TECHNISCHE UNIVERSITÄT WIEN
Vienna University of Technology

DIPLOMARBEIT

Hyphenation of Raman spectroscopy and ultrasound particle manipulation for increased signal sensitivity – An experimental characterization with the example of polymer particles in aqueous environment

Institute of Chemical Technologies and Analytics

Supervisor
Univ. Prof. Dr. Bernhard LENDL

And

Dipl-ing. Dr. techn. Stefan Radel and Dipl.Ing. Karin Wieland

By
Hamid Rasoulimehrabani
Josef Baumann Gasse 8a-513
1220 Wien

Vienna, May 2018   ………………………………

So then you're free? 'Yes, I'm free,' said Karl and nothing seemed more worthless than his freedom.

Franz Kafka, America

In memory of my father

To my mother

With love and eternal appreciation

Contents

Abstract

In this thesis two techniques, namely Raman spectroscopy and ultrasound particle manipulation, have been successfully combined to achieve a powerful analytical measurement technology for the acquisition of Raman spectra of PMMA particles in suspension in order to increase sensitivity of Raman spectroscopy.

The experimental setup has been characterized and optimized for the investigation of micrometer-sized PMMA particles and the immobilization thereof in defined areas by employing ultrasound particle manipulation. A commercial confocal Raman microscope as well as Raman probe for process analytical monitoring were employed for collecting Raman spectra of PMMA particles of defined size (~ 3.4 μm) in aqueous environment. Using Raman spectroscopy solely allows to detect only weak signal in the spectra of the suspended particles. Ultrasound enhanced Raman spectroscopy has been developed by using the acoustic radiation forces acting within an ultrasound standing wave field (f ~ 2 MHz) to actively position the particles in suspension within and outside the focus of the Raman laser. This work demonstrates that the limit of detection of otherwise hardly detectable signal is drastically improved by combining a Raman probe with a piezoelectric device for ultrasound generation compared to conventional Raman spectroscopy. The analysis are able to describe how successful the enhancement factor of Raman intensity is after using ultrasound particle manipulation. To demonstrate the improved sensitivity of such a combination, different concentrations of PMMA in distilled water have been investigated and compared. The results indicate that the intensity of the Raman signal depends on the stability of the ultrasound standing wave field which is dependent on the ultrasound frequency, the material properties of PMMA particle and the surrounding medium and the concentration of the particles in suspension.

Furthermore, a gel immobilization technique for fixing the spatial arrangement of the particles in the nodal planes was applied for visualization of the particle arrangement in the force field and for accessing the signal enhancement achieved by combining conventional Raman spectroscopy

8

with ultrasound particle manipulation in a more stable way. Suspended particles can be kept within a gel-block, for subsequent investigation of single cut layers under the microscope. The spatial distribution of the particles can be sustained even when the force field is removed. This provides the direct analysis of the influence of ultrasound standing waves on the location of PMMA particles. The experiments presented here, provide detailed insights into the experimental design and the effects of different parameters on the obtained Raman signal for the investigated method.

Acknowledgment

My thanks to …

My thesis supervisor Bernhard Lendl for the useful comments, remarks and engagement through the learning process of this master thesis.

I would like to thank Stefan Radel for introducing me to the topic as well for the support on the way. He was always open whenever I ran into a trouble spot or had a question about my research or writing.

Especial thanks to Karin Wieland for her wonderful collaboration. She supported me greatly and was always willing to help me. She definitely provided me with the tools that I needed to choose the right direction and successfully complete my thesis. Karin was the first reader of this thesis, and I am gratefully indebted to her valuable comments on this thesis.

I am grateful to all of the colleagues who have supported and helped me so much throughout this period.

My thanks to…

My dear mother and my dear Forough through good time and bad, your kindness and extensive support have been ever presented in this important time of my life for which I am eternally grateful.

This thesis is dedicated to the memory of my father who I lost last year…

Introduction

The combination of ultrasound particle manipulation and Raman spectroscopy is investigated during this thesis. Spectroscopic techniques are based on the interaction between matter and electromagnetic radiation. Due to this interaction, molecules get excited and the change in energy resulting in a frequency shift is detected. In Raman spectroscopy, a laser acting as monochromatic light source is employed for molecule excitation. Raman spectra provide a fingerprint consisting of vibrational frequencies of the measured molecules to identify the investigated sample. Raman scattering is an inelastic scattering process where the frequency of a back scattered photon shifts to lower (Stokes) or higher (anti-Stokes) frequencies compared to the incoming photon [1].

The primary axial radiation force exerted by an ultrasound wave (standing wave) can be used to move particles in suspension into the nodal planes. The application is employed in a set up where the cavity of an acoustic resonator encompasses suspended particles. Upon ultrasound particle manipulation, the initial homogenously distributed particles are forced into the pressure nodes of the standing wave field. Typically, the collection of suspended particles in the nodal planes does not take longer than a few seconds. Focusing the Raman sensor in the nodal planes with the agglomerated particles yields significant enhancement of the Raman signal compared to the same particle concentration homogenously distributed in the suspension.

1. Theoretical background

1.1.1 The Raman Effect

The Raman Effect was first theoretically predicted by A.Smekal in 1923; followed by quantum mechanical descriptions by Kramers and Heisenberg in 1925 and Dirac in 1927. The first experimental evidence of Raman effect was observed by Sir C. V. Raman in 1928. He was awarded with the Nobel Prize in physics for his discovery of the phenomenon of the inelastic scattering of light. If light is reunified for a very short time with particles and then scattered again, it carries the information of particles [2]. Raman spectroscopy provides detailed information about chemical composition, crystal structure and chemical bonds. The Raman Effect is based on the changes of the wavelength of light when it interacts with a sample which allows the chemical identification of the investigated sample. When the incident light with a defined wavelength λ interacts with the sample, electrons get excited to a higher energy level (virtual energy state) for a short time. When they fall back to ground state, it leads to three possible outcomes: The scattering of photons off the particles without change of frequency is called Rayleigh scattering and that with change of frequency to lower or higher photon energy is called Raman scattering. Raman bands of the spectrum of the scattered radiation at frequencies lower than the incident frequency (v_0-v_{vib}) are referred to as Stokes bands and those bands with higher frequency than the incident frequency (v_0+v_{vib}) are called anti-Stokes [2, 3]. Usually, the Raman shift is numerically represented in wavenumbers (cm^{-1}) and calculated as follows, equation 1:

Equation 1) $\qquad\qquad$ Wavenumber: $\tilde{v} = \dfrac{1}{\lambda}$

Where λ is the wavelength. A Raman spectrum plotted in wavelength scale would be very narrow and crowded and because of that wavenumber as the inverse of the wavelength is used for depicting Raman spectra. Increasing wavenumber means increasing energy difference between

incoming and scattered photons. Hence, a Raman spectrum is usually plotted going from low to higher energy difference.

The energy of the electromagnetic wave is directly proportional to its frequency f multiplied by Planck's constant h, equation 2:

Equation 2)
$$E = hf = \frac{hc}{\lambda}$$

As described in equation 3, a change in polarizability α is required for a molecule to be Raman active where Q is the physical displacement of the molecule. The intensity of the Raman signal is directly proportional to the intensity of the incoming Raman photons I_0, the polarizability α and the inverse of the excitation wavelength λ to the power of four (equation 4)[5].

Equation 3)
$$\left(\frac{\partial \alpha}{\partial Q}\right)_0 \neq 0$$

Equation 4)
$$I_{Raman} \propto \alpha \left(\frac{1}{\lambda}\right)^4 I_0$$

Induced molecular dipole moment is generated as result of the interaction of molecule with incident electromagnetic wave or light. That interaction of light and molecule to produce the dipole moment, generate some isolating dipole moment which emits radiation or light scattering. The basis of this induced dipole moment is polarizability. In particular with respect to Raman effect the most important is polarizability as function of the nuclear coordinate with the vibrations of the molecule [2].

The most basics expression in dealing with light scattering and electrodynamic of the interaction of molecule with light is (equation 5):

Equation 5)
$$\vec{P} = \tilde{\alpha} \vec{E}$$

Where P is induced dipole moment, α is the polarizability tensor and E is the incident electric field. Molecular polarizability is the ease with which the electron density distribution which can be distorted by an electric field.

In oscillating electric field induces as oscillating molecular dipole moment (equation 6):

Equation 6): $E = E_0 \cos(2\pi vt)$

The incident electric field (E_0) from the electromagnetic radiation is an oscilating electric field at frequency v of that incident light. The expression of dipole moment P is following (equation 7):

Equation 7): $P = \alpha E_0 \cos(2\pi vt)$

Figure 1 shows graphical understanding of polarizability and how that associate with chemical bands and the vibrational motions.
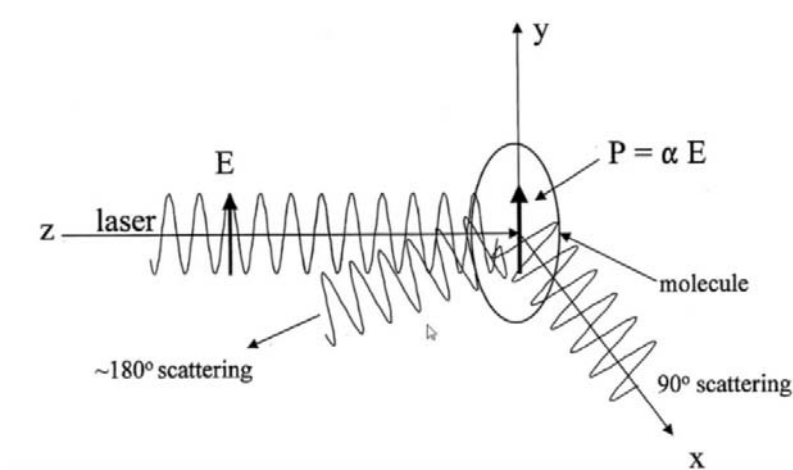
Figure1) Polarizabilty ellipsoid of the molecule by interaction with laser

Polarizability of the molecule can be describes as Taylor expansion. That indicates the static polarizability in addition to a small vibrational displacement (equation8):

Equation 8): $\alpha = \alpha_0 + \dfrac{\partial \alpha}{\partial Q} Q + \cdots$

Where α_0 is static or equilibrium polarizabtility that consider for a molecule that's not in motion and then there is vibrational modulation of molecular polarizability with respect to Q which is normal vibrational coordinate (equation 9):

Equation 9): $\qquad$ $Q = Q_0 \cos(2\pi v_{vib} t)$

The Q value expressed a normal vibrational coordinate and Q_0 is the maximum value of Q and v_{vib} is the frequency of the vibrational molecule and is time.

The taylor expansion gives us two components for limited to static linear polarizability and the vibrational modulation (equation 10):

Equation10) $\qquad$ $\alpha = \alpha_0 + \frac{\partial \alpha}{\partial Q} Q_0 \cos(2\pi v_{vib} t)$

In cooperating the polarizability from the static and vibrational component in to my original expression for the induced dipole moment, I see there is a term for the induced dipole moment and therefore scattering occurs at the frequency of the incident radiation. Then I have the component which combines the incident radiation frequency with the vibrational frequency of the molecule, and the vibrational modulation of the polarizability (equation11):

Equation11): $\qquad$ $P = \alpha_0 E_0 \cos(2\pi vt) + \frac{\partial \alpha}{\partial Q} Q_0 E_0 (\cos(2\pi vt))(\cos(2\pi v_{vib} t))$

With using trigonometric identity (equation12):

Equation12) $\qquad$ $\cos A \cdot \cos B = \frac{1}{2}[\cos(A-B) + \cos(A+B)]$

I applied this trigonometric identity to the expression of equation 11, then I will have three expressions of light scattering from oscillating molecular dipole moments (equation13):

Equation13) $\qquad$ $P = \alpha_0 E_0 \cos(2\pi vt) + \frac{\partial \alpha}{\partial Q} \frac{Q_0 E_0}{2} [(\cos(2\pi(v-v_{vib})t) + (\cos(2\pi(v+v_{vib})t)]$

The energy difference between the incident and scattered photons is represented schematically by Figure 2. The energy is released in form of light which is detected by a CCD (charged coupled device) detector.
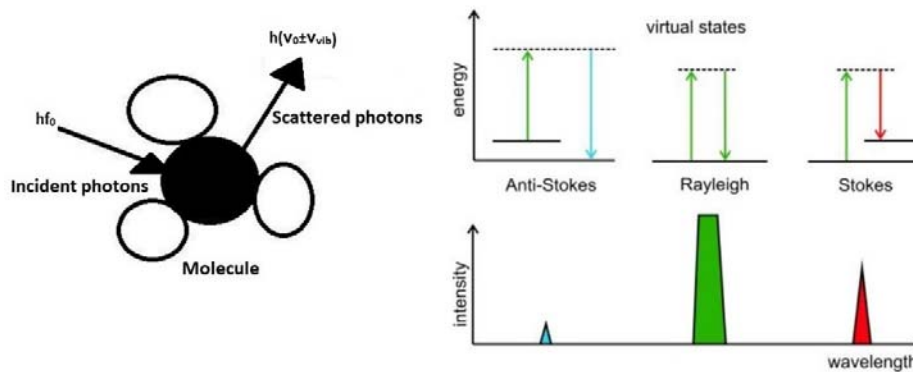
Figure 2) Interaction of incident photons with the molecule and scattered photons with the schematic diagram of a Raman spectrum showing Raman effect (Rayleigh, stokes and anti-stokes scattering)

The lateral resolution can be defined by the diffraction limit (equation 14), Δx is the shortest distance between two points which are distinguishable, λ is the wave length of the incident beam and NA is numerical aperture[1] of the objective.

Equation 14) $$\Delta x = 0.61 \times \frac{\lambda}{NA}$$

To obtain the highest collection efficiency with the maximum spatial resolution we have to choose the objective with the highest numerical aperture (Figure3) which means that more light will be collected by the objective [6]. However, higher NA also means lower working distance which can be problematic with very rough sample surfaces [7] [4].

---

[1] numerical aperture is the ability of the lens to gather light and resolve fine the details of the specimen, NA= n sin θ, which n is the refractive index of the media between cover glass that sample is on it and the objective front lens and θ is half of the angular aperture

Low numerical aperture   High numerical aperture

A   B   C

NA = 0.12 $\theta = 7°$

NA = 0.34 $\theta = 20°$

NA = 0.87 $\theta = 60°$

$NA = n \sin(\theta)$ where $n = 1.0$
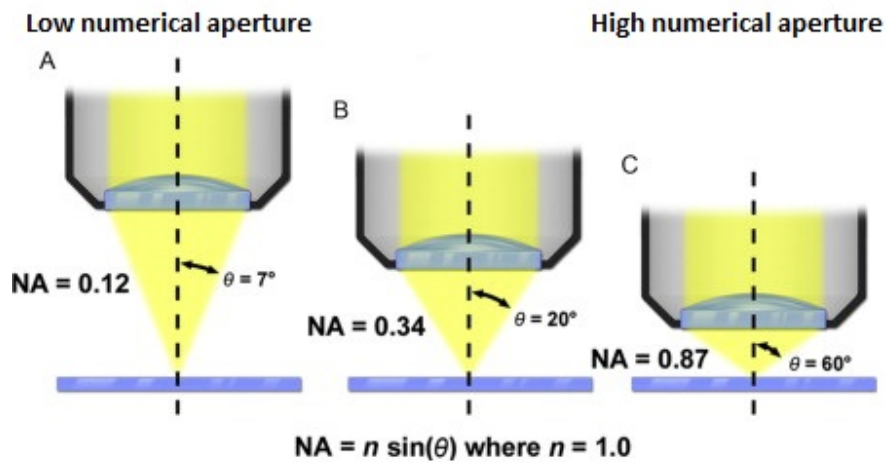
Figure 3) the amount of light collected through the objective depends on the NA [8].

1.1.2 Confocal Raman Microscopy

Confocal microscopy allows you to improve the vertical and horizontal resolution by adding a confocal hole of a defined size in front of the detector. Hence, only photons of the specific sample layers can be detected. In conventional Raman microscopy, the lateral resolution is influenced by the numerical aperture (NA) of the objective and the excitation wavelength λ of the laser. However, using confocal Raman microscopy, the lateral resolution is roughly improved by a factor of 1/3 compared to conventional Raman microscopy. The laser which is used as monochromatic light source, is focused onto the sample through an objective. The backscattered photons of the sample are collected by the same objective lens and focused onto the aperture in front of the detector (Figure4). The sample is entirely illuminated by the excited light, its highest intensity is at the focal point of the lens. Out of focus light is rejected by the pinhole in front of the detector, while light in focus is detected (see figure 4). By the use of variable pinhole sizes, the Raman signal of the defined sample layers, can be selected. The laser spot size is determined by $\frac{\lambda}{2NA}$ where λ is the wavelength of incident photons, and NA is the numerical aperture of the focusing lens and the size of the pinhole [4][5].
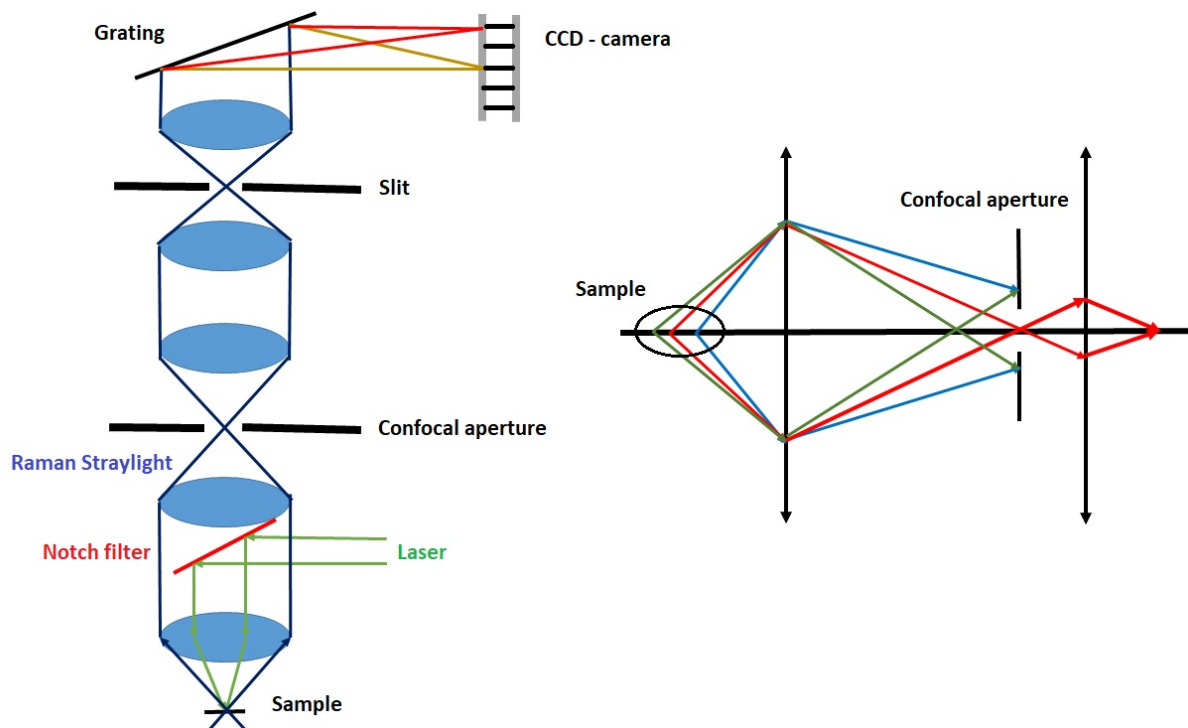
Figure 4) Schematic of an inverted confocal microscopy with its block diagram of the optical section

1.2.1 Separation of suspended particles via ultrasound

Particles suspended in a medium are manipulated by acoustic radiation force. For particle manipulation, acoustic resonators and thus standing wave fields are usually used [9]. An acoustic standing wave field is used to separate and manipulate particles based on the size and density of particles along the axial direction. Ultrasound resonators consist of a reflector placed on the opposite side of an ultrasound transducer leading to the superposition of incident and reflected wave. The resulting quasi standing wave consists of nodal and anti-nodal planes, depending on the particle size as well as on density of the suspended particles and medium, the particles are concentrated in the nodal region of the standing wave. For this purpose, there is a transducer which includes a piezoelectric material charged by a voltage signal to produce an acoustic standing wave in the resonator. In a standing wave, particles within fluids are collected at nodal or anti-nodal planes perpendicular to the direction of sound propagation[10][11][12](Figure5).

18
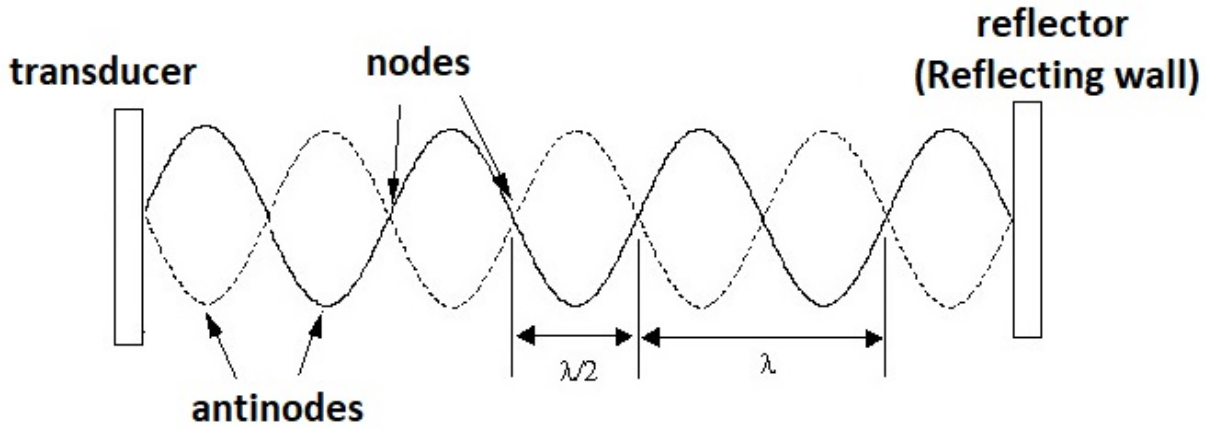
Figure 5) Nodal and anti-nodal plane layers of the standing wave where the particles can be collected

Due to the primary acoustic radiation force the particles move to the nodal or anti-nodal pressure points of the acoustics standing wave. It consists of two main inputs: axial and transverse radiation force [13]. The primary axial radiation force pushes particles in the axial z direction and the particles are driven to the nearest pressure node/antinode plane. The primary transverse radiation force has an effect on the distribution of the particles collected in the nodal plane (XY) [14] while secondary forces make the particles attract or repel each other[15].

The primary axial radiation force $F_z{}^{rad}$ is the main force acting on the particles and dragging them into nodal or anti-nodal planes determined by the radius α of the particles, the acoustic energy E_{ac} (Equation 16) brought into the medium and the acoustic contrast $\phi(\tilde{\kappa}, \tilde{\rho})$. $F_z{}^{rad}$ with a wavelength λ and $\lambda \gg \alpha$ propagating in z direction is given by equation 15 [17][16]:

Equation 15)
$$F_z^{rad} = 4\pi \cdot \phi(\tilde{\kappa}, \tilde{\rho}) \cdot (ka)^3 \cdot E_{ac} \cdot \sin(2kz)$$

with wavenumber k= $\frac{2\pi}{\lambda} = 2\pi$f

Equation 16)
$$E_{ac} = \frac{p_a^2}{4\rho_0 c_0^2}$$

p_α ... acoustic pressure amplitude

ρ_0 ... density of medium

c_0 ... speed of sound in medium

Equation 17)
$$\phi(\tilde{\kappa}, \tilde{\rho}) = \frac{1}{3}\left(\frac{5\tilde{\rho}-2}{2\tilde{\rho}+1} - \tilde{\kappa}\right)$$

The acoustic contrast factor $\phi(\tilde{\kappa}, \tilde{\rho})$ (equation17) depends on the density ratio $\tilde{\rho} = \frac{\rho_p}{\rho_0}$ and compressibility ratio $\tilde{\kappa} = \frac{\kappa_p}{\kappa_0}$ with the compressibility being defined as $\kappa = \frac{1}{\rho \cdot c^2}$. The subscript 0 denotes the respective value of the surrounding medium and the subscript p denotes the respective value of the particles. For $\rho_P > \rho_0$, the acoustic contrast factor is a positive number leading to an accumulation in the nodal planes of the ultrasound standing field. In contrast, for $\rho_P < \rho_0$, $\phi(\tilde{\kappa}, \tilde{\rho}) < 0$ results in an accumulation in the anti-nodal planes. [18] [21] [22]

1.2.2 Hard Piezoelectric materials on a layered resonator

To achieve particle motion control, acoustic systems are manufactured based on a layered resonator with the main part being a piezoelectric element glued to a carrier layer (Figure6). For higher acoustic intensities, piezo materials based on lead zirconate titanate (PZT ceramic) are most suitable in high power acoustic applications especially as ultrasound transducer because of its high efficiency to transform the electrical to mechanical energy [19,20]. Modified lead zirconate titanate is used as ceramic disc with diameters up to several millimeters or in other shapes such as squares or rectangular shape. They have a high mechanical quality factor and

good toleration for high temperatures. Electrodes are mostly made of silver with at least 5μm of layer thickness [21].

The simplest arrangement to build a resonator for the investigation of particles in a liquid suspension with a standing ultrasound field is generated by two PZTs and a commercial UV/Vis cuvette (see figure 6). The piezoelectric transducers with two electrodes are glued to the opposite side of the cuvette glass walls which act as isolator between the PZT and the suspension [15].
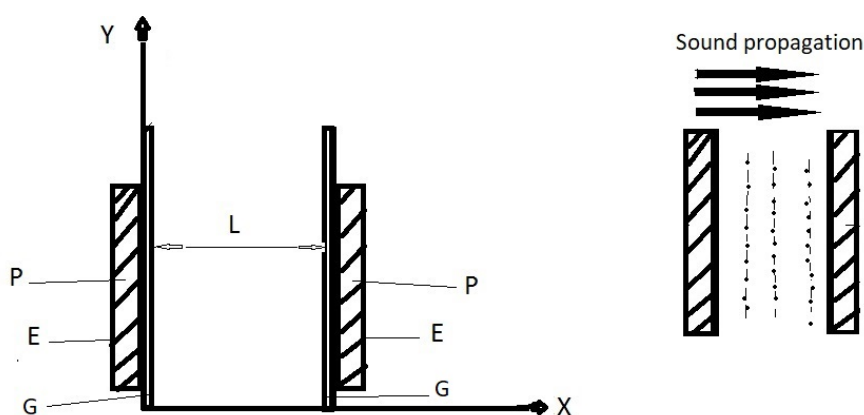

Figure 6) Piezoelectric resonator, sound propagates in x-direction. P: Piezoelectric element, E: Electrodes, G: glass wall, L: liquid (suspension)

Hard PZT Materials are used for ultrasound transducers because of their properties which hardly change under mechanical stress and high electrical power. Here i used PZT PIC 181 which is a modified lead zirconate titanate. Due to its characteristic material properties such as high mechanical resistance, resistance to different temperatures and stability over time it is an appropriate material for ultrasound applications.

1.2.3 Immobilization of ultrasound manipulated particles

To experimentally determine the particle distribution when an acoustic force is applied, studies with particle immobilization in gel were performed. As long as the force is applied, the particles are agglomerated in the nodal planes while they homogenously redistribute in the medium when the ultrasound is off. Immobilization of the suspended particles in a polymer gel matrix is one of the best techniques used to study agglomeration of micro sized particles due to acoustic forces even when the force field is removed. The immobilized particles within a gel block can be easily cut into layers and examined subsequently. Most of the studies investigating immobilization of particles use gel because of its simplicity and excellent particles blocking capabilities without influencing particle properties[23]. However, the gel suffers from limited mechanical stability. Additionally, if microorganisms e. g. yeast cells are fixed in the gel matrix, the structure is also easily destroyed by cell growth inside the gel.

2. Methods and Materials

Raman experiments are performed using different Raman spectrometers. Raman spectroscopy is a nondestructive optical method based on a laser beam focused onto the sample. Detailed information of chemical composition and crystal structure of chemical components can be obtained by Raman spectroscopy.

2.1 Horiba Jobin-Yvon LabRAM 800 HR

Horiba Jobin-Yvon LabRAM 800 HR is a high resolution confocal Raman system which operates with laser sources emitting visible continuous laser radiation typically below 100 mW. This spectrometer presents advanced confocal Raman imaging resolution down to 240 nm (considering 100x objective with N.A=0.9 and 532 nm laser excitation wavelength) (equation 18).

Equation 18) $\qquad$ Diffraction limit: $\Delta x = 0.61 \dfrac{\lambda}{N.A}$

$$\text{Confocal} \sim \frac{2}{3} \Delta x$$

This instrument consists of three main parts (Figure 7):

a) Monochromatic laser excitation source – an internal HeNe (633nm) laser and an external frequency – doubled Nd: YAG laser (532 nm, Oxxius LMX-532).
b) Optical Microscope with Halogen lamp, motorized XYZ-stage and color camera.
c) Spectrograph equipped with a 300 grooves/mm and a 1800 grooves/mm grating coupled to a synapse open-Electrode-CCD Camera.

The laser power on the sample depends on the magnification of the objective lens, therefore the laser spot size varies for different objectives/magnifications. The size of the laser spot can be

estimated with the airy disk approximation (An airy disk is the central bright circular region of the pattern produced by light diffracted when passing through the aperture) (equation19).

Equation19) $$\text{Laser spot diameter} = 1.22\frac{\lambda}{N.A}$$

Where λ is the wavelength of the excitation laser and N.A is the numerical aperture of the objective. The laser spot size of a 633 nm Raman laser with 20x objective as used for most of the experiments in this work is 3.8 μm^2 (table 1):

Table1: Calculated laser spot size for 20* magnification at 633 nm excitation wavelength

Objective	N.A	Laser spot diameter [μm]	Laser spot area [μm^2]
20	0.35	2.2	3.8
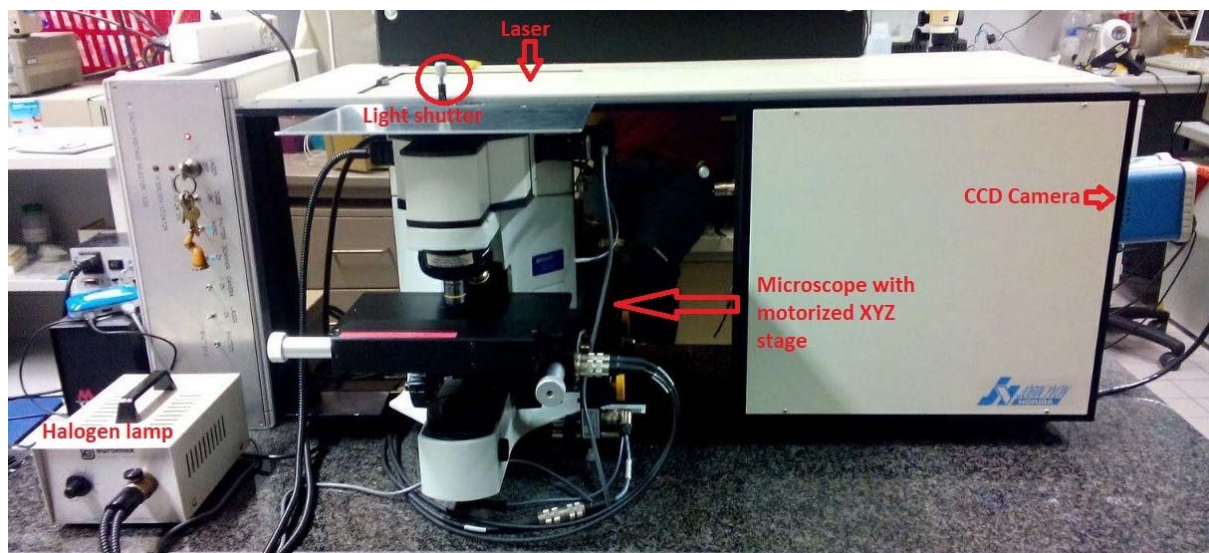
Figure 7) Horiba Jobin-Yvon LabRAM 800 HR with its three main parts

Prior to analysis with Raman spectroscopy, the sample on the stage can be visualized using the optical microscope, the Halogen lamp and the digital camera. The resulting image can be captured and saved using Horiba Jobin-Yvon LabRAM 800 HR control software (Labspec6):

1) The sample can be visualized via the digital camera by turning on the white light illumination and putting the shutter into the correct position (down).
2) In the software (Labspec6), click on the video icon on top toolbar, use the joystick to move the motorized XYZ-stage.
3) Stop the video image by clicking on the stop icon on the top right side of toolbar on the screen.
4) To collect a Raman spectrum, turn off the white light illumination and change the position of the shutter (up).
5) The Raman signal can be collected either in "Real Time Display" mode which is primarily used for adjusting parameter settings or in "Spectrum Acquisition" mode where an acquisition time and a specific number of accumulations for one single spectrum can be set (Figure 8).
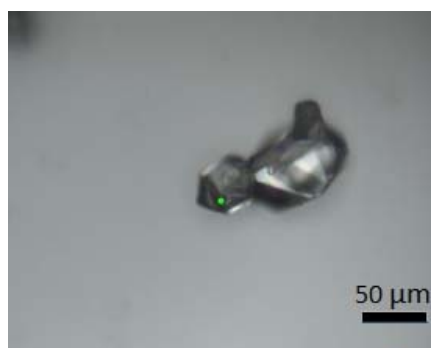
Figure 8) Horiba Jobin-Yvon LabRAM 800 HR -Crystal of Paracetamol 20x magnification (Nikon, N.A.0.35)

All the spectra in this work were collected with 633 nm excitation wavelength, 20× objective, 300 g/mm grating, a confocal hole of 500 µm and an entrance slit of 100 µm.

2.2 Calibration with silicon

Elemental silicon is often used to calibrate Raman Spectrographs. If the instrument is well calibrated, a sharp Raman band at around 520 cm^{-1} should be visible. Silicon is used for calibration purposes because it doesn't emit fluorescence and shows sharp, defined Raman bands. It does not degrade over time and it is easy to handle. Figure 9 shows a typical Raman spectrum of silicon including a list of parameter settings which can be fully controlled by LabSpec6:
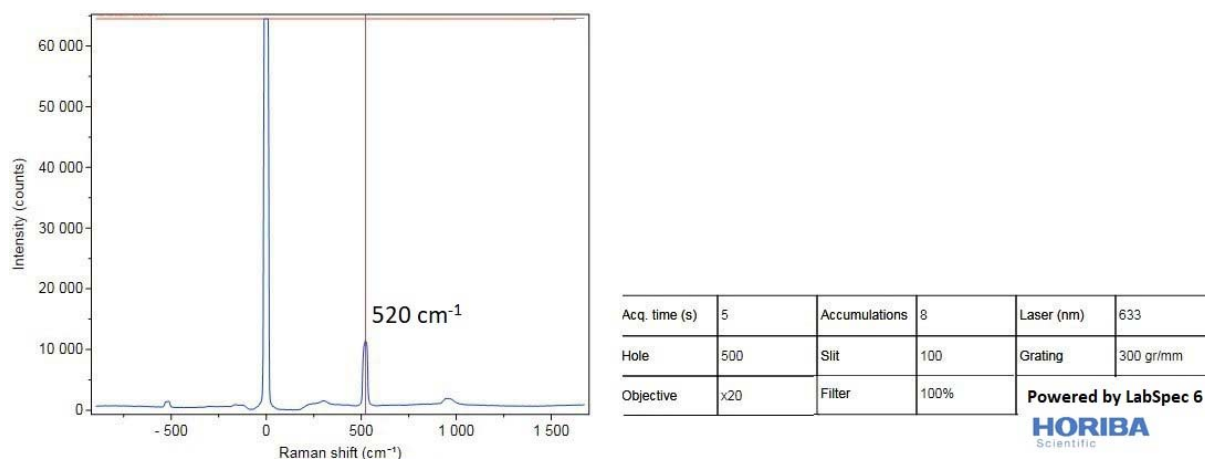

Acq. time (s)	5	Accumulations	8	Laser (nm)	633
Hole	500	Slit	100	Grating	300 gr/mm
Objective	x20	Filter	100%	Powered by LabSpec 6	

Figure 9) A characteristic Raman spectrum of silicon with according parameter settings

2.3 Kaiser Optical Systems RXN-1-785 nm

RAMAN RXN1 Analyzer from Kaiser Optical Systems RXN, Inc. is a compact Raman probe for PAT[2] purposes. It is easy to use and ideal for analyzing, monitoring and controlling chemical processes. All the experiments and measurements in this work have been done with 785 nm laser excitation wavelength covering a spectral range of 200-1800 cm^{-1} Raman Shift.

---

[2] Process Analytical Technologies (PAT)

RAMAN RXN1 Overview: Monochromatic light is coupled into an optical fiber connected to the probe head (Multi RxnProb 785 nm). After light sample interaction the back scattered light is detected by a fiber coupled spectrograph.

The following steps are necessary to perform a Raman experiment. After running iC Raman software, create a new experiment and set the integration time interval (can be changed manually later). To check the quality of the spectrum, it is recommended to collect a reference spectrum. The next step is entering a name for the reference spectrum and selecting the sample type (e.g. selecting "Solvent" and the corresponding functional groups which is useful to auto define characteristic Raman bands; if a functional group is not included in the list, just leave it as "None" and click on "Next"). After positioning the probe, the spectra acquisition can be started and spectra are continuously collected and displayed on the screen. Figure 10 shows the Raman Kaiser Optical Systems RXN probe included in experimental setup.
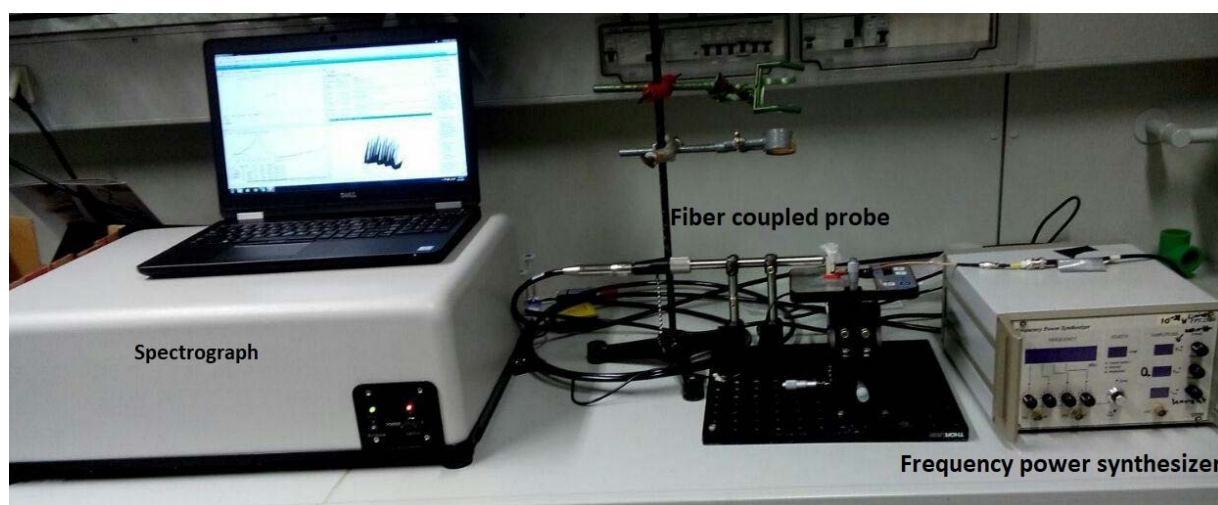
Figure 10) Kaiser Optical Systems RXN-1-785 nm, Raman probe (MultiRxn probe 785 nm) set in front of the cuvette

General procedure for performing Raman experiments with Kaiser Optical Systems RXN is placing the sample on a substrate (microscope slide or CaF_2) or in a transparent cuvette and then turn on the laser by turning the key and wait for approximately 30 minutes for the laser to stabilize.

Open the software and start collecting spectra. During Raman experiments, the sample and probe were covered with a black curtain to avoid interferences by the light in the laboratory. Also, the laser beam needs to be covered to avoid eye damage of the operator due to laser radiation.

As shown in figure 11 the Raman probe uses a single lens to both focus the laser on and collect the Raman signal from the sample. Lenses with different working distances can be selected. The most efficient Raman signal collection will take place with the highest numerical aperture. This occurs with the shortest working distance of the lens. With short working distance, the probe must be positioned closer to the sample for it to be in focus, which may not be physically possible (e.g. the lens may not be able to focus through the cuvette glass wall, resulting in the measurement of the container rather than of the sample). Therefore, the optical components of such a system have to be chosen carefully.
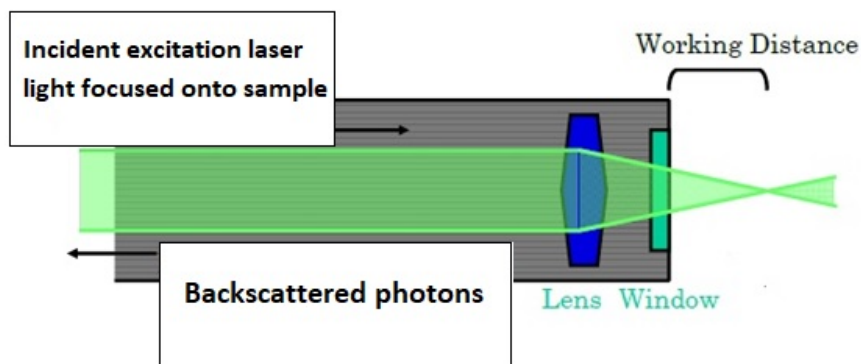
Figure 11) Schematic presentation of probe (In our case there is only one lens, no additional window) [Raman spectroscopy a valuable tool for PAT applications, Dr. Bruno Lenain]

2.4 Reference spectra of PMMA

Poly (Methyl Methacrylate) microspheres (PMMA; Bang Laboratories, Inc.) with a diameter of 3.36 µm +/- 0.54 µm were used for all the experiments with ultrasound particle manipulation. Experiments were performed in a UV/Vis cuvette (a Hellma Macro-Cuvette 6030-OG) with and without magnetic stirrer. Different PMMA concentrations suspended in water (starting from 9.3 g/l to 1.116 g/l) were prepared. Raman spectra with 18×30s of integration time were collected using Horiba Jobin-Yvon LabRAM 800 HR spectrometer and Raman spectra with 3×5s of integration time were collected using Kaiser Optical Systems RXN spectrometer.

In this project, PMMA was chosen due to insolubility in water, having defined particle size around 3.4 µm which proofs applicability of the used system in biotechnology fields because microorganisms usually are in a similar size range, having a narrow particle size distribution and its capability as a good Raman scatterer. A reference Raman spectrum of PMMA is depicted in figure 12 and table 2 including band assignments.
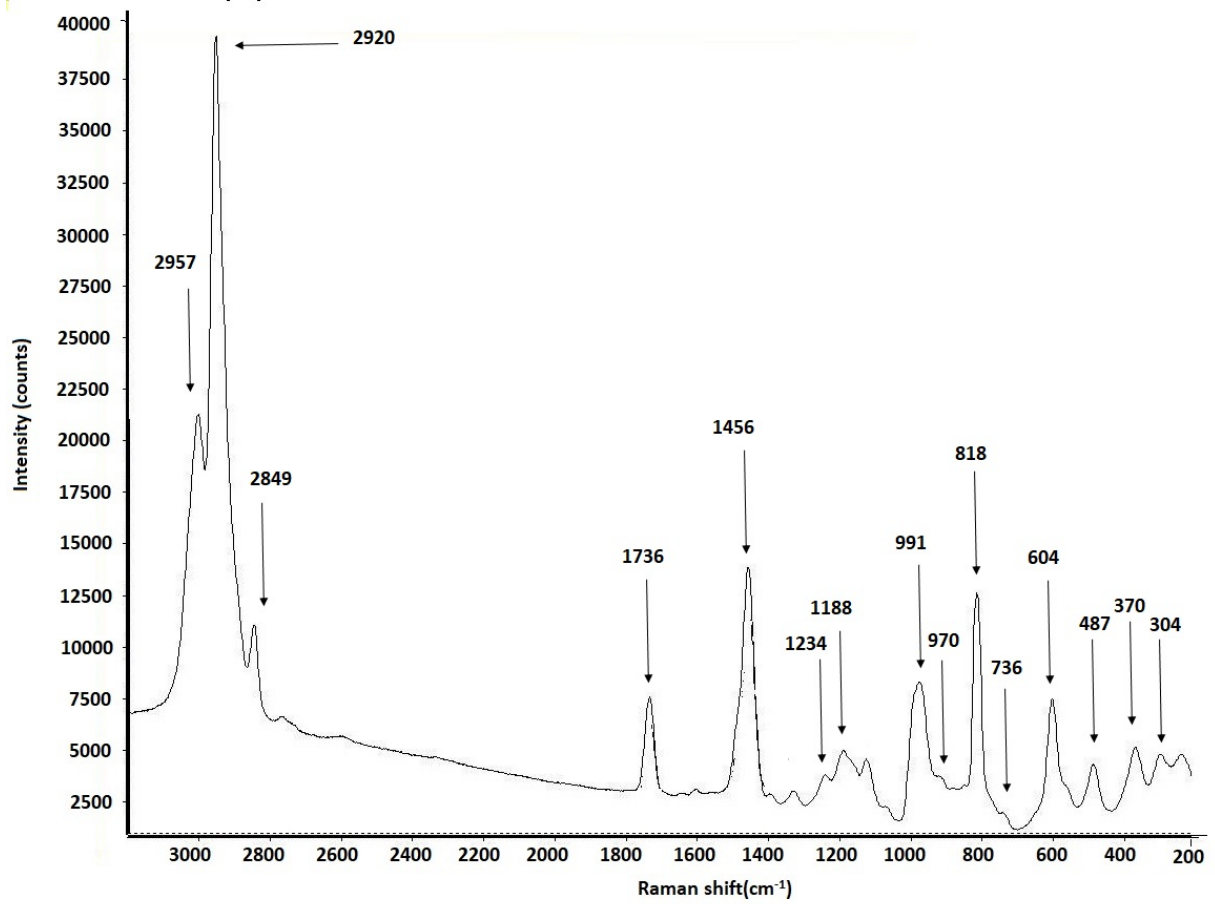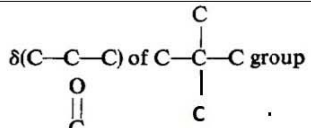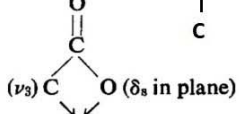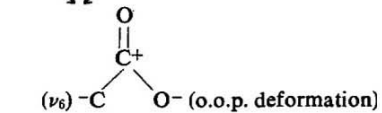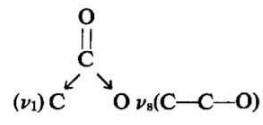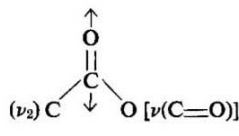
Figure 12) Raman spectra and band assignment of the PMMA particles covering different spectra range depending on the Raman system used to collected the spectrum [28]

Table 2: band assignment of the PMMA particles covering different spectra range [28]. Abbreviations: vs=very strong; s=strong; m=medium; w=weak; vw=very weak

Wavenumber(cm^{-1})	Band assignment	Wavenumber(cm^{-1})	Band assignment
304 w	δ(C—C—C) of C—C—C group (with C substituents)	991 ms	O—CH$_3$ rock
370 m	(ν_3) C—O (δ_s in plane)	1188 mw	ν_a(C—O—C—)
487 m	(ν_6) —C—O$^-$ (o.o.p. deformation)	1234 w	(ν_4) C—O or C—O stretch
537 w	δ(C—C—C) skeletal mode	1400 vw	CH$_2$ twist or wag
604 s	(ν_1) C—O ν_s(C—C—O)	1456 ms	δ_a(C—H) of α-CH$_3$
736 vw	ν(C—C) skeletal mode	1736 mw	(ν_2) C—O [ν(C=O)]
818 vs	ν_s(C—O—C)	2849 vw	Combination band involving O—CH$_3$
970 ms	α-CH$_3$ rock	2920 vw	Combination band involving O—CH$_3$ and ν_s(CH$_2$)
		2957 m	ν_s(C—H) of O—CH$_3$ with ν_s(C—H) of α-CH$_3$ and ν_a(CH$_2$)

Reference spectra of PMMA in solid form (figure 13) and mixed with deionized water (figure14), homogenously distributed in water (figure 15) and of the sediment (particles in suspension settled in the bottom of the cuvette) were collected with the Kaiser Optical Systems RXN. Also, a spectrum of a cuvette's glass wall (figure16). A spectrum from the optical glass consists of very strong and broad photoluminescence throughout and peaking at approximately 1400 cm^{-1} which completely obscuring the fingerprint region of the Raman spectrum [34]. Also water inside the cuvette (figure17) was recorded for comparison. For water, due to hydrogen bonding interactions, the bending and stretching vibration modes lie around 1630 cm^{-1} and in the range of 2750–3800 cm^{-1}. Therefore, the ν_2 mode lies around 1630 cm^{-1}, while the ν_1 and ν_3 lie in the range of 2750–3800 cm^{-1}[35].
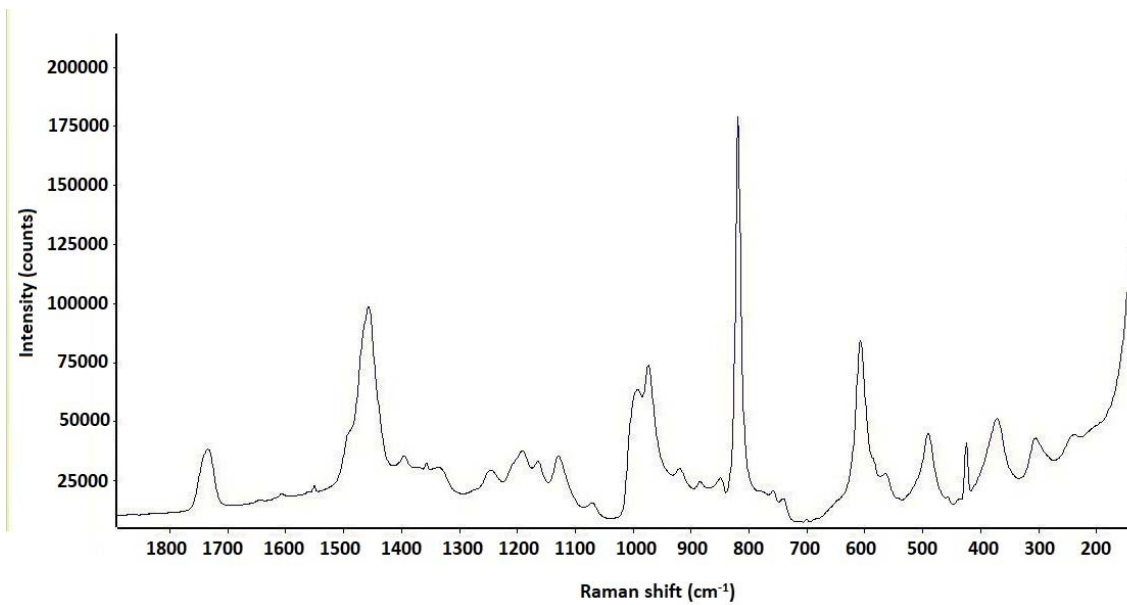
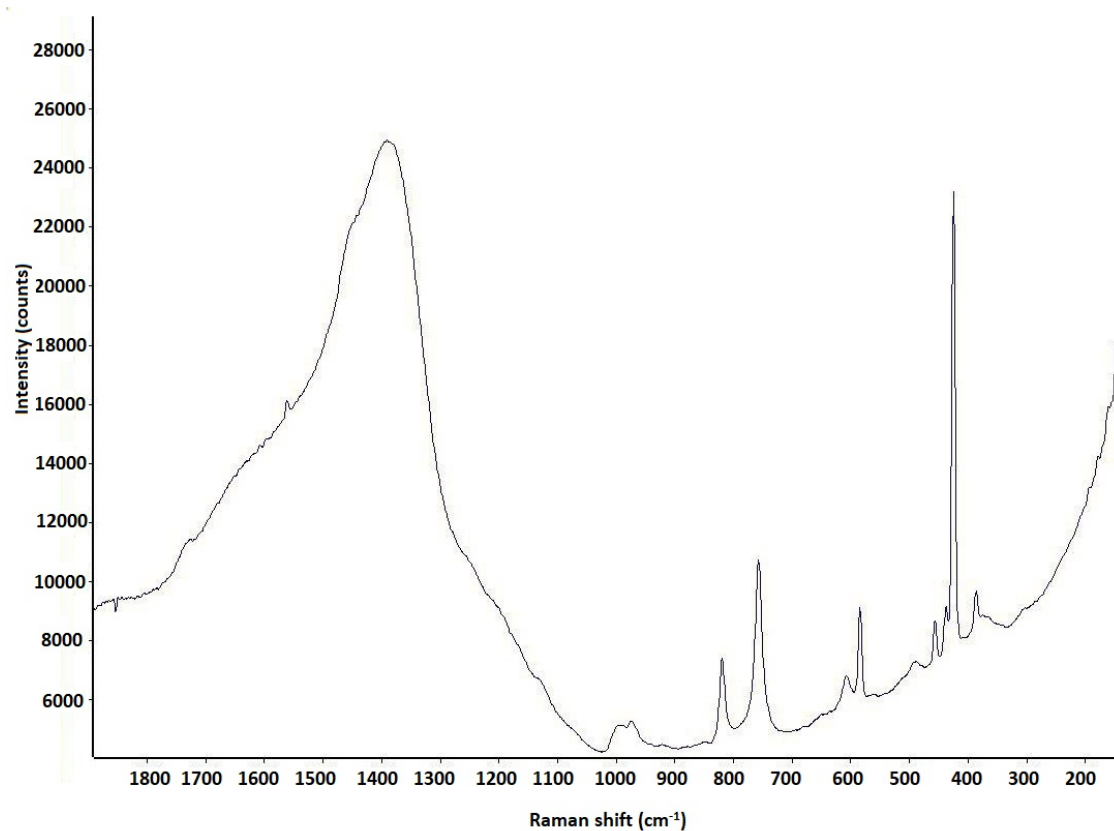Figure 13) reference spectra of pure powder of PMMA on the microscope slide

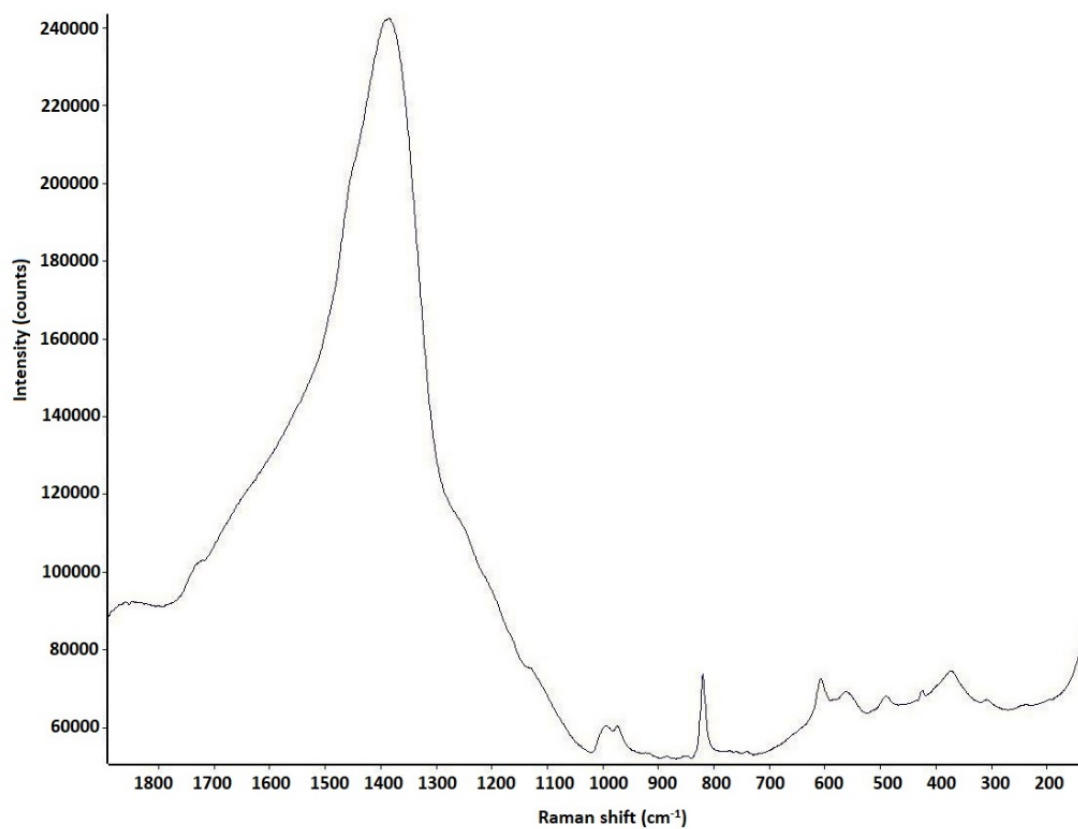Figure 14) reference spectra of PMMA with one droplet of water on a microscope slide

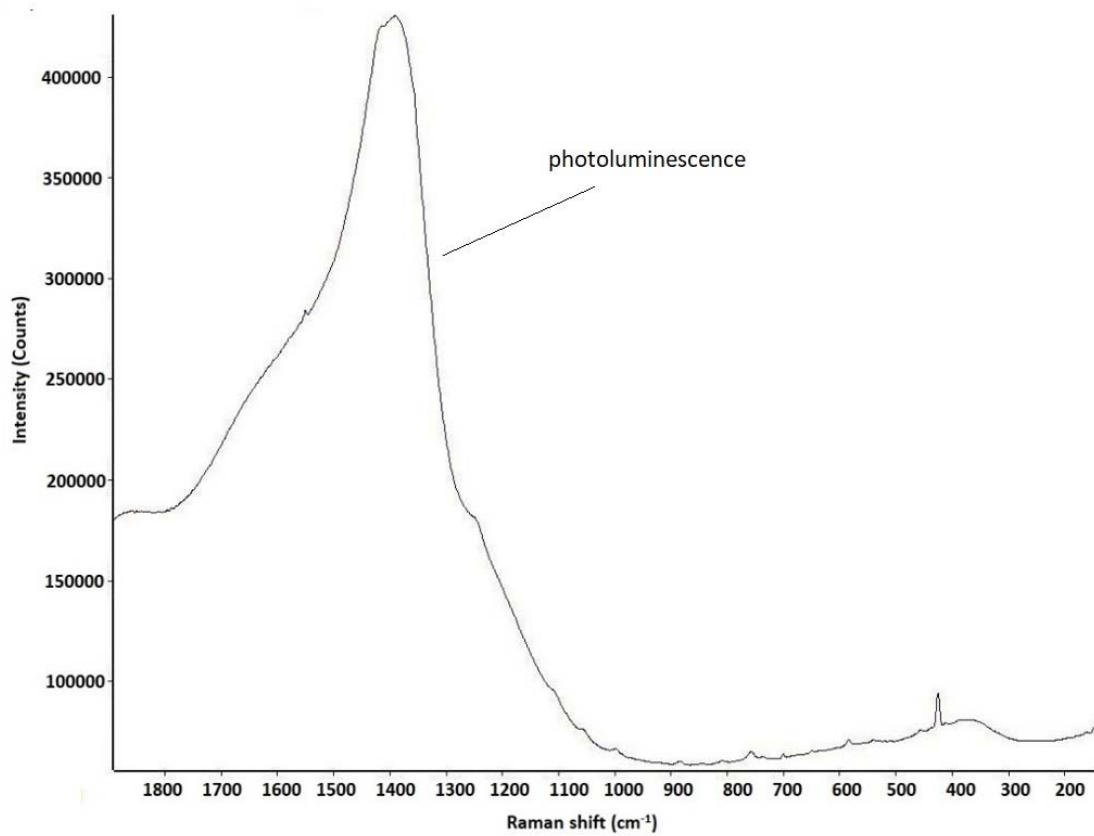Figure 15) reference spectra of Sediment of PMMA inside the cuvette

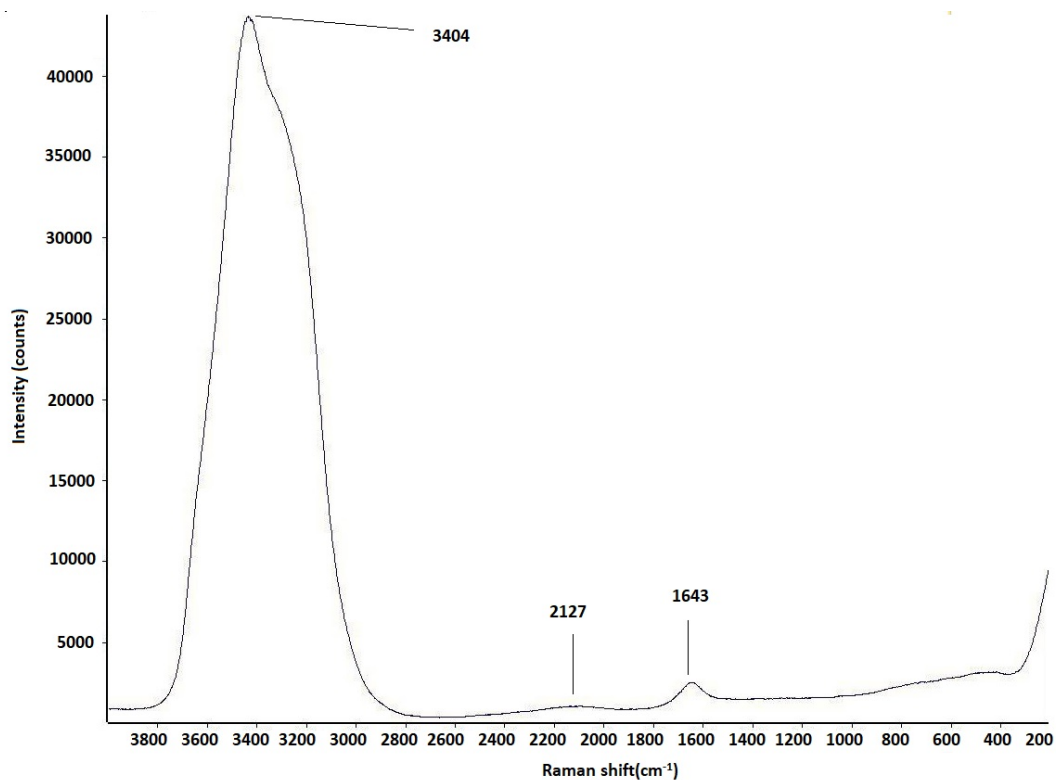Figure 16) reference spectra of optical glass of empty cuvette

Figure 17) reference spectra of water inside the cuvette

2.5 Data acquisition with Opus 7.5

Opus 7.5 (Bruker, Germany) was used for spectra processing. The following methods were used:

1) Baseline correction of Raman Spectra is necessary primarily to remove fluorescent background. In order to perform a baseline correction in Opus software, load the spectrum file and select "Baseline Correction" in the "Manipulation" section.

2) Smooth: Most of the spectra are superimposed by noise. Therefore, different algorithms are employed for smoothing the spectra to improve signal to noise (S/N) ratio. However, the number of points that are used for smoothing needs to be chosen very carefully since smoothing contains the risk of losing small spectral features. For smoothing spectra in OPUS, load the spectrum file and select "Smooth" in the "Manipulation" section.

3) Integration: Once a calibration curve has been established, integration of specific spectral features in the Raman spectrum can used for quantitative analysis. In OPUS, the integration can be found in the "Evaluation" section. For each Raman band, an integration method can be established by setting appropriate integration limits and selecting an integration method. Figure 18 shows the integration method used in this work. All the spectra collected with Horiba Jobin-Yvon LabRAM 800 HR were integrated between 2918-2984 cm^{-1}. Similarly, the spectra collected with the Kaiser Optical Systems RXN probe were interpreted between 790-840 cm^{-1}. Both bands are characteristic for PMMA and were used for quantitative comparison of different PMMA concentrations.
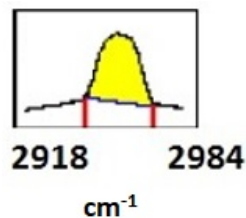

Figure 18) Integration method to calculate intensity the area of a selected band

2.6 One way ANOVA test for independent measurements

The one way Anova test is designed for several groups of samples, to compare the means of three or more different populations of groups. It is used to determine if there are any statistically significant differences between the means of three or more independent groups. Anova uses a null and the alternative hypothesis. The null hypothesis is a statement that claims that the mean for all three groups is the same (equation20). The alternative hypothesis states that there are at least two group means that are significantly different (equation21)[25].

Equation20) $H_0: \mu_1 = \mu_2 = \ldots = \mu_k$ where k is the number of groups in independent samples

Equation21) $H_a: \mu_i \neq \mu_k$ where i and k indicate unique groups

To determine whether a set of means is equal, I need to use the proper variances in the F ratio (equation22). In one way ANOVA test the F ratio is:

Equation22) $$F = \frac{\text{The variance between the groups}}{\text{The variance within the groups}} = \frac{MS_{between}}{MS_{within}}$$

The total sample size is N. and the total degree of freedom is df_{total}. Also, the "between groups"-degree of freedom is $df_{between}$ and the "within groups"-degree of freedom is df_{within} (equation23):

Equation23) $$df_{within} = df_{total} - df_{between}$$

The total sum of squares (SS) is computed as follows (equation24):

Equation24) $$SS_{total} = \sum_{ij} X_{ij}^2 - \frac{1}{N} \left(\sum_{ij} X_{ij}\right)^2$$

The within sum of square is computed as shown in the calculation below (equation25):

Equation25) $$SS_{within} = \sum SS_{within\ groups}$$

Now the mean sum of squares between (equation26) and within (equation27) is computed as follows:

Equation26) $$MS_{between} = \frac{SS_{between}}{df_{between}}$$

Equation27) $$MS_{within} = \frac{SS_{within}}{df_{within}}$$

ANOVA uses the F-test to determine whether the variability between group means is larger than the variability of the observations within the groups. For larger F ratios, means of the groups are different and the hypothesis H_0 has to be rejected.

2.7 Agar Gel Experiment

Agar "Agar Extra Pure Merck 226 K17703215" is an ultra-purified agar. Agar (2-5% w/w) was dissolved in distilled water. Ultra purified agar was used for immobilization of particles that

usually are only concentrated in the nodal planes of an US standing wave field while the acoustic radiation forces are applied [26,27]. The Agar concentration was limited to 2.5% because for higher concentration the viscosity of the solution increases and thus prevents a sufficient particle movement toward the pressure nodal planes. The agar dissolved in water was prepared in an Erlenmeyer flask and heated up on a magnetic stirrer with a heating plate. Once the suspension began to boil, the heating plate was turned off and different concentrations of PMMA particles were added.

2.5% Agar was prepared in 100ml distilled water. Then 5.58 g/l PMMA particles were added to the agar gel in the cuvette. After 2 minutes, the ultrasound was turned on and set to 2.04 MHz, 0.8 W, 0.23 A, 29 V which are the parameters for optimal PMMA particle trapping. After 1 min, line scans covering a distance of 1 mm in Y direction were collected with a step size of 50 μm. The starting point for the line scan was set such that the focus of the laser is on the inside of the glass of the cuvette, which in our case corresponds to a distance of 0.5 mm between probe head and cuvette wall. Due to the additional energy input by the frequency power synthesizer, the gel takes longer to cool down.

2.9 Cuvette

Most of the experiments were performed using a Hellma Macro-Cuvette 6030-OG with10 mm light path which is transparent in the range from 360 to 2500 nm. Its outer dimensions are (H×W×D) 45×12.5×12.5 mm and its inner dimensions are 45×0.95×12.5 mm. For ultrasound particle manipulation, two piezoelectric elements were attached on opposite sides of the cuvette and connected to an amplifier (figure19). The experimental setup used a cuvette stand and was performed with and without a stirrer. Most of the spectra from inside of the cuvette were collected with red laser excitation (633nm), the confocal hole set to 500 μm, the slit set to 100 μm and a 300 g/mm grating with 20× magnification. The recording time was 18x30 s at room temperature.
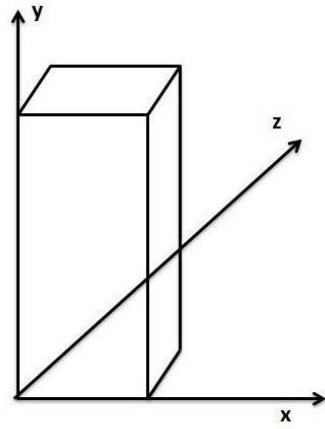
Figure 19) Cuvette 6030-OG- with two piezoelectric ceramics (PZT) glued to opposite sides of the cuvette

3. Results and discussion

3.1 Measurements with the Horiba Jobin-Yvon LabRAM 800 HR confocal Raman microscope

The confocal Raman microscope can be used collecting single spectra or Raman maps of a great variety of samples (e. g. cells, polymers, metals, bones and many more). Here, Raman spectra were collected on defined spots using 633 nm laser excitation with 20x magnification. Using the 20× objective a spatial resolution of roughly 1 µm is achievable.

3.2 Defining the focus point of the probe

The objective used in this experiment is calibrated for air as medium between lens and sample. To account for the changing optical properties due to different refractive indices of glass and water, the actual focus point was calculated by the following equations. Equation 28 shows Snell's law which describes how the angle of the beam path (entrance angle θ_1 and exit angle θ_2) changes when light passes from one medium with refractive index 1 to another medium with a different refractive index 2. In our case, the light passes through three different media on its way from the objective lens to the sample: air, glass and water (figure 20)

Equation 28) Snell's law: $\dfrac{n_1}{n_2} = \dfrac{sin\theta_2}{sin\theta_1}$
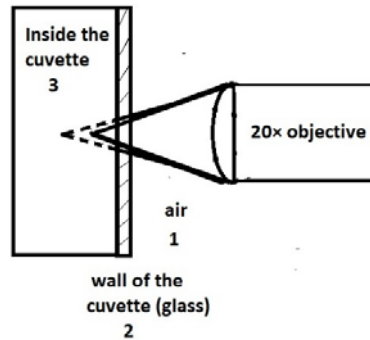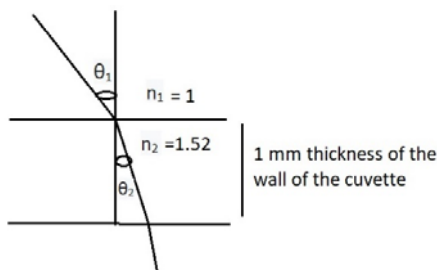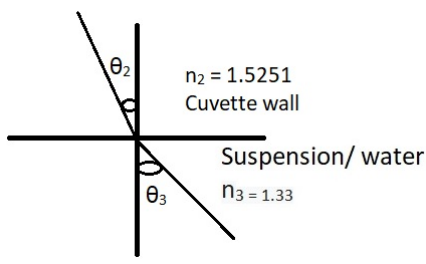
Figure 20) Schematic drawing of the changing focal length of an objective due to different refractive indices of the media between lens and investigated sample. Solid line indicates the focus point in air. Dotted line shows the actual focus point of the lens with light going through air, glass and water.

With n_1 as the refractive index of air being 1, n_2 = 1.5251 (refractive index of the wall of the cuvette; Schott Superwite B270) and θ_1 = 20.49° which is the angle of the incident laser beam in air medium calculated from the numerical aperture of the objective (Equation 29; see chapter 1.1.2), the angle of refraction at the wall of cuvette θ_2 can be determined using Snell's law. Similarly, the refraction angle θ_3 was determined for light passing from glass (cuvette wall) to water. The calculation steps are shown hereafter:

Equation 29) $n1 \sin(\theta_1)$ = N.A. -> arcsin (0.35) = 20.49° = θ_1

$$\frac{n_1}{n_2} = \frac{\sin\theta_2}{\sin\theta_1} = \text{arcsin} \left(\sin(22.49°)\frac{1}{1.5251}\right) = 13.27° = \theta_2$$

$$\frac{n_2}{n_3} = \frac{\sin \theta_3}{\sin \theta_2} = \arcsin \left(\frac{1.5251}{1.3317} \cdot \sin(13.27°)\right) = 15.24° = \theta_3$$

Based on this calculation, the difference between air and corrected focus point was determined graphically from the resulting sketch (6.6 mm for 20x objective). Similarly, the focus point of the Kaiser Optical Systems RXN probe with 2.4 mm focal length on air was determined to be 550 µm longer in combination with our set-up with $\theta_1 = 22.62°$, $\theta_2 = 14.61°$ and $\theta_3 = 16.79°$. Figure 21 shows the comparison of the beam path in air (dotted black lines) and the corrected beam path due to refraction of light at the interface between media with different refractive index resulting in a 550 µm longer focal length compared to air.
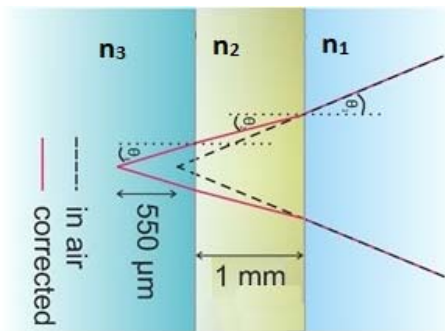

Figure 21) the focus point of the probe changes due to the media with different refractive index (n_1, n_2, n_3) being between the lens and the analyte that should be investigated. Based on Snell's law, the actual focus length of the objective in our set-up was determined to be 550 µm longer (red line) compared to air (dotted black line).

To experimentally determine the focus point in the cuvette, a line scan with defined step size (50µm) was performed along the x- axis with the probe head directly in front of the wall of the

cuvette defined as point zero. Line scans were repeated twice. The highest intensity was found at 800 μm investigated for a suspension with 9.3 g/l PMMA stirred at 700 rpm (Figure22).
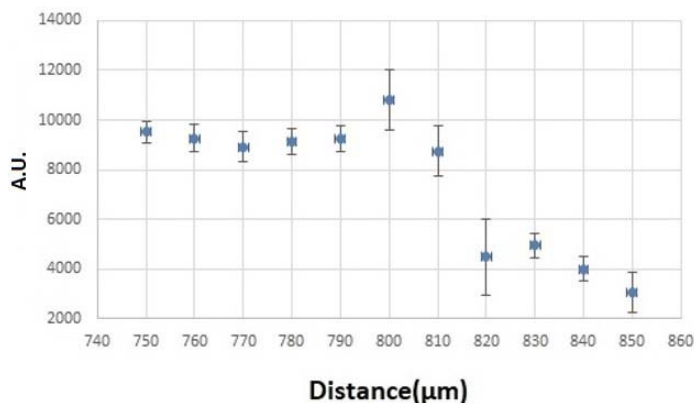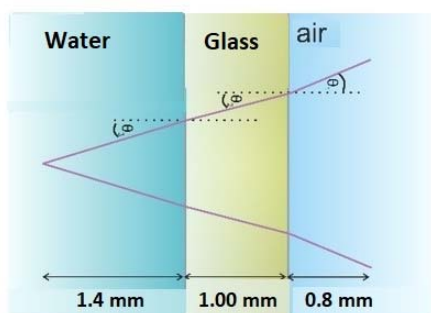

Figure 22) Sketch showing focus point 1.4 mm inside the cuvette with 800 μm distance between probe head and wall of the cuvette (left). Intensity distribution for different x-distances between head of the probe and cuvette (right).

3.3 Experiments with Kaiser Optical Systems RXN

Kaiser Optical Systems RXN analyzer was used to acquire the Raman spectra using 785 nm excitation. iC Raman software was used for collecting, analyzing and visualizing data from Kaiser Optical Systems RXN Raman spectrometer.

3.4 Effect of setup configurations of the probe with Kaiser Optical Systems RXN Analyzer on Raman signal

Experiments with pure powder of PMMA inside the cuvette with changing distance between head of probe and the surface of the cuvette were performed to investigate if the stirrer speed in the previous experiment (section 3.2) had any influence on the determination of the maximum

intensity in the cuvette. To reduce the amount of sample used in the experiment, the path length of the cuvette was reduced to approximately 2mm by placing a CaF_2 substrate as temporary second wall in the cuvette (figure 23).
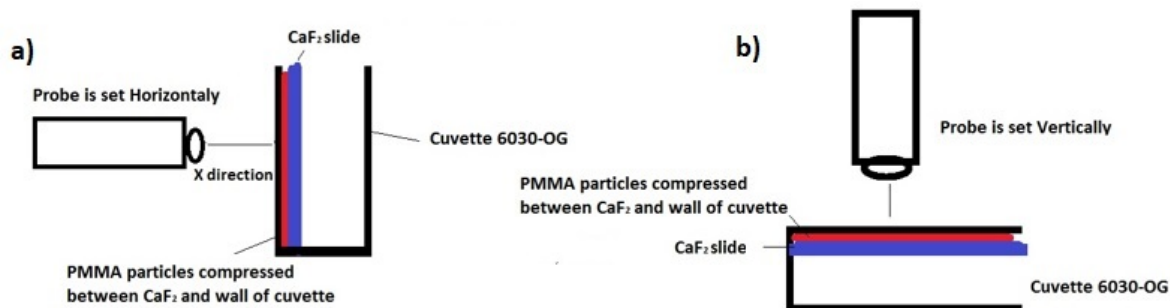
Figure 23) Different setup configuration of probe and cuvette (a: Horizontally, b: Vertically)

All the experiments have been done with a 1s exposure time and 3 scans to prevent saturation of the detector. In the first experiment, the probe is set vertically to the surface of the cuvette (see Figure 23 b). This experiment was repeated three times, in which out of all the experiments the highest intensity was around 0.65 mm (figure 24). Then, the probe was set horizontally (see Figure 23 a). For this arrangement, the highest PMMA intensity was around 0.60 mm of distance between the head of the probe and the wall of the cuvette (Figure 24). This experiment was also repeated three times (see table 6,7,8 in appendix).
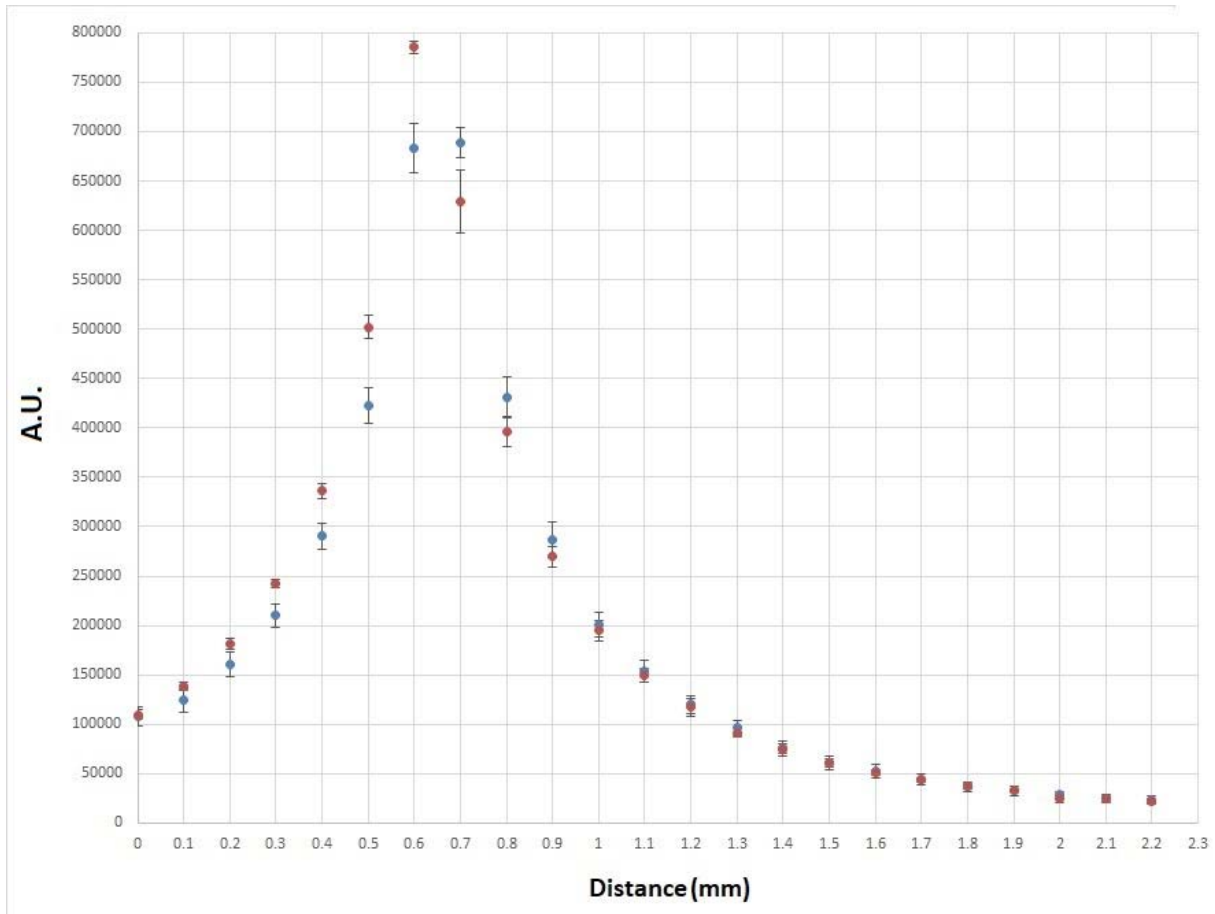
Figure 24) The highest PMMA intensity signal is between 0.6 and 0.7 mm distance between head of the probe and the wall of the cuvette for both arrangements (Vertical position: red series, Horizontal position: blue series)

Normalizing data is the process of scaling spectra in a defined region to make single spectra comparable to each other when they have different intensity ranges. Equation 30 was used to bring all values (see table 8 in appendix) into the range [0, 1]. Normalized data is shown in figure 25 for better comparison.

Equation 30)
$$X' = \frac{X - Xmin}{Xmax - Xmin}$$
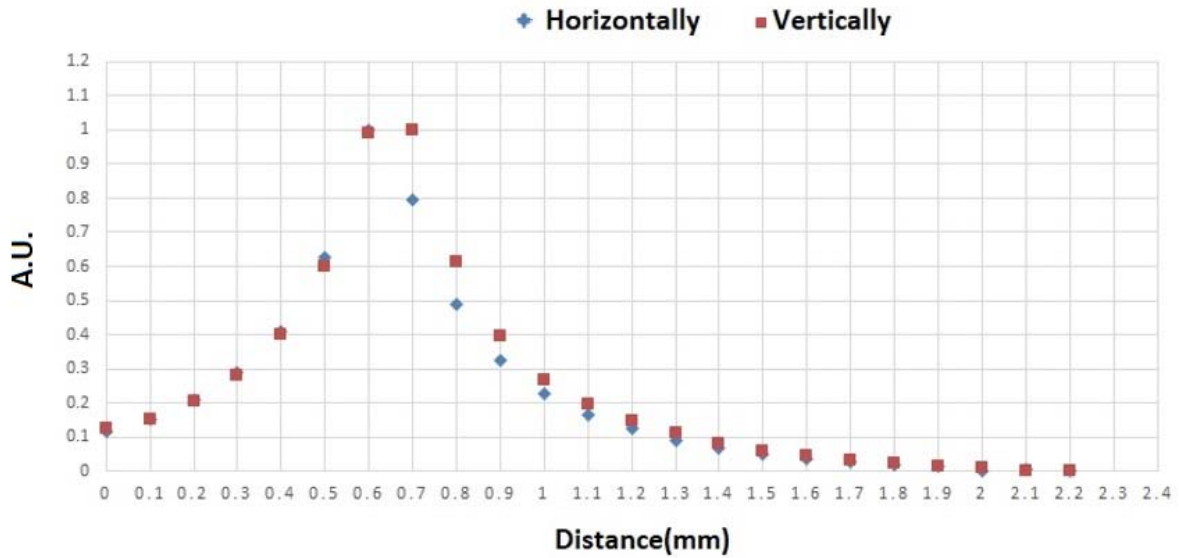
Figure 25) Normalized intensity distribution for both configuration showing the maximum intensity is around 0.6 mm

As can be seen in figure 24, the arrangement of the probe and cuvette has no influence as to where the highest intensity in the cuvette was detected. To statistically evaluate the data shown in the figures 23 and 24, one way ANOVA test was performed (see chapter 2.6). First, one way ANOVA test was caluclated with the three runs of experiments performed with horizontally set probe (see table 7 in appendix) and then was calculated with vertically set probe (see table 6 in appendix). The results of the calculation are shown in table 3 and table 4:

Table 3: One way ANOVA test for three runs (probe set horizontally)

	Run1	Run2	Run3
Sum(counts)	4637600	4431216	4484555
Average	201634	192661	194980
$\sum_i X^2_{ij}$	1.89E+12	1.78E+12	1.82E+12
St. Dev	208363	205412	207852
SS	9.55E+09	9.28E+11	9.5E+11
n	23	23	23

Finally, with having already calculated the mean sum of squares, the F-ratio is computed as follows (see chapter 2.6):

$$F = \frac{MS\ between}{MS\ within} = \frac{499001278}{42937401556} = 0.012$$

The following null H_0 and alternative H_a hypotheses need to be tested:

H_0: $\mu_1 = \mu_2 = \mu_3$

H_a: Not all means are equal

The above hypotheses will be tested using the F-ratio for a One-Way ANOVA. Since F=0.012, It is concluded that the null hypothesis Ho is not rejected.

Using the P-value approach: The p-value is p = 0.9884, and since p = 0.9884 ≥ α, it is concluded that the null hypothesis is not rejected.

Therefore, there is not enough evidence to claim that not all 3 population means are equal, at α=0.5 significance level.

Table 4: One way ANOVA test for three runs (probe set vertically)

	Run1	Run2	Run3
Sum(counts)	4274861	4611428	4182112
Average	185863	200496	181830
$\sum_i X^2_{ij}$	1.7E+12	1.8E+12	1.6E+12
St. Dev	199161	200611	190163
SS	8.7E+11	8.9E+11	8E+11
n	23	23	23

Finally, with having already calculated the mean sum of squares, the F-ratio is computed as follows (see chapter 2.6):

$$F = \frac{MS\ between}{MS\ within} = \frac{2218782248}{38690755594} = 0.057$$

The following null H_0 and alternative H_a hypotheses need to be tested:

H_0: $\mu_1 = \mu_2 = \mu_3$

H_a: Not all means are equal

The above hypotheses will be tested using an F-ratio for a One-Way ANOVA.

The above hypotheses will be tested using the F-ratio for a One-Way ANOVA. Since F=0.057, It is concluded that the null hypothesis Ho is not rejected.

Using the P-value approach: The p-value is p = 0.9443, and since p = 0.9443≥α, it is concluded that the null hypothesis is not rejected.

Therefore, there is not enough evidence to claim that not all 3 population means are equal, at α=0.5 significance level.

Since the means are comparable, i can use all three measurement runs and can calculate the mean and standard deviation. As seen in figure 24 both configuration shows the same maximum at 0.6 mm distance which is an agreement with our calculation.

3.5 Intensity of the spectra of the PMMA particles suspended in the cuvette measured with Horiba Jobin-Yvon LabRAM 800 HR

PMMA particles are suspended in distilled water with different concentrations (see appendix), starting with 9.3 g/l. For the first experiment, it was hard getting PMMA spectra from inside of the cuvette. Only spectra from the sediment could be obtained. The main purpose of this investigation was to demonstrate that Raman spectroscopy could be used for getting spectra from PMMA particles within the cuvette. Also, appropriate parameter settings that can be used for all different PMMA concentrations needed to be determined.

The Raman intensity signal depends on the excitation wavelength, the scattering cross section of the analyte and also on its concentration. The shorter the wavelength of laser, the higher the intensity of the Raman signal, but a shorter wavelength will also increase fluorescence background. Because of that, all the experiments were done with a red Raman excitation laser (633nm). One option for obtaining better Raman spectra is to increase the concentration of PMMA or to increase the measurement time to 18×30 seconds. That was the longest exposure time possible to prevent saturation of the detector for all concentrations investigated. Then, a clear spectrum from inside the cuvette could be recorded. A comparison between the Raman spectra recorded inside the cuvette and the sediment shown in figure 26.
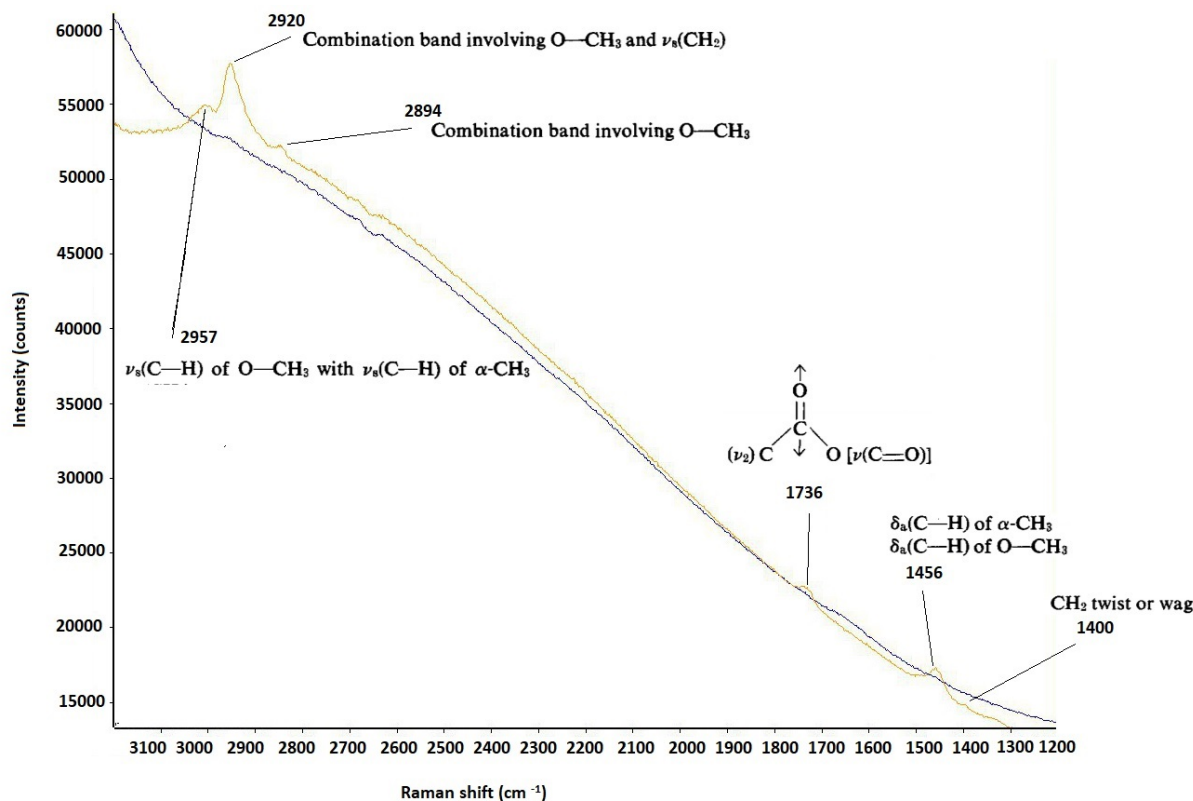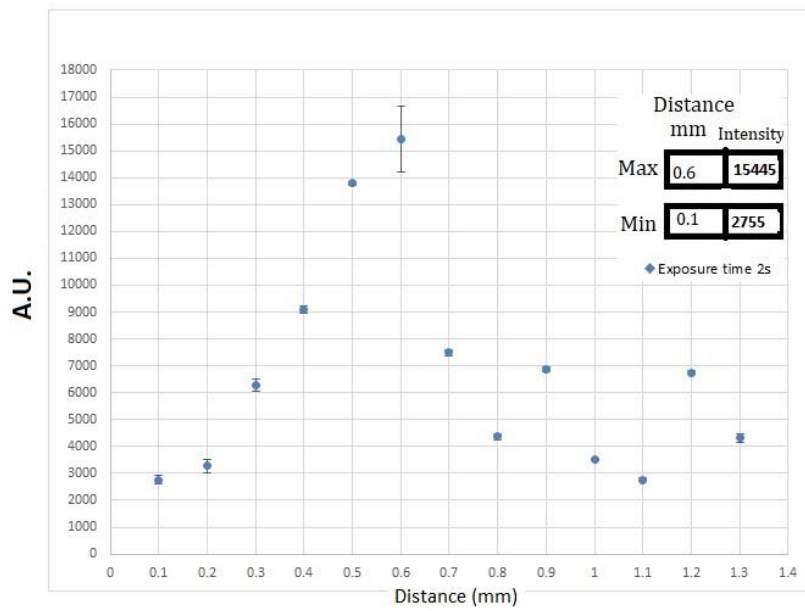
Figure 26) Comparison between the Raman spectra recorded inside the cuvette (Stirred PMMA suspension, blue) and the sediment (red).

3.6 Changing integration time versus distance with Kaiser Optical Systems RXN

In this experiment, the stirrer speed was set to 1500 rpm and the number of accumulation per spectrum was set to 3. The distance between the head of the probe and the glass of the cuvette was varied with 0.1 mm step size. To find optimal exposure time, each distance run was performed using different exposure time (1s, 2s, 3s, 5s, 10s) to get maximum Raman signal of reasonable time and without risking saturation of the detector (figure27). For the band which is not sorted in the spectrum, the integrated area might be negative. In this case the area was set to zero because it means that there is no analyte that can be detected. Normalized data is shown in figure 28 for better comparison.

Chart 1 (top):

Y-axis: A.U. (0 to 9500)
X-axis: Distance (mm) (0 to 1.4)

	Distance mm	Intensity
Max	0.6	8654
Min	1.3	626

◆ Exposure time 1s

Chart 2 (bottom):

Y-axis: A.U. (0 to 18000)
X-axis: Distance (mm) (0 to 1.4)

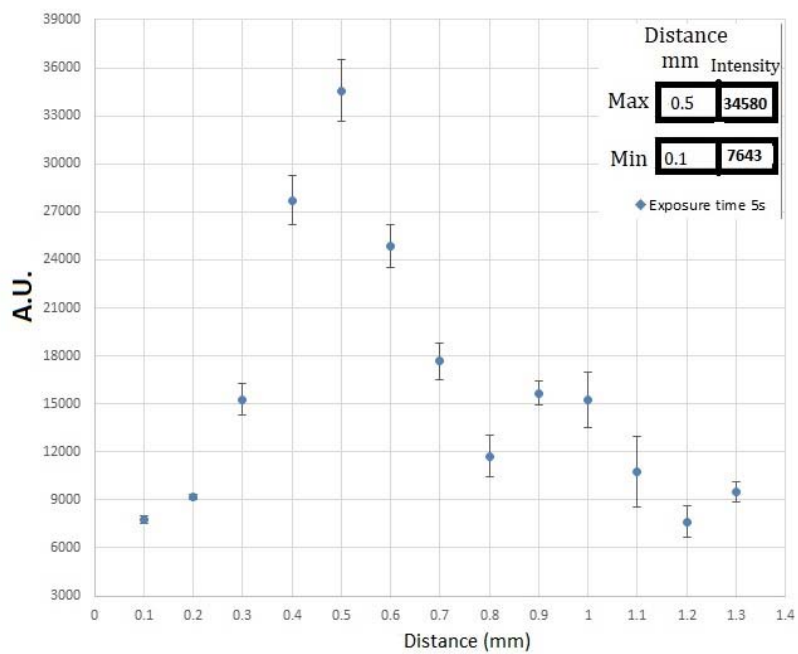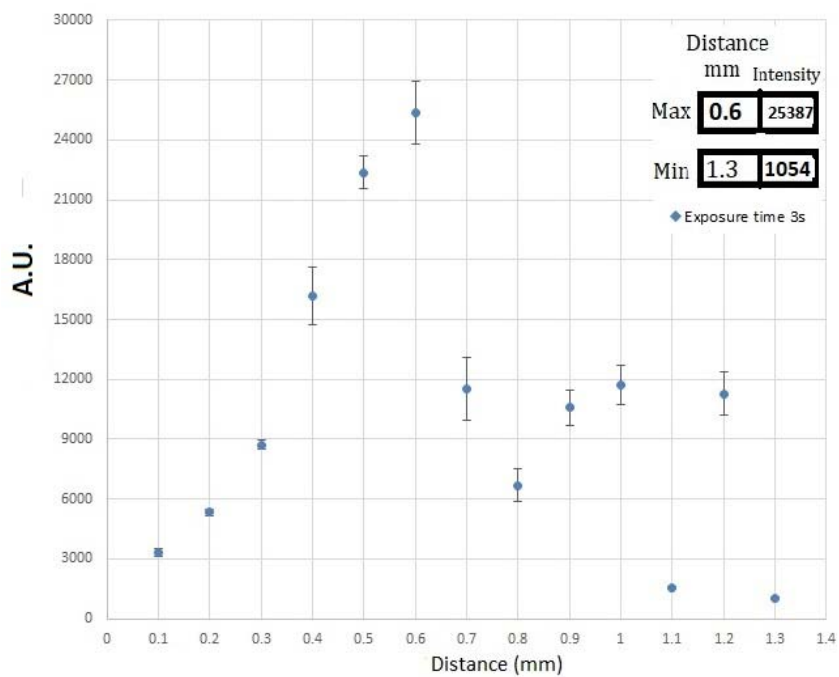|	Distance mm	Intensity
Max	0.6	15445
Min	0.1	2755
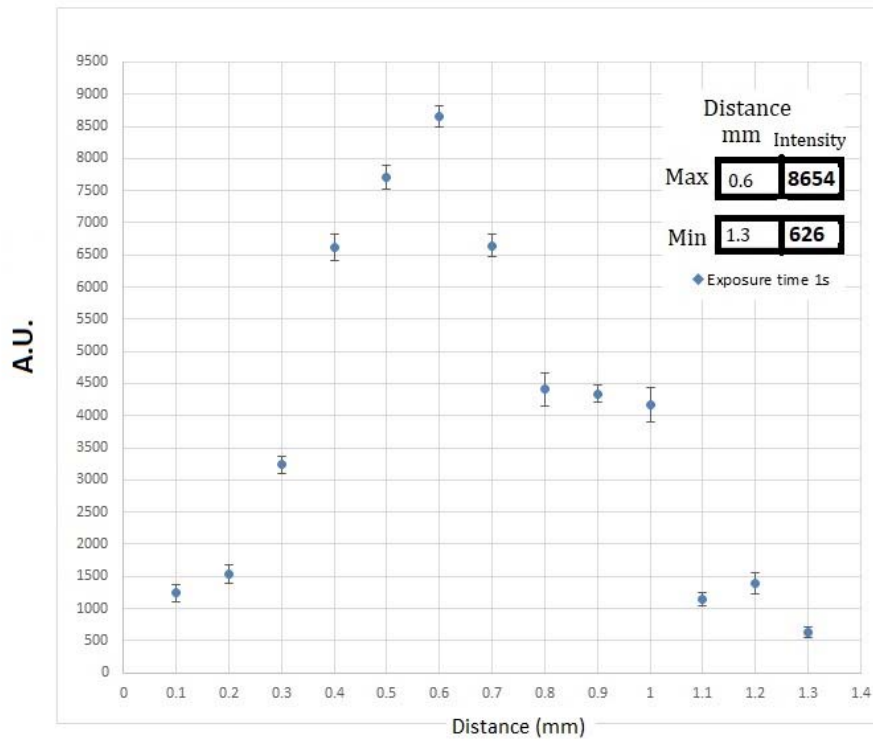
◆ Exposure time 2s

Figure 27) Different exposure times with changing distance between head of the probe and wall of the cuvette
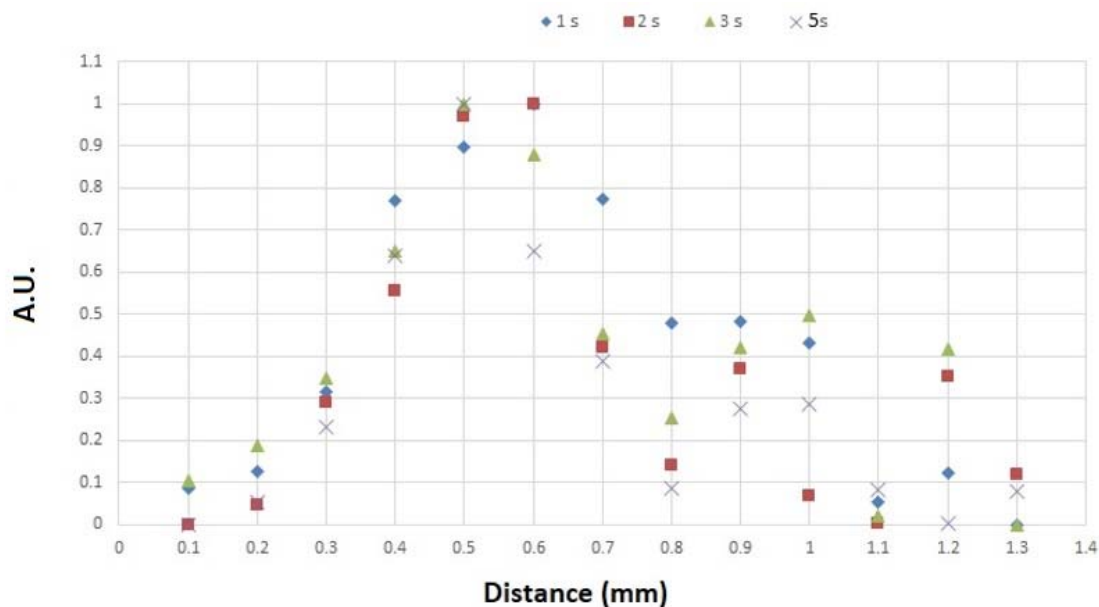
Figure 28) Normalized intensity distribution for different exposure time with changing distance between head of probe and wall of the cuvette

With 10s of exposure time, the detector was saturated (result shown in table 9 in appendix). A CCD camera consists of pixels. The backscattered photons are collected at the detector (=pixels of the CCD) where the photon signal is transformed to an electron charge. The exposure time is the time that photons are collected on the CCD pixels before the read-out. However, there is only a certain number of photons one single pixel of the CCD camera can collect before it is saturated. Depending on the fluorescence that might have in our system and depending on how good of a Raman scatterer our sample is, the detector is sooner or later saturated. So, to have a Raman spectrum of good quality (low noise and high signal intensity), the exposure time (Signal intensity) and number of accumulations (noise improvement) have to be set appropriately. Since I want to have comparable spectra for quantification purposes, i need to keep parameter settings constant. This means that I have to make sure that it stays in the dynamic range of the camera during the whole experiment when different PMMA concentrations are used. As can be seen in figure 27, the highest intensity could be achieved with highest exposure time which is accordance to the theory of Raman spectroscopy: the higher the energy put into the

system, the better the Raman signal (more intense Raman signal) will be detected. However, considering the standard deviation of all the measurements, it seems that spectra do not get more stable with increasing integration time (see Figure 27). What i would expect is that with increasing integration time all the disturbances that i have in our system e.g. due to stirrer speed would be averaged out. So during the experiments to get maximum Raman signal within reasonable time and without risking saturation of the detector i used 5s as exposure time.

3.7 Experiments with changing stirrer speed

The speed of the stirrer was adjusted to different speeds to find the effect of stirrer speed on the intensity of the Raman spectrum. In the series of experiments, the speed of the stirrer was changed from 50 rpm to 100, 200, and 300 …1500 rpm. Measurements were started 1 min after each stirrer speed was set. The same procedure was repeated for the same concentration of PMMA 9.3g/l with two different 'x' distances, in which 'x' is the distance between the head of the probe and the wall of the cuvette. Each measurement was repeated 3 times at the exact same measurement position for each stirrer speed at x+800 μm and x+1000 μm (see table1, 2 and 3 in appendix) to exclude that i might be measuring particles "attached" to the wall of the cuvette instead of particles in motion. The first set of experiments was performed using the Horiba Jobin-Yvon LabRAM 800 HR spectrometer. Figure 29 shows the different stirrer speeds for x+800 μm and x+1000 μm. One way ANOVA test was calculated based on the values listed up in table 5 and table 6 containing data of 3 repetitions of x+800 μm and x+1000 μm.
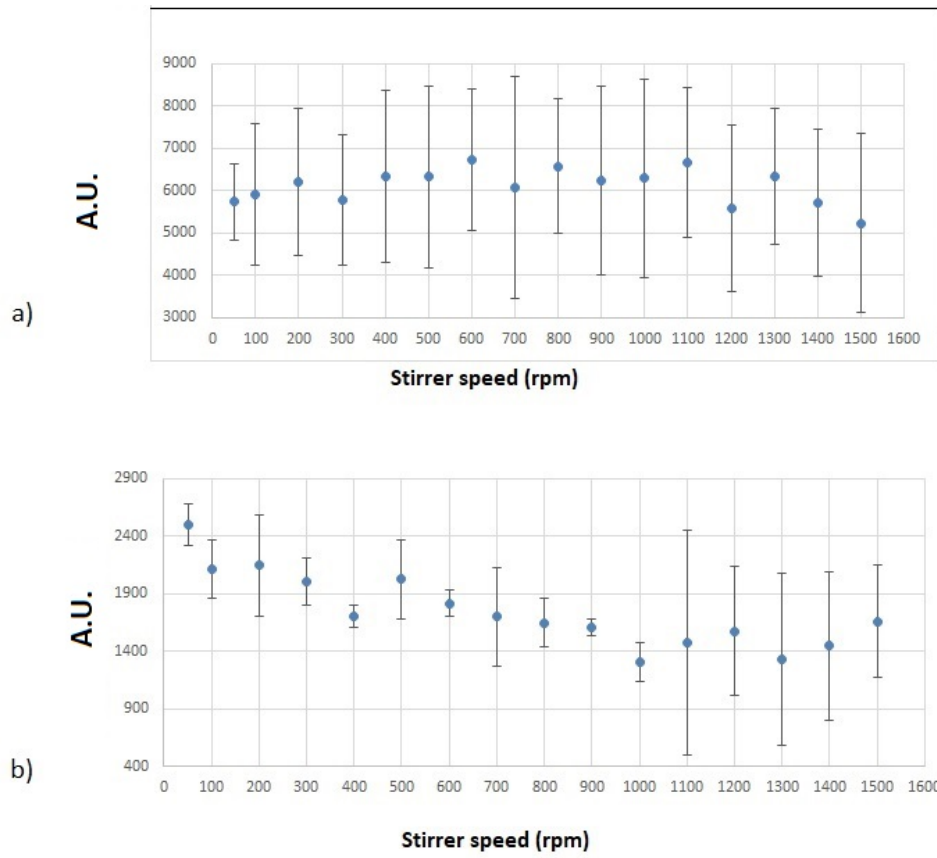
Figure 29) Mean and standard deviation of PMMA Raman signal at different stirrer speeds for a) x+800 μm and b) x+1000 μm

Table 5: One way ANOVA test for three runs of stirred PMMA particles at different stirrer speeds for x+800µm

	Run1	Run2	Run3
Sum(counts)	113339	65723	114106
Average	7083	4107	7131
$\sum_i X^2_{ij}$	8E+08	3E+08	8E+08
St. Dev	857	576	837
SS	1E+07	5E+06	1E+07
n	16	16	16

Finally, with having already calculated the mean sum of the squares, the F-ratio is computed as follows:

$$F = \frac{MS\ between}{MS\ within} = \frac{48009200}{589670} = 81$$

The following null H_0 and alternative H_a hypotheses need to be tested:

H_0: $\mu_1 = \mu_2 = \mu_3$

H_a: Not all means are equal

The above hypotheses will be tested using an F-ratio for a One-Way ANOVA.

Since it is observed that F=81, means that the variation among group is more than i expect to see by chance it is then concluded that the null hypothesis is rejected. Therefore, there is enough evidence to claim that not all 3 population means are equal, at α=0.5 significance level.

A higher F ratio is due to the more difficult detection of any consistent patterns. Or, if I do find consistent patterns, I will be less confident in these patterns, because with more random variation, the patterns could actually be due to chance.

Table 6: One way ANOVA test for three runs of stirred PMMA suspension at different stirrer speeds for x+1000μm

	Run1	Run2	Run3
Sum (counts)	140346	135249	157477
Average	8771	8453	9842
$\sum i\ X^2 ij$	1.3E+09	1.2E+09	1.6E+09
St. Dev	1434	1626	1417
SS	3.1E+07	4E+07	3E+07
n	16	16	16

The calculation was repeated for the three runs recorded at x+1000 μm with the F-statistic computed as follows:

$$F = \frac{MS\ between}{MS\ within} = \frac{8474318}{2237276} = 3.7$$

Since it is observed that F=3.7 and thus > 0 it is then concluded that the null hypothesis H_0 is rejected.

Using the P-value approach: The p-value is p = 0.0302, and since p = 0.0302≥α, it is concluded that the null hypothesis is not rejected.

Therefore, there is enough evidence to claim that not all 3 population means are equal, at α=0.5 significance level.

 As a next step, t-test for the comparison of two means between run 1 and run 2, run 1 and run 3 and run2 and run 3 at x+800 μm and similarly at x+1000 μm experiment was calculated to compare their variance together. But the results were the same as ANOVA test, which indicated not all the two population of the means are equal (the results shown in the table 23 and 24 in appendix).

To compare the result of measurements in x+800 µm and x+1000 µm, is concluded that the effect of stirrer speed in x+1000 µm is very higher than x+800 µm, so in x+800 µm might be have some protective effect when i am at the edge of the cuvette wall. Because the measurement in x+800 µm is more stable in different range compare to x+1000 µm. i also have very big standard deviation in higher stirrer speed, which means that using the same integration time with the same exposure time, the signal gets less stable with increasing stirrer speed (figure 28).

As a next step, the effect of the stirrer speed on the intensity of the Raman signal was studied with the Kaiser Optical Systems RXN Analyzer at 0.5 mm distance between head of the probe and wall of the cuvette because the highest Raman signal was detected in this distance (see chapter 3.6). Experiments were performed using 3×5 s of integration time at defined measurement spot in the cuvette, changing the stirrer speed from 50 rpm to 1500 rpm using 100 rpm steps. The experiment was repeated three times with the same parameters. Mean and standard deviation of the obtained data for all three repetitions (listed up in table 11 in appendix) are depicted in figure 30.
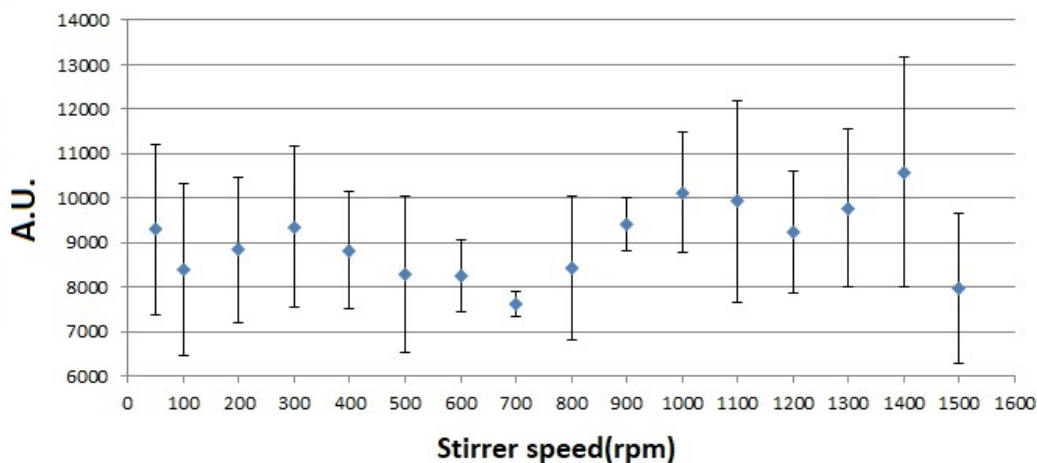

Figure 30) Effect of stirrer speed on Raman signal of 9.3 g/l PMMA particles in suspension

From the quantum mechanics i know that light and matter are dual in behavior, it means that they display wave nature properties, same as diffraction[27]. Theoretically with changing stirrer speed, different intensity of Raman signal is not expected. The speed of light is faster than speed of particles so it should not have any effect on the Raman signal. Also, using an exposure time of 3x5s for each spectrum, any disturbances in the stirred suspension should be averaged out. Thus, i should see relatively stable Raman signal for all stirrer speeds which doesn't change too much.

The experiments indicate that the stirrer speed has a minor to no effect on the Raman signal (see Figure 27). However, most of the obtained intensity values show a great standard deviation. The signal stability would be improved by using higher integration time to reduce the impact of the effects causing these intensity variations. However, increased integration time would risk saturation of the detector. In Raman spectroscopy, the back scattered photons are collected and detected by the CCD camera. Particles in motion may increase the light scattering by diffracting the light into different directions even more than stationary particles while the collection angle of the objective remains constant. Particles in motion might lead to changing "scattering patterns". Agglomerated particles might have a directed scattering direction which might or might not coincide with the viewing corn of the objective thus causing great variance in signal stability. One way ANOVA test was also performed to compare the means of individual runs of experiments (results shown in table 11 in appendix). The results indicate that means are not comparable.

3.8 Settled phase of PMMA

To check the maximum intensity of PMMA particles in water that can be achieved with the available Raman setups, Raman spectra of highly concentrated PMMA (sediment) were recorded with Kaiser Optical Systems RXN Analyzer. The sediment (the settled phase) of PMMA was obtained by letting the particles in suspension settle at the bottom of the cuvette for 24 hours. Figure 31 shows *th*e spectra collected from the settled phase of PMMA, when the laser spot is focused on the sediment and when it is a few micrometers above the sediment. All Raman

measurements were performed at room temperature. As can be seen in figure 31, the spectrum collected from the sediment exhibits characteristic PMMA bands at 970 cm^{-1}, 813 cm^{-1}, 604 cm^{-1} overlaid by glass (broad band around 1400 cm^{-1}). While the spectrum recorded above the sediment shows the characteristic Raman band of glass only (see table 12 in appendix).
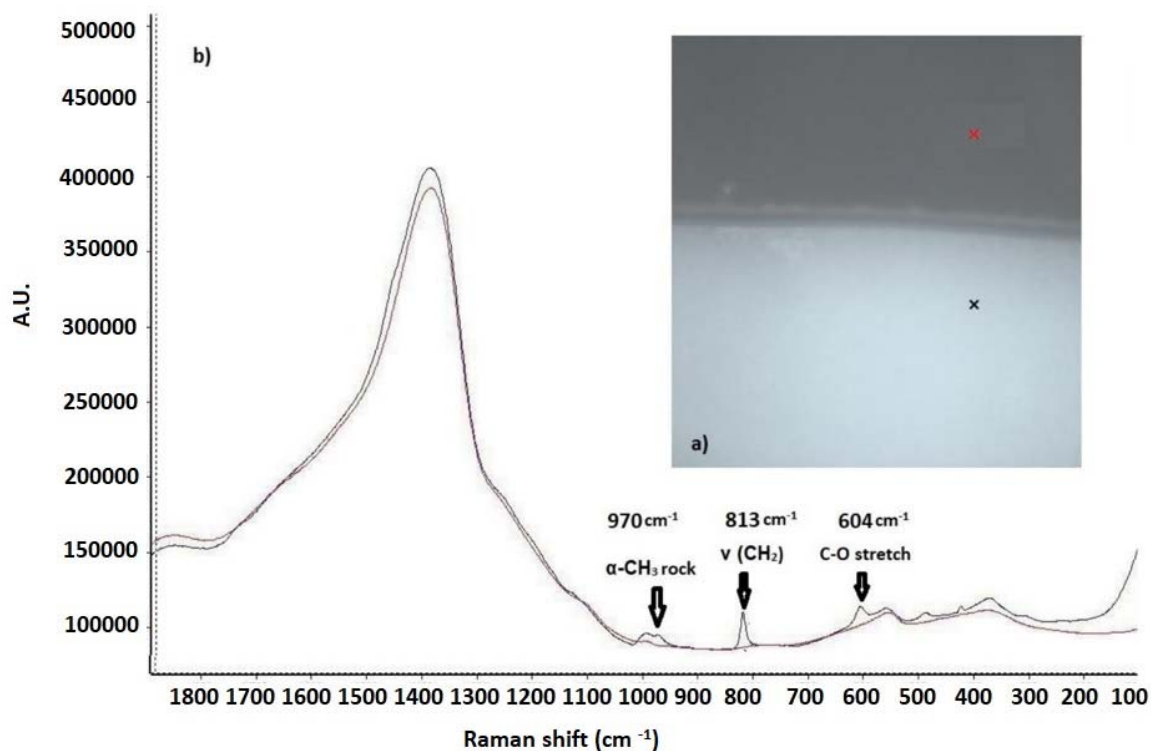

Figure 31) a: Microscope image (20 × magnification) showing phase separation after 24 hours between PMMA particles (lower part) and water (upper part), b: Raman spectra collected with the focus on the sediment (black) and a few micrometers above the sediment (red)

Again, exposure time (1s, 2s, 3s, 5s, and 10s) and distance between head of the probe and the glass wall of the cuvette were changed to define optimal parameter settings for measurement of PMMA sediment (Figure32). The position when the probe touches the wall of the cuvette was set as the zero reference of the x position. By increasing the distance between the probe and cuvette, it can be seen that the Raman signal of PMMA increases as well. While for the first

measurement position X was 0.1 mm, the focus of the probe was deep inside the sediment. Because of all the scattering effects going on in the sediment, there is less signal coming back to the detector. However, with increasing the distance i could determine the maximum PMMA intensity at 0.6 mm. Since i can assume that the concentration distribution is homogenous in the sediment, the increasing Raman intensity is not due to the higher PMMA concentration, But due to the less scattering effect/loss of energy in the system. By further increasing the x distance, the Raman signal of PMMA decreases again, because now there are less PMMA particles and more glass of the cuvette in the focus point of the laser (see table 9,10 in appendix).

1 s	
Distance (mm)	Intensity (counts)
0.1	16725	min
0.6	143429	max

2 s	
Distance (mm)	Intensity (counts)
0.1	30647	min
0.6	290381	max

3 s	
Distance (mm)	Intensity (counts)
0.1	43780	min
0.6	439317	max

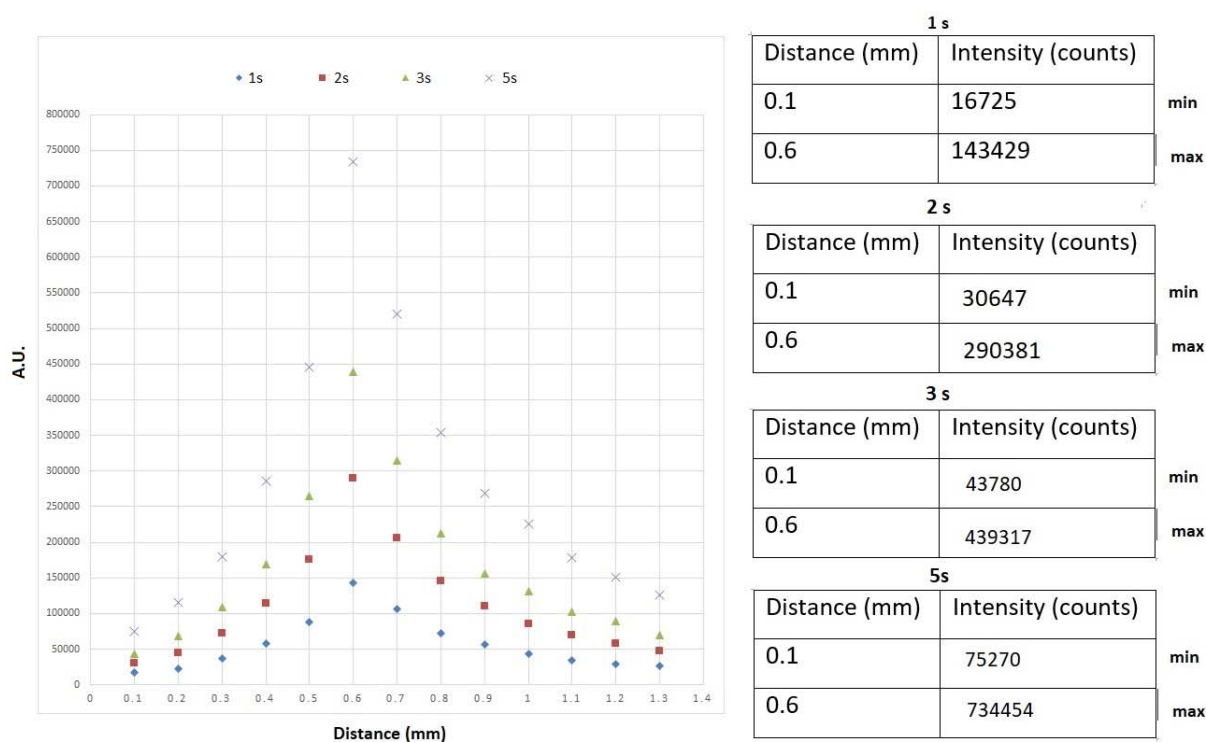| 5s	
Distance (mm)	Intensity (counts)
0.1	75270	min
0.6	734454	max

Figure 32) Four experiments of measuring the sediment of PMMA inside the cuvette with changing exposure time and changing distance between head of the probe and wall of the cuvette. For each single spectrum 3 scans were accumulated.

While Raman spectra with good quality were obtained with 1, 2, 3 and 5 s of integration times, saturation of the detector was reach with 10 s of integration time (see the results in table 13 in appendix). Since the integration of Raman signal is proportional to the integration time, we

wanted to use the highest integration possible to have the best quality of Raman spectrum for our measurements. This is why I used 5 s of integration for future measurements.

3.9 Separation of PMMA particles using ultrasound particle manipulation

Up to now, the Raman signal obtained from PMMA particles in suspension was very weak. In order to increase the Raman signal, i want to employ ultrasound particles manipulation to accumulate PMMA particles in the focus point of the Raman laser. Since the Raman signal is proportional to the analyte concentration, i expect a significant increase in signal intensity by setting the laser focus on particle agglomerations in the nodal planes of the ultrasound standing wave field. An ultrasound standing wave field is generated from the superposition of the reflected and incident acoustic wave. Due to the ultrasound standing wave field, suspended particles are collected in the nodal planes.

Micro-sized particles are collected in the nodal planes of the standing ultrasound field mainly due to the primary axial radiation force acting on them [20]. Particle separation with respect to resonator efficiency depends on the frequency and the properties of the particles (see chapter 1.2). Typical frequencies used for manipulation of PMMA as a micrometer sized particle are around 2 MHz. The speed of sound in water C_0 is approximately $1500ms^{-1}$. Therefore, the wavelength of the acoustic wave is 750µm. When a standing wave field is built up, the pressure nodal planes are approximately 375µm apart.

The purpose of this experiment is to investigate changes in Raman signal along and between layers of concentrated PMMA particles in the nodal planes of standing waves.

The effect of the standing wave field on suspended particles is shown in figure 33 resulting in approx. 115 µm thick layers of agglomerated PMMA particles. Figure 34 clearly highlights the effect of ultrasound particle manipulation on the Raman signal (9.3 g/l). A well-defined PMMA signal can be detected in the nodal planes whereas there is no PMMA signal measurable between

the nodal planes. This means that all the particles are agglomerated in the nodal planes or at least all the particles that are above the LOD (limit of detection)[3] are collected in the nodal planes.
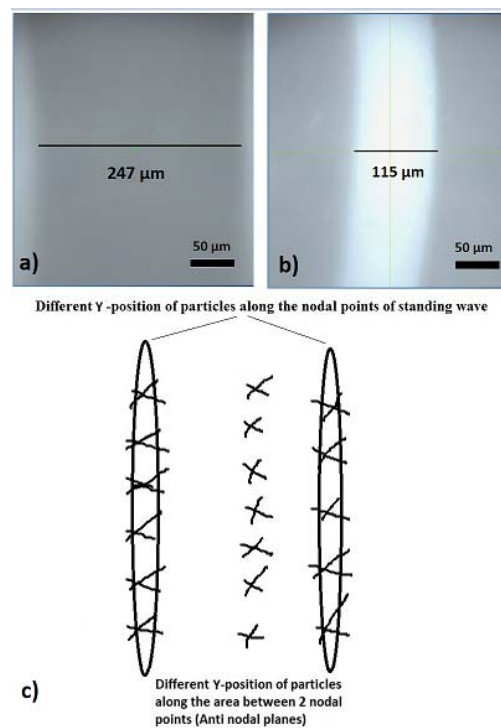

Figure 33) a: effect of standing wave on suspended particle, b: the diameter of concentrated lines, c: nodal and anti-nodal planes

---

[3] Limit of detection: if we decrease concentration of PMMA particles further and further in one point although we know still there are particles inside the medium but we cannot measure them any more
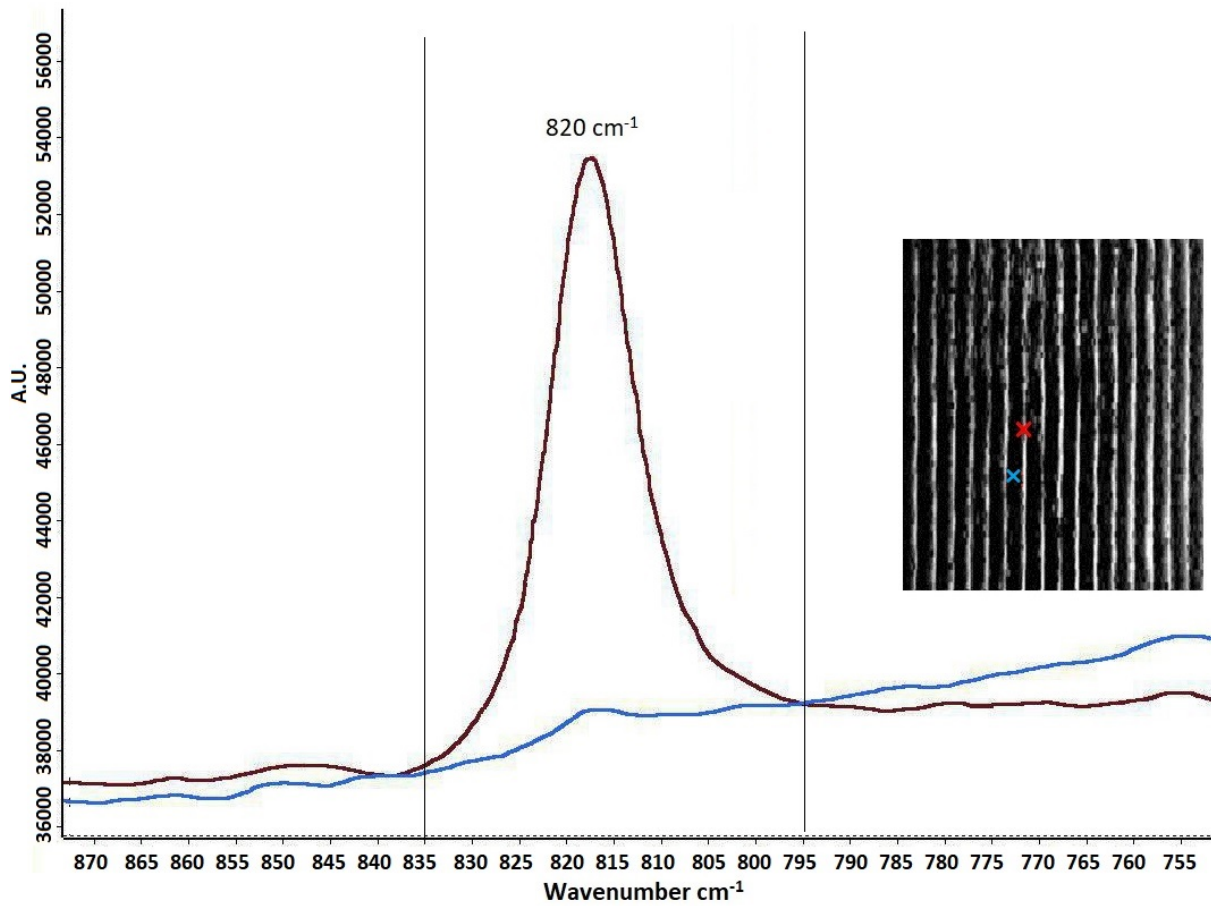
Figure 34) Characteristic PMMA band at 820 cm^{-1} shown representatively for measurements on the nodal plane (red) and between the planes (blue) corresponding measurement positions are shown exemplarily by color coded crosses(right image)

As a next step, a Raman spectrum of the stirred suspension with the sound being turned off was recorded. A comparison of spectra recorded on and between the lines with ultrasound being turned on including a spectrum of the PMMA suspension (5.58 g/l) when sound is off is shown in figure 35.
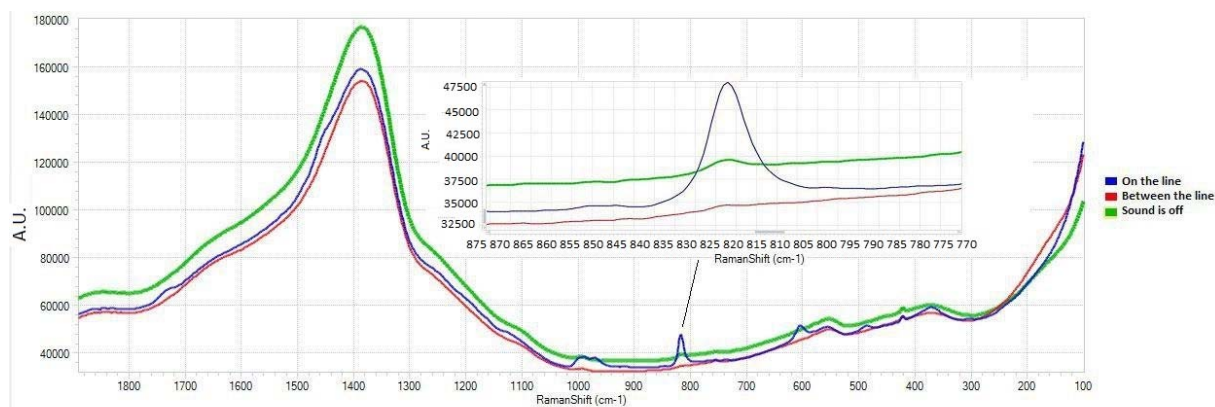
Figure 35) a: Comparing three spectra of PMMA when sound is on with focus set on the line (agglomerated PMMA particles; blue spectrum) and between the lines (red spectrum) and when sound is off (green spectrum). b: The integrated PMMA band used for studying intensity distribution.

Seven different concentrations of PMMA were examined to investigate the enhancement effect of ultrasound particle manipulation on the Raman signal. Line scans along the y-axis with 50 µm step size and a total length of 1 mm were performed while ultrasound was on (Figure 36). A sketch of agglomerated particles in the nodal planes by using the acoustic radiation forces exerted by an ultrasound standing wave of approximately 2MHz and the results of the experiment indicated in figure 37a. Also, to see the signal enhancement induced by ultrasound particle manipulation, Raman spectra between and on the nodal planes were recorded and compared to each other. Experiments were performed at 400 rpm stirrer speed starting at 0.5 mm distances between head of the probe and cuvette (figure 37b).
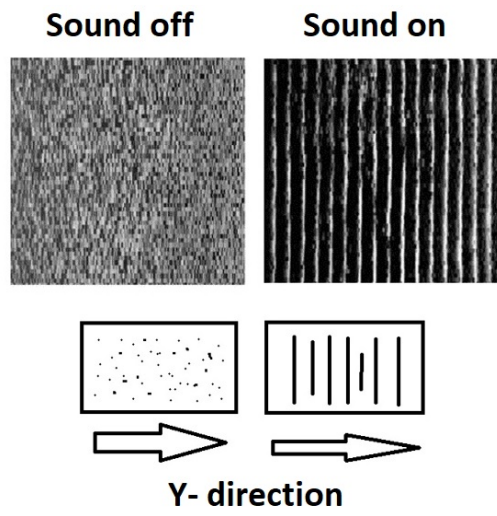
Figure 36) Scanning in Y direction when sound is off (left side) and on (image on the right side)(see tables 4,5 in appendix)
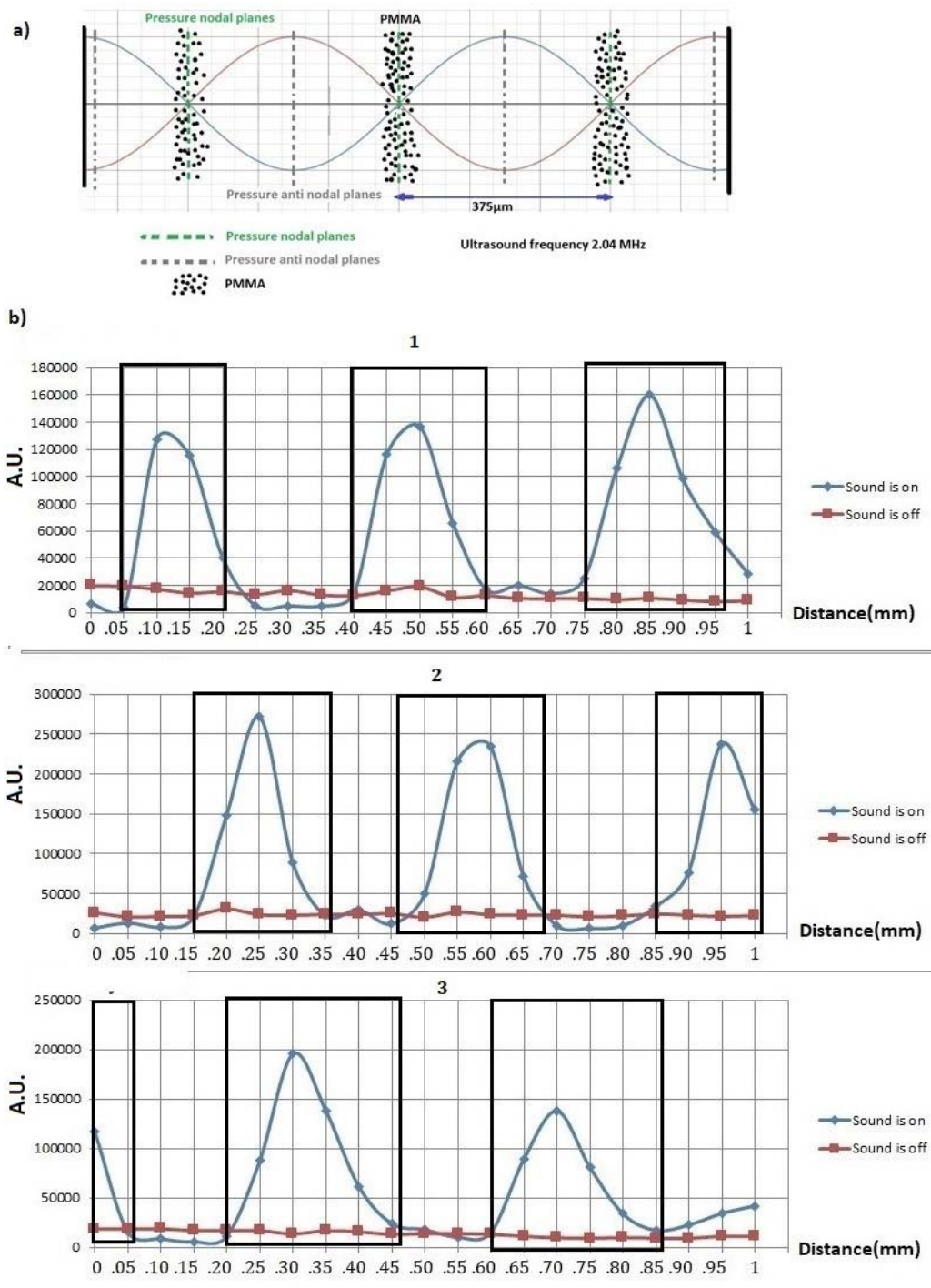
Figure 37) a: Sketch of ultrasound particle manipulation with particles being agglomerated b) Intensity distribution of integrated PMMA band along the line scan (on and between PMMA accumulations) with ultrasound being turned on. Areas of the accumulated particles are shown in rectangular region. Line scans were repeated twice.

Line scans in the direction of the sound propagation indicate the presence of particles in the nodal planes very well. However, consecutive line scans on identical measurement positions also indicate that the ultrasound wave field is not very stable over time since significant changes of the positions of the agglomerated particles in the micrometers scale are observed. One possible explanation would be the secondary axial radiation force which also act on the particles and might be responsible for continuous particle rearrangement within a nodal plane. Thus, making it less stable over time.

The intensity distribution of 3 consecutive line scans shows great variation in terms of Raman intensity and the position of accumulated PMMA particles. The frequency of the ultrasound field was regulated manually which directly impacts the stability of the Raman measurements. Another impact of the ultrasound is the additional amount of energy that is brought into the system causing the suspension to locally heat up. An increase in temperature influences the motion of the particles in a stirred suspension as well as the speed of sound in the medium and consequently the resulting Raman signal along a defined line scan.

While the collection of the PMMA particles in the nodal planes could be observed very well a lower packing density in the upper region of the resonator was visible. For low concentrations of PMMA during the measurement, the low number of particles in the nodal planes were not stable but trembling more than higher particle concentration.

Figure 38 shows the average of the integrated PMMA band at seven different concentrations (1.11 g/l, 1.48 g/l, 1.86 g/l, 3.72 g/l, 5.58 g/l, 7.44 g/l, 9.3 g/l) for stirred suspensions without ultrasound particle manipulation (see tables 14,15,16,17,18,19 and 20 in appendix). As can be seen, single values (especially for higher concentration) show unusually high standard deviation. This could result from insufficient stirring of the suspension in the cuvette leading to the superposition of stirred and settling particles. However, to have comparable results, the stirrer speed was kept constant for all the measurements. Figure 39 shows the average of the integrated PMMA band when the sound was on and the focus of the probe was set on the lines of the agglomerated PMMA particles. As can be seen in comparison to figure 38, the signal is a lot more

intense with ultrasound particle manipulation. However, the linear dependency of the Raman signal and the particle concentration in the beaker is lost.
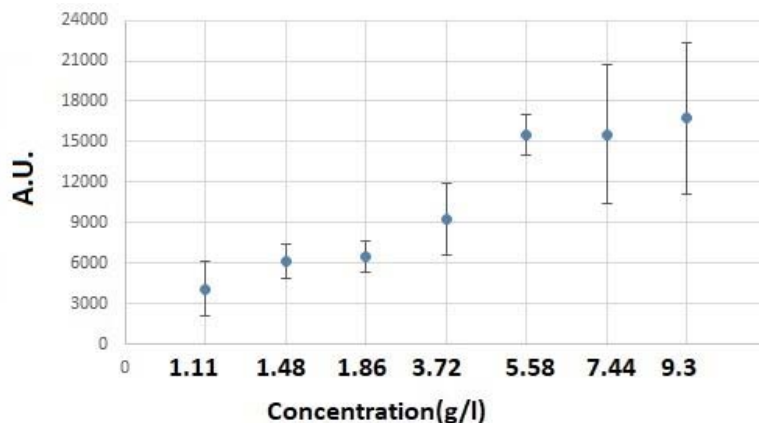

Figure 38) Mean and standard deviation of 3 measurements per PMMA concentration in stirred suspension (700 rpm) without ultrasound particle manipulation
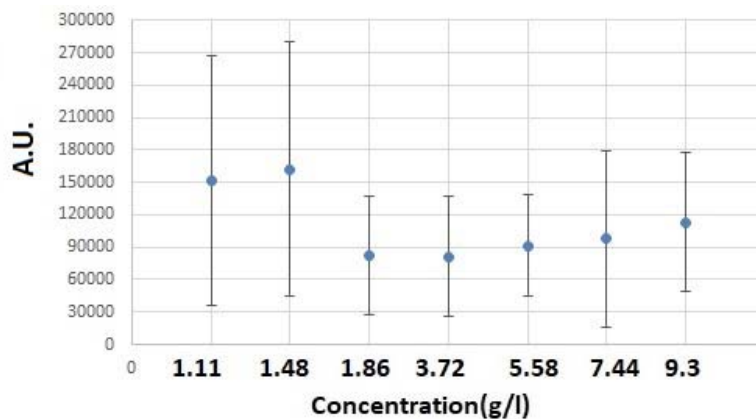
Figure 39) Mean and standard deviation of 3 measurements per PMMA concentration in stirred suspension (700 rpm) with ultrasound particle manipulation. Measurements were performed in the nodal planes of the standing wave field where PMMA particles were agglomerated

The sensitivity of this measurement can be determined by calculation of the enhancement factor (EF). This analysis is able to describe how successful the enhancement of Raman intensity is after

using ultrasound particle manipulation. In this study, EF was calculated by using following equation (equation 31):

Equation 31)
$$EF = \frac{\frac{\sum_{i=1}^{n} A_{US,i}}{n}}{\frac{\sum_{i=1}^{n} A_i}{n}}$$

A_{US} is the band area of one measurement in the nodal plane and n is the number of focus point of the probe on the nodal planes during each measurement with ultrasound particle manipulation. A_i is the band are of PMMA particles and n is the number of focus point of the probe in the PMMA suspended particles during each measurement without ultrasound particle manipulation. The results are shown in table 7. It can be seen that the enhancement factor decreases for higher concentrations. This is not unexpected, because for lower concentration the ratio of the number of PMMA particles agglomerated in the nodal planes to the number of particles homogenously distributed in the suspension without ultrasound particle manipulation is higher than for higher concentrations.

Table 7: Enhancement factor of each concentration

Concentration (g/l)	Enhancement factor (EH)
1.11	36
1.48	26
1.86	12
3.72	8
5.58	5
7.44	6
9.3	6

3.10 Effect of time on particles agglomerated in nodal planes

Experiments were performed to examine time-dependency of particle agglomeration in the nodal planes of the ultrasound standing wave field. In other words, we wanted to see if more particles are concentrated in the nodal planes with more time between turning ultrasound on and performing Raman measurements and if at a certain point saturation is reached. Also, the next aim of this experiment was to investigate the stability of the lines. Line scans with a step size of 50 µm were repeated after different time lapses (1 min, 15 min, 30 min) between turning on the ultrasound and starting Raman measurements. To calculate the enhancement factor with ultrasound on, a line scan of identical measurement positions was collected with ultrasound off. The EF was then determined using equation 31 based on the average Raman signal on the nodal planes with ultrasound particle manipulation and the average Raman signal without ultrasound

particle manipulation. The calculated value is EF=9.Single experiments were repeated three times using 5.58 g/l PMMA (figure 40).
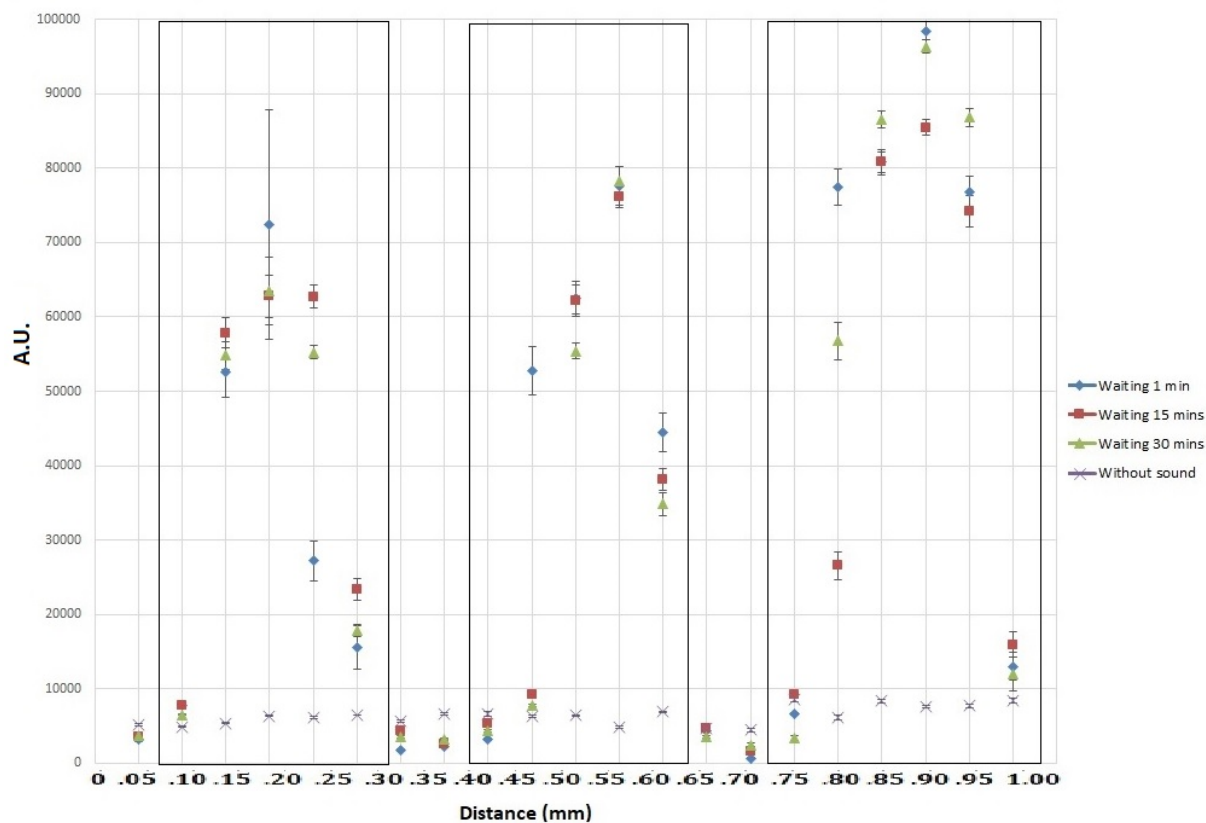

Figure 40) Time-dependency of particles agglomeration in nodal planes. Area of the accumulated particles are shown in rectangular region

For low concentrations the arrangement of particles in the nodal planes is better visible because there are less particles that can be trapped, thus resulting in a less stable Raman signal. Also, depending on the stirrer speed (suspension was stirred at constant rpm to assure homogenous distribution in x, y and z-direction), the wave field might not be stable enough to stay intact and might break down from time to time.

The factors influencing maximum separation rate on the suspended particles are the input power (amplifier), the stirrer speed and PMMA concentration. Based on our experiments (figure 40), no time dependency of particle agglomeration in the ultrasound standing wave field can be

observed for the given PMMA concentration and the chosen time lapses in the range of 1 to 30 min. Maybe, the time between turning ultrasound on and starting Raman measurements should have been reduced to a few seconds to see any time dependency. However, i could observe increasing PMMA signal throughout signal line scans which was unexpected. Since this effect was observed for all three runs, we can conclude that it is a reproducible effect. Nevertheless, the nodal planes seem to be fairly stable between single measurements. Also, i can assume that the collection of the PMMA particles in nodal planes takes under one minute.

3.11 Investigating the nodal planes of the ultrasound standing wave field

Here, i investigated the signal distribution within a single nodal plane. In order to do so, line scans along the x-axis of a selected nodal plane were performed of defined measurement positions (step size: 50 μm). The experiment was repeated 3 times using 5.58 g/l PMMA in aqueous solution (Figure 41).
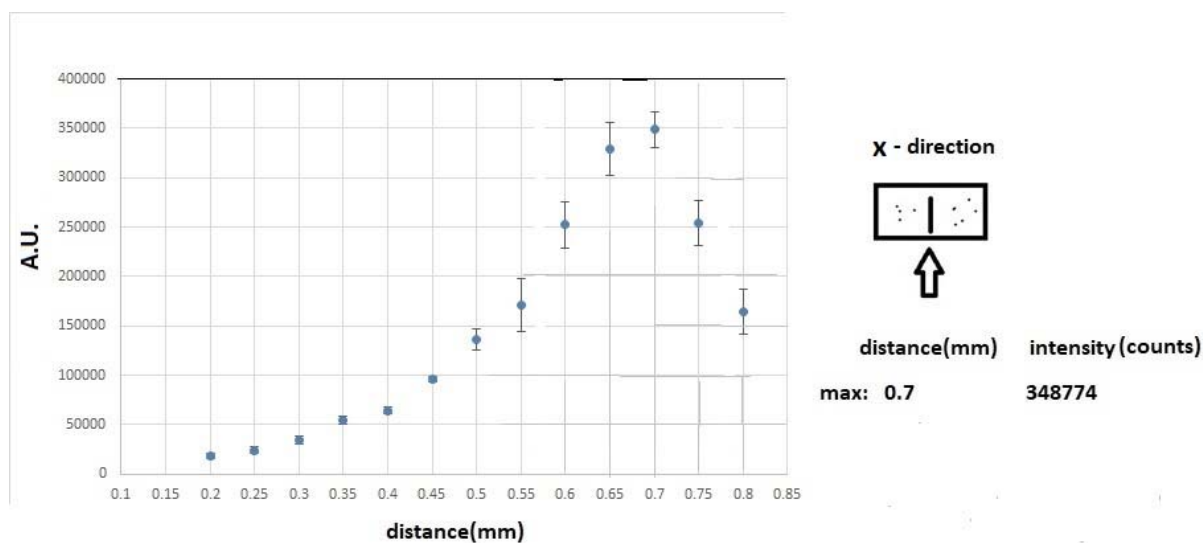

Figure 41) Line scans along a selected nodal plane (x-direction) and resulting PMMA intensity distribution (mean and standard deviation); sketch of experiment is shown on the right side

The results shows that the highest intensity of the area of the agglomerated particles is around 0.7 mm which means that in this distance the probe is focused on the line. Considering the standard deviation I can conclude that nodal plane observed here was stable over time.

3.12 Studying particle distribution due to ultrasound particle manipulation in a stable environment (gel matrix)

The aim of this study was to investigate the effects of ultrasound manipulation on suspended particle in more stable condition to improve SNR (signal to noise ratio) of the Raman spectra. Previous experiments were greatly influenced by noise due to constant motion of particles leading to increased scattering effects influencing the Raman signal background. The other point of this study was the investigation of particle distribution as a result of ultrasound particle manipulation which usually can only be studied as long as the acoustic field is applied. Since i wanted to exclude any effect that the ultrasound wave field might have on our Raman signal stability, i aimed for investigating the separated particles without sound. However, without sound there is no separation. To overcome this limitation the particles were immobilized in agar gel for later, detailed study with the microscope [25]. After immobilization in agar gel, the gel cube was cut into flat layers of $\simeq$ 1 mm thickness for subsequent investigation under the microscope. Additionally, line scans along the propagation direction of the ultrasound waves were recorded at 3 different positions (1 repetitions each) to get a more stable impression of the PMMA Raman signal. The use of this method of immobilization during acoustic manipulation gathered more information about the spatial arrangement of suspended particles because of the selective retention of particles. Light microscopy confirmed the presence of specific regions (Figure 42) where particles were retained effectively in the layers corresponding to the standing wave's pressure nodal planes. For gel solutions with low concentration in liquid state, the acoustic properties of sound wave resonance are essentially the same as for pure water (density $\rho=1000kg/m^3$, sound speed $c\approx1500m/s$)[26] .The image of immobilized particles

and stable lines in figure 42 shows retained concentrated PMMA particles on the nodal planes. Three pressure nodes and suspended particles which are not concentrated in the same area as an effect of when ultrasound is turned off and some particles are not fixed enough in the gel yet.
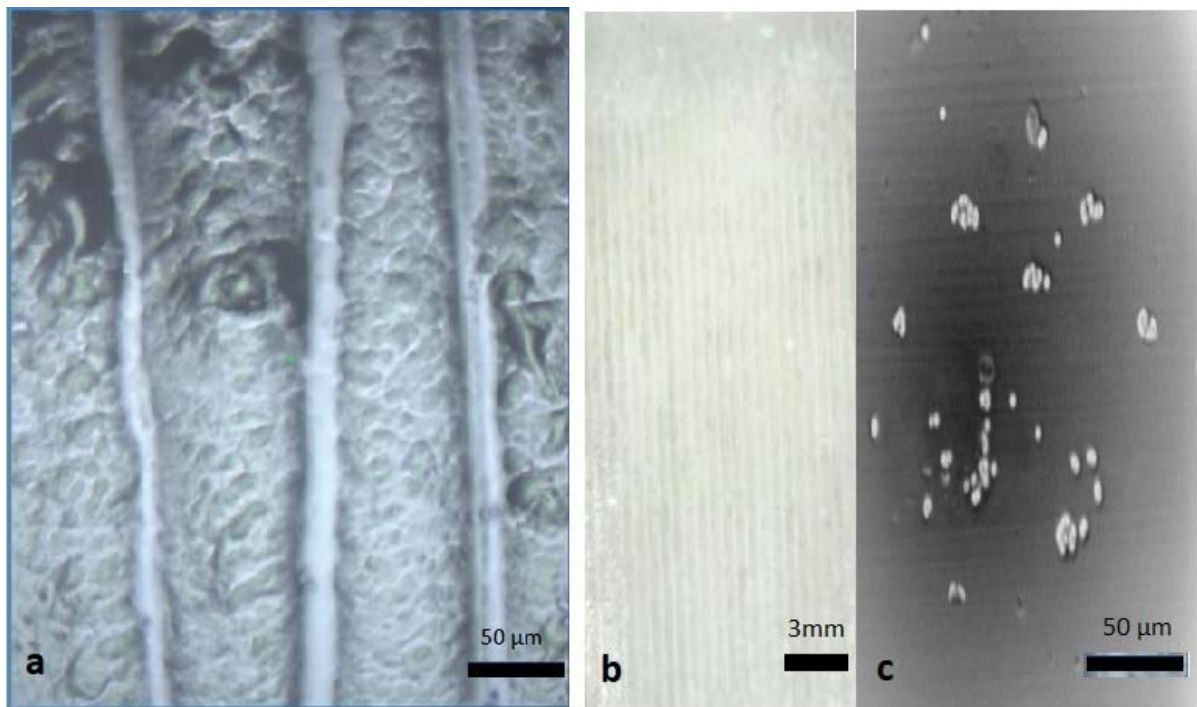

Figure 42) Agar gel experiment: a) Agar gel block with layers of concentrated PMMA particles (white lines).b) 20x magnification of PMMA particles immobilized in agar gel concentrated by ultrasound wave on the three nodal planes. C) Suspended particles which are not concentrated in the nodal planes as an effect of when ultrasound is turned off

A direct investigation of the immobilized particles behavior under ultrasound manipulation can lead to improve the design of the acoustic system. Figure 43 shows the reference spectra of 2.5 % agar gel with 5.58 g/l PMMA when sound is on and the focus of the laser is on the line. Additionally, Raman spectra were collected with the focus of the laser being between the lines. As reference, the spectrum of agar gel without PMMA was also added to figure 43 for better comparison.
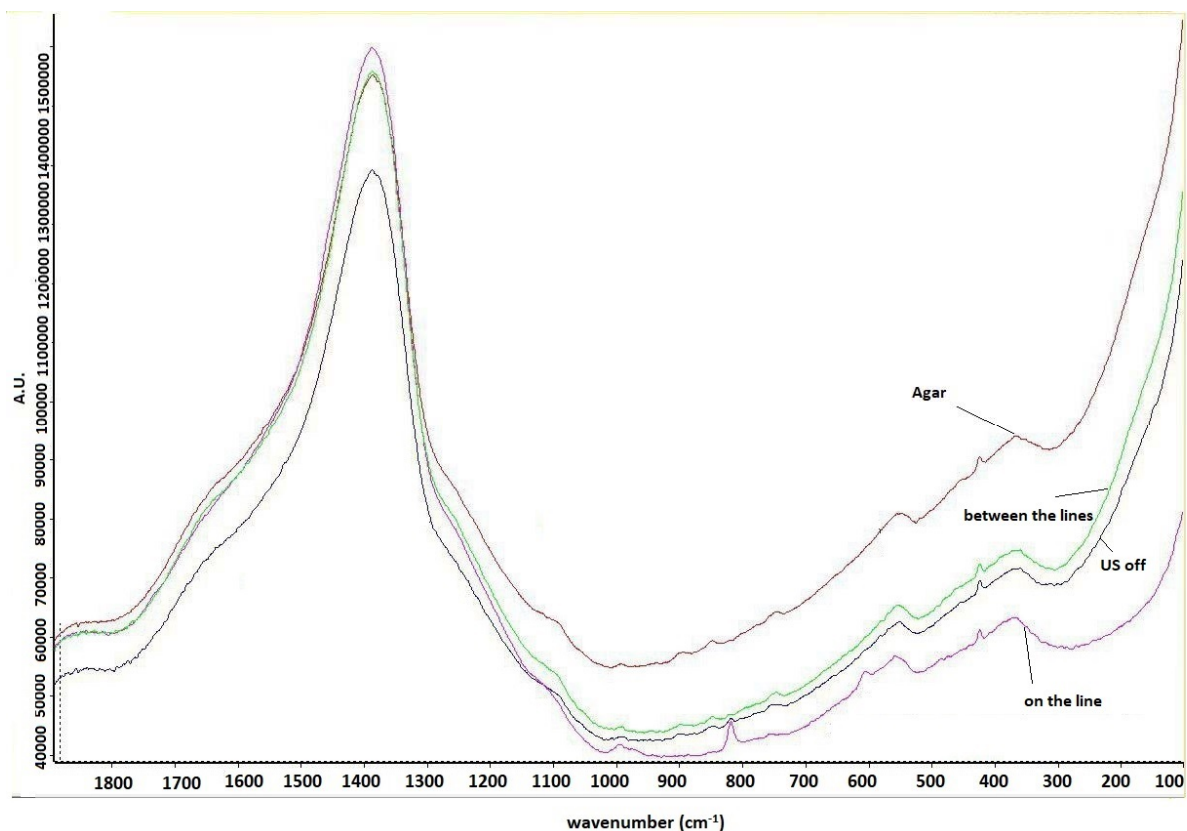
Figure 43) Reference spectra of 2.5 % Agar gel with 5.58 g/l PMMA without ultrasound particle manipulation (blue), when sound is on and the focus of the laser is on the line (pink), when the focus of the laser is between the lines (green) and Agar gel without PMMA (red)

Figure 44 shows the results of the Agar experiment and the effects of particle immobilization in Agar gel on the intensity of the Raman signal (see table 22 in appendix). Line scans with 50µm step size covering a total region of 1 mm were performed to study the difference in Raman signal on and between the lines of particles immobilized in the gel matrix.

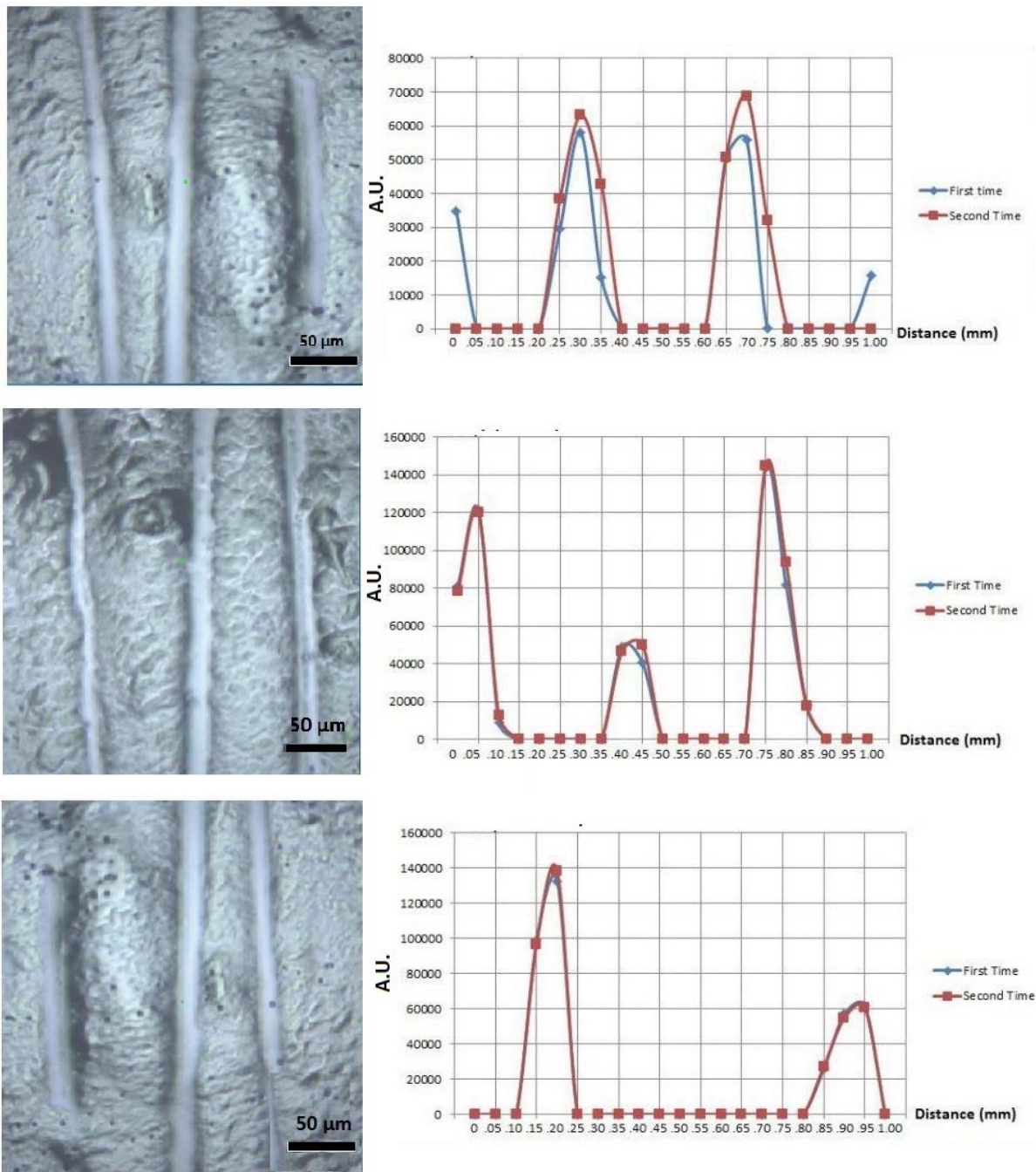*Figure 44) Areas of agglomerated PMMA particles. Two line scans were performed on identical measurement positions. Three different areas were investigated.*

The polymerization process of Agar gel produced a transparent gel block with PMMA particles fixed in the nodal planes after the ultrasound has been turned off. As can be seen in figure 43, it

is also suitable for investigating the position of PMMA bands with Raman microscopy. Since the particle separation stays intact in the gel even after the sound was turned off, the direct study of the effects of ultrasound standing waves on the location of agglomerated PMMA particles was possible. The scans are reproducible and show lower variance and lower standard deviation for repeated measurements. However, i have different signal intensity between different nodal planes, which might be due to the different focus spot of the laser on the particles, because i did scans along the gel so i might not have the same focus everywhere. Also, i might have more and less particles agglomerated. As can be seen in figure 42, the thickness of the lines with agglomerated PMMA particles varies which also impacts the Raman signal. The spectra between the lines did not show any PMMA signal. Thus, the integration of the area of the PMMA marker band yielded a negative value which was set to zero in the plots of figure 44.

One challenge faced in this experiment was the additional energy input by the acoustic wave resulting in a local increase in temperature. Since particles were fixed in the gel by cooling it down, the time for solidification and thus for immobilization of particles increased. To remove this effect the amplitude of sound was slowly reduced to decrease the energy transfer to the gel block and favor the cooling down process. However, the sound field still had to be present until the gel system was cooled down and the agglomerated PMMA particles were fixed in the gel block.

4. Conclusions and outlook

Raman imaging of PMMA particles in aqueous environment was successfully performed using two different Raman set-ups: the confocal Raman microscope (Horiba Jobin-Yvon LabRAM 800HR-633nm) and a Raman probe optimized for process monitoring (Kaiser Optical Systems RXN-1-785 nm). Herein, the developed technique allowed to obtain higher signal intensity of the Raman spectrum for micro-sized particles in suspension. While there are hardly few Raman bands of particles visible in the spectra obtained with conventional Raman spectroscopy. Here, i showed one way to overcome this limitation by hyphenation of Raman spectroscopy with ultrasound particle manipulation. The spectroscopic fingerprint of the particles are perfectly visible once the ultrasound has been turned on.

In this step, a method for the acquisition of the spectra of the PMMA particles in suspension was developed. This was achieved by the combination of ultrasound particle manipulation with Raman spectroscopy. The separation of the suspended particles in the cuvette was successfully right from the beginning when ultrasound manipulation was applied. The obtained results confirmed that the acoustic radiation force exerted on the particles leads to local concentration of the particles at defined areas in the standing ultrasound field. This results in a significant enhancement in Raman signal intensity and therefore better detection efficiency of particles in aqueous solution with improved signal to noise ratio. In this work, different parameters such as focal length, stirrer speed and particle concentration were varied for detailed characterization of the hyphenated technique. The sensitivity of these measurements was determined by calculation of the enhancement factor of Raman intensity, after using ultrasound particle manipulation.

The method can show great potential for studying polymerization and observing crystal versus suspension. Furthermore, design a new prototype for in-line application of ultrasound enhanced Raman spectroscopy with the new experimental setup of the glass tank is recommendable. Besides, depending on the set frequency, in the future using the improved amplifier with changing the frequency automatically is advisable. For future prospects, it might be advisable to further investigate the effect of stirrer speed temperature controlling on the signal intensity of

the particles. Time-dependent measurements should be performed to see if and how much the collection process in the nodal planes of the ultrasound standing wave field depends on the particle concentration. Also, for future measurements using a device called a stage micrometer which is particularly useful for determining the distance between the probe objective and the sample can be proposed to obtain more accurate results.

5.1 List of figures

5.2 List of the tables

Appendix

Tables

Table 1: Mean of PMMA Raman signal at different stirrer speeds for x+800 µm, 9.3 g/l PMMA

Stirrer speed(rpm)	First time			Mean	Second Time		Mean		Third Time		Mean
50	6763	7528	5162	6484.333	4906	4547	4726.5	7505	3536	6951	5997.333
100	7860	6868	7477	7401.667	5475	2749	4112	5474	5401	7748	6207.667
200	8744	7524	7942	8070	4511	4737	4624	6501	6104	5250	5951.667
300	6763	6614	7508	6961.667	4102	4003	4052.5	5815	6734	6398	6315.667
400	8389	6432	7775	7532	4449	3538	3993.5	7179	8036	7278	7497.667
500	8017	6568	7171	7252	3396	4344	3870	6756	7989	8787	7844
600	7961	7858	7312	7710.333	5097	4516	4806.5	8324	7251	7458	7677.667
700	6694	7851	7952	7499	3396	2700	3048	7800	8249	6999	7682.667
800	5762	7830	7099	6897	5655	4022	4838.5	8760	7398	7747	7968.333
900	8521	7001	5969	7163.667	5239	2115	3677	7719	8074	7715	7836
1000	7099	7056	6836	6997	4072	3291	3681.5	7522	9412	7680	8204.667
1100	7392	7595	8038	7675	4003	5223	4613	7126	7787	8092	7668.333
1200	6585	7388	7819	7264	3435	3439	3437	5520	6103	6552	6058.333
1300	7217	7271	9589	8025.667	4689	4970	4829.5	5395	6926	6103	6141.333
1400	6958	4972	4999	5643	4319	3736	4027.5	7639	7132	7730	7500.333
1500	5246	3978	5065	4763	3536	3236	3386	6936	7409	8320	7555

Table 2: Mean and standard deviation of PMMA Raman signal at different stirrer speeds for x+800 µm, 9.3 g/l PMMA

Stirrer speed(rpm)	Mean	Mean 2	Mean 3	Average	Standard deviation
50	6484	3267	3267	4339.556	1857.432
100	7402	3751	3751	4967.778	2107.81
200	8070	4135	4135	5446.667	2271.873
300	6962	3631	3631	4741.111	1923.058
400	7532	3966	3966	5154.667	2058.831
500	7252	3876	3876	5001.333	1949.135
600	7710	4155	4155	5340.222	2052.576

700	7499	4100	4100	5232.667	1962.702
800	6897	3849	3849	4864.667	1760.052
900	7164	4032	4032	5075.778	1808.165
1000	6997	3999	3999	4998	1731.185
1100	7675	4388	4388	5483.333	1898.039
1200	7264	4232	4232	5242.667	1750.526
1300	8026	4663	4663	5783.778	1941.533
1400	5643	3522	3522	4228.667	1224.849
1500	4763	3132	3132	3675.333	941.947

Table 3: *Mean of PMMA Raman signal at different stirrer speeds for x+1000 µm, 9.3 g/l PMMA*

Stirrer speed (rpm)	First time		Mean	Second time		Mean		Third time		mean
50	2370	1946	2632	2361	2392	3016	2704	2882	2491	1927	2433
100	2347	2212	1195	1918	2093	1925	2009	2457	2508	2220	2395
200	2203	2521	1031	1918	2874	2423	2648	1885	1819	1879	1861
300	1764	1874	1913	1850	2530	1937	2233	2456	1597	1721	1924
400	1791	2171	1474	1812	2437	869	1653	1545	1515	1836	1632
500	985	2221	1746	1650	2008	2161	2084	2669	2083	2255	2335
600	2092	1606	1407	1701	1508	2110	1809	2687	1134	1985	1935
700	537	2103	1024	1221	1902	2229	2065	1638	1307	2474	1806
800	1962	2077	1563	1867	1798	1439	1618	1378	1890	1100	1456
900	1408	1278	1882	1522	1663	1627	1645	1617	1364	1942	1641
1000	1531	1697	441	1223	1221	1767	1494	1323	838	1422	1194
1100	949	933	1563	1148	2982	2162	2572	1310	1278	778	696
1200	1459	1369	430	1086	1540	2832	2186	1410	1379	1548	1445
1300	321	920	-68	627	2694	1532	2113	752	1875	1114	1247
1400	1377	581	340	766	1873	2233	2053	1485	1439	1632	1518
1500	1482	1139	1237	1286	1483	2933	2208	1815	1211	1401	1475

Table 4: *Scanning in Y direction when sound is off (left side) and on, X+800 micrometer, PMMA 9.3 g/l*

Distance (µm)	First time	Second time	Third time	Mean
Y	33990	54281	21642	36637
Y-100	-2283	-55	82	27
Y-200	38568	215	-218	12999
Y-300	-848	8956	22447	10467

Y-400	108354	2398	6119	38957
Y-500	-168	-1130	-1684	0
Y-600	-275	217	942	386

Table 5: *Scanning in Y direction when sound is off and on, X+1000 micrometer, PMMA 9.3 g/l*
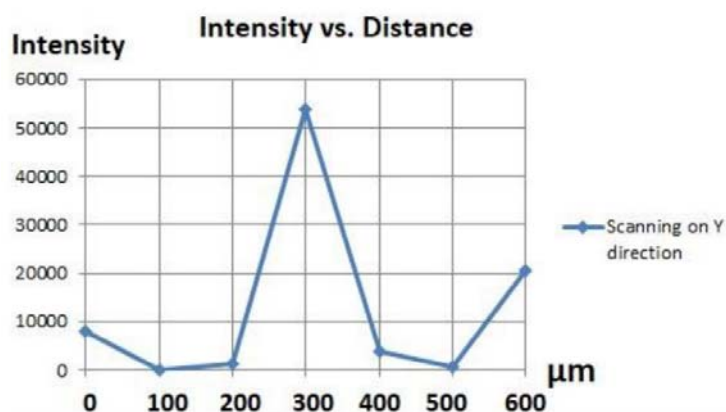
Distance (µm)	First time	Second time	Third time	Mean
Y	10562	7418	6495	8158
Y - 100	-2542	-2508	-1773	0
Y - 200	-2722	1930	1582	1170
Y - 300	42250	59086	60197	53844
Y - 400	8844	-836	2862	3902
Y - 500	-1601	1483	-96	494
Y - 600	1765	30977	28845	20529

Table 6: *Different setup configuration of probe and cuvette vertically*

Intensity(counts)					
Distance(mm)	First Time	Second Time	Third Time	Mean	Standard Deviation
0	101851	119013	101749	107537.7	9938.061
0.1	118927	137828	115197	123984	12133.44
0.2	155959	174666	151931	160852	12131.62
0.3	205211	223602	202010	210274.3	11652.54
0.4	294255	301715	275942	290637.3	13261.88

0.5	424681	439730	404090	422833.7	17891.67
0.6	696692	698386	653940	683006	25186.14
0.7	683300	705821	676861	688660.7	15206.02
0.8	426099	453428	412927	430818	20658.76
0.9	281858	307448	272759	287355	17985.95
1	195238	215681	192943	201287.3	12517.99
1.1	147526	165718	147703	153649	10452.44
1.2	113199	129954	116225	119792.7	8929.092
1.3	90496	105348	92708	96184	8012.953
1.4	70034	84253	73065	75784	7489.306
1.5	55795	69274	58551	61206.67	7121.115
1.6	47157	59804	50354	52438.33	6576.092
1.7	38625	50136	43281	44014	5790.401
1.8	32789	42241	36250	37093.33	4782.1
1.9	28606	37700	31164	32490	4689.767
2	25228	32823	26766	28272.33	4015.319
2.1	21816	29005	23872	24897.67	3702.624
2.2	19519	27854	21824	23065.67	4303.993

Table 7: *Different setup configuration of probe and cuvette horizontally*

		Intensity (counts)			
Distance(mm)	First Time	Second Time	Third Time	Mean	Standard Deviation
0	115628	108427	105887	109980.7	5052.938
0.1	143664	136997	135087	138582.7	4502.997
0.2	187106	181619	175659	181461.3	5725.128
0.3	247472	242054	238704	242743.3	4424.459
0.4	342761	337352	328463	336192	7219.238
0.5	497201	515482	493672	502118.3	11707.01
0.6	778851	790748	786971	785523.3	6079.182
0.7	657637	594061	634931	628876.3	32217.56
0.8	405587	378453	404519	396186.3	15366.8
0.9	280358	258993	269504	269618.3	10682.96
1	206715	187654	190724	195031	10234.41
1.10	156135	142066	148769	148990	7037.103
1.20	126635	109771	114804	117070	8657.349
1.30	97027	88436	89758	91740.33	4625.857
1.40	80175	70848	74923	75315.33	4675.861
1.50	65918	58463	59378	61253	4065.83
1.60	54587	48789	49774	51050	3102.472
1.70	46406	42506	42261	43724.33	2325.62

1.80	40356	35534	35429	37106.33	2814.784
1.90	34590	32152	32286	33009.33	1370.536
2.00	20355	26616	26609	24526.67	3612.771
2.10	28101	23117	24512	25243.33	2571.225
2.20	24335	21078	21931	22448	1688.928

Table 8: *Normalized variables for two different configuration of the probe*

	Normalized	
Distance(mm)	Horizontally	Vertically
0	0.11471	0.126912
0.1	0.152193	0.151621
0.2	0.208385	0.207012
0.3	0.288694	0.281265
0.4	0.411157	0.402004
0.5	0.628602	0.600617
0.6	1	0.991504
0.7	0.794717	1
0.8	0.489779	0.612613
0.9	0.323914	0.397072
1	0.226168	0.267763
1.1	0.165832	0.19619
1.2	0.124001	0.145324
1.3	0.090807	0.109854
1.4	0.069282	0.079205
1.5	0.050853	0.057304
1.6	0.037483	0.04413
1.7	0.027882	0.031473
1.8	0.01921	0.021075
1.9	0.01384	0.014159
2	0.002724	0.007823
2.1	0.003663	0.002752
2.2	0	0

Table 9: four different experiments of measuring the sediment of PMMA inside the cuvette with changing exposure time and changing distance between head of the probe and wall of the cuvette for each single spectrum 3 scans were accumulated

			Exposure time(s)		
Distance(mm)	1	2	3	5	10
0.1	1283	2788	3339	7707	15822
0.2	1593	3302	5152	9218	20699
0.3	3097	6051	8697	14306	33157
0.4	6670	9046	15386	26047	49651
0.5	7675	13752	23039	36343	78201
0.6	8474	14073	20377	26310	57421
0.7	6692	7546	11013	18863	0
0.8	4371	4372	6645	10213	0
0.9	4395	6954	10289	15600	0
1	4007	3536	11961	15926	0
1.10	1039	2835	1536	10103	0
1.20	1571	6774	10220	7821	0
1.3	604	4122	1042	9996	0
Max	8474	14073	23039	36343	78201
Min	604	2788	1042	7707	15822

Table 10: Normalized of four different experiments of measuring the sediment of PMMA inside the cuvette with changing exposure time and changing distance between head of the probe and wall of the cuvette for each single spectrum 3 scans were accumulated
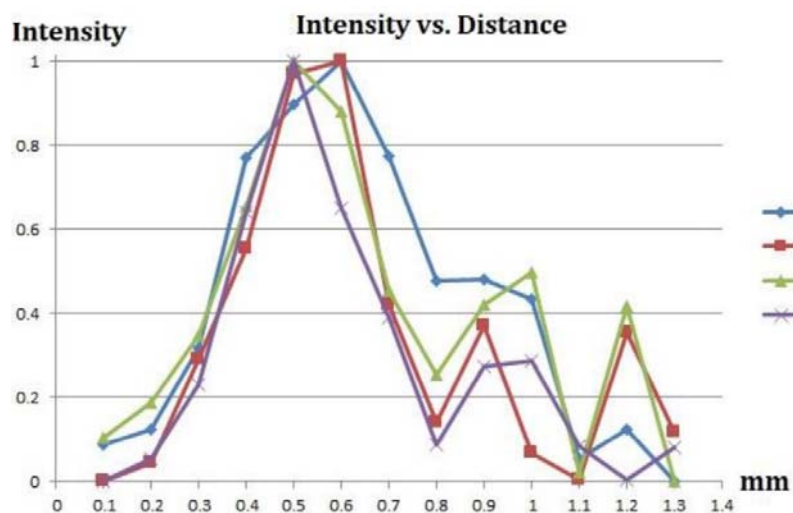
Normalized				
Distance (mm)	1S	2S	3S	5S
0.1	0.086277	0	0.104423	0
0.2	0.125667	0.045547	0.186844	0.052766
0.3	0.316773	0.289145	0.348002	0.230444
0.4	0.770775	0.554541	0.652089	0.640453
0.5	0.898475	0.971555	1	1
0.6	1	1	0.878983	0.649637
0.7	0.773571	0.421622	0.453289	0.38958
0.8	0.478653	0.140363	0.254717	0.087512
0.9	0.481703	0.369163	0.420376	0.275623
1.00	0.432402	0.068675	0.496386	0.287016
1.1	0.055273	0.004165	0.022458	0.083671
1.2	0.122872	0.353212	0.417239	0.003981
1.3	0	0.11821	0	0.079934

Table 11: *Effects of different stirrer speed on the intensity of the spectra with ANOVA test*
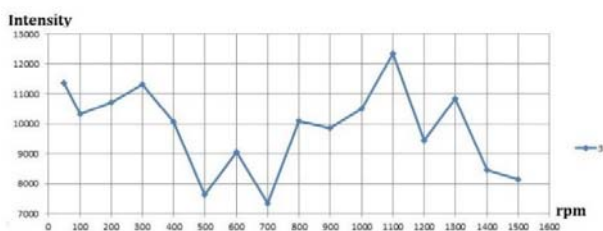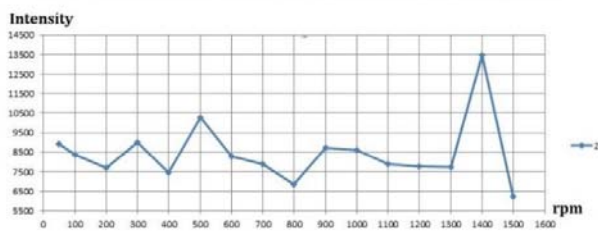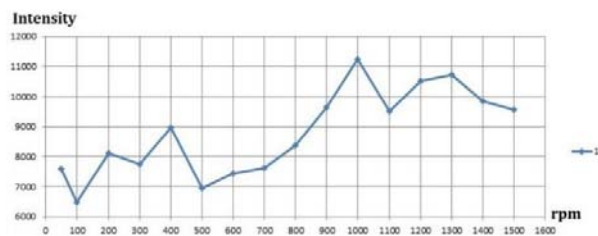
Stirrer speed	Intensity1	Intensity2	Intensity3
50	7587	8943	11366
100	6473	8373	10337
200	8118	7705	10705
300	7761	8988	11311
400	8976	7447	10073
500	6949	10267	7637
600	7447	8299	9054
700	7613	7910	7334
800	8363	6855	10090
900	9636	8730	9850
1000	11241	8620	10506
1100	9517	7905	12352
1200	10513	7782	9432
1300	10737	7730	10846
1400	9857	13464	8449
1500	9558	6231	8135
	Max	Max	Max
	11241	13464	12352

	Min	Min	Min
	6473	6231	7334

	Run 1	Run 2	Run 3
Sum (counts)	140346	135249	157477
Average	8771	8453	9842
$\sum i\ X^2ij$	1.3E+09	1.2E+09	1.6E+09
St. Dev	1434	1626	1417
SS	3.1E+07	4E+07	3E+07
n	16	16	16

Finally, with having already calculated the mean sum of squares, the F-statistic is computed as follows:

$$F = \frac{MS\ between}{MS\ within} = \frac{8474318}{2237276} = 3$$

The following null H_0 and alternative H_a hypotheses need to be tested:

H_0: $\mu_1 = \mu_2 = \mu_3$

H_a: Not all means are equal

The above hypotheses will be tested using an F-ratio for a One-Way ANOVA.

Since it is observed that F=3 and thus > 0, it is then concluded that the null hypothesis H_0 is not rejected. Therefore, there is enough evidence to claim that not all 3 population means are equal, at α=0.5 significance level.

Table 12: *Different experiments of the sediment of PMMA inside the cuvette with changing exposure time and distance between head of the probe and wall of the cuvette*

		Exposure time s		
Distance (mm)	1	2	3	5
0.1	16725	30647	43780	75270
0.2	21864	45301	68624	114967
0.3	36814	72004	108890	179985
0.4	57405	113763	169216	285512
0.5	87748	175358	264314	445865
0.6	143429	290381	439317	734454
0.7	105826	205510	314230	519934
0.8	71742	145515	211915	354491
0.9	56729	110437	156492	268759
1	43954	85674	131456	225248
1.10	34448	70094	103055	178236
1.20	28853	57493	88676	150816
1.3	26403	47640	70186	126193
max	143429	290381	439317	734454
min	16725	30647	43780	75270

Table 13: Normalizes of four different experiments of measuring the sediment of PMMA inside the cuvette with changing exposure time and changing distance between head of the probe and wall of the cuvette for each single spectrum 3 scans were accumulated.
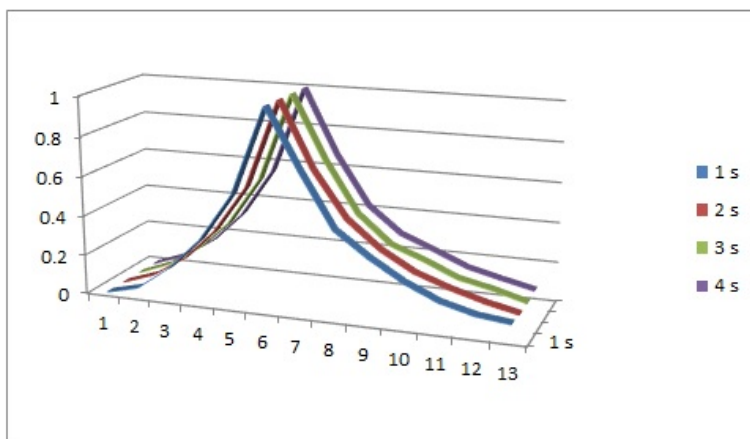

Distance (μm)	Normalized1	Normalized 2	Normalized 3	Normalized 4
0.1	0	0	0	0
0.2	0.040559	0.056419	0.062811	0.060221
0.3	0.158551	0.159228	0.164612	0.158855
0.4	0.321063	0.320004	0.317128	0.318943
0.5	0.560543	0.557151	0.557556	0.562203
0.6	1	1	1	1
0.7	0.703222	0.673239	0.683754	0.674567
0.8	0.434217	0.442252	0.42508	0.423586
0.9	0.315728	0.307199	0.284959	0.293528
1	0.214902	0.211859	0.221663	0.227521
1.1	0.139877	0.151875	0.14986	0.156202
1.2	0.095719	0.10336	0.113506	0.114605
1.3	0.076383	0.065425	0.06676	0.077252

Table 14: Intensity distribution integrated PMMA band along the line scan (on and between PMMA accumulations) with ultrasound turned on. Area of the accumulated particles are shown in rectangular region,- 1.16 g/l PMMA
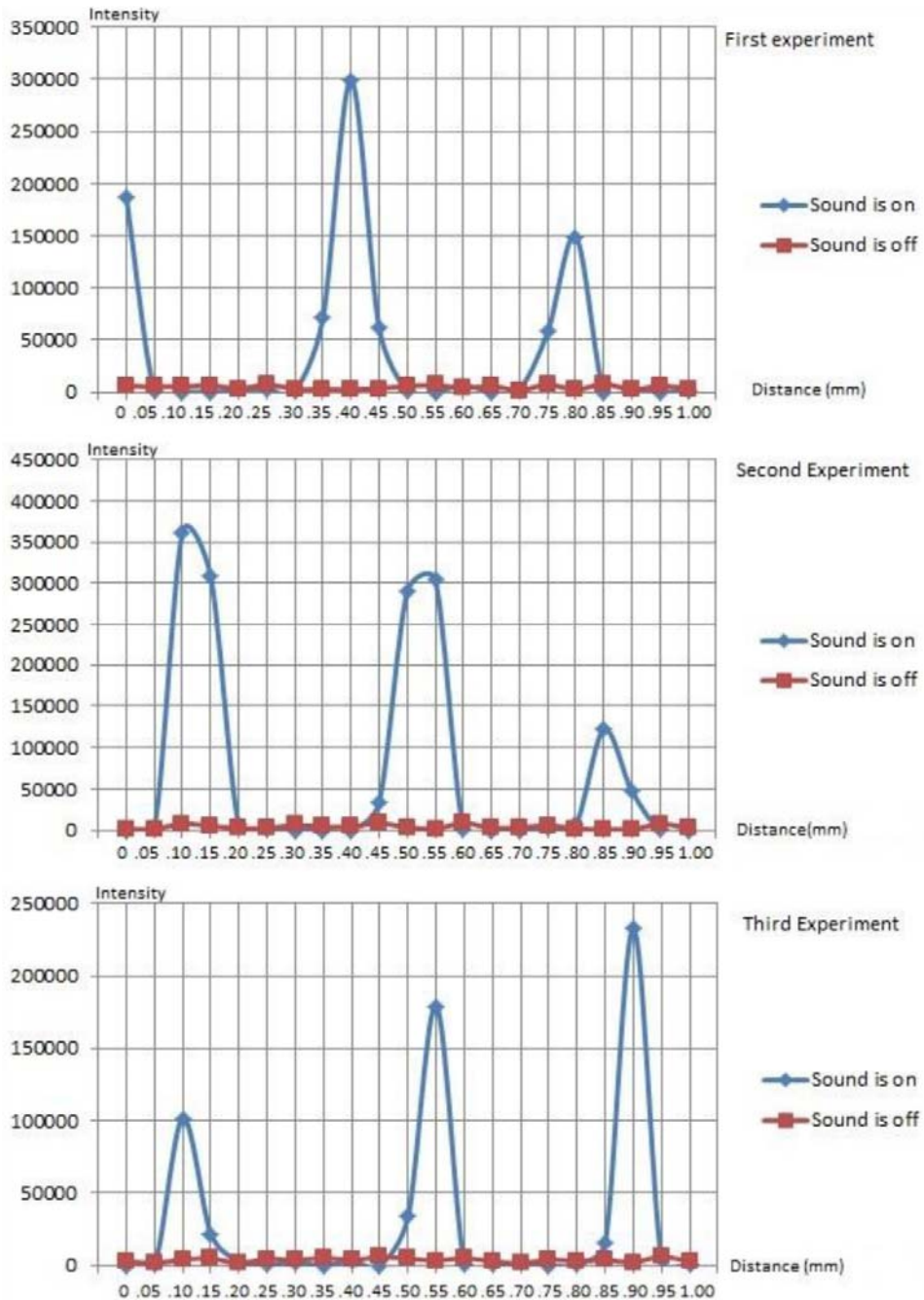
	First experiment		Second experiment		Third experiment	
Distance (µm)	Sound on	Sound off	Sound on	Sound off	Sound on	Sound off
0	186441	5801	0	1176	0	2679
0.05	492	5058	3341	1619	353	1563
0.10	0	5214	362306	7871	101485	4067
0.15	0	6478	309707	5258	21918	4915
0.20	1895	3079	6623	2355	3191	1430
0.25	3315	7078	1476	2483	474	4607
0.30	721	2883	0	6277	2028	3826
0.35	71263	2388	0	4517	0	5329
0.40	299410	2268	0	4373	3181	3903
0.45	61288	3251	34100	8552	0	5894
0.50	735	5744	290694	3544	33914	4809
0.55	148	6735	304054	1981	178939	3518
0.60	6381	3867	242	8921	874	5073
0.65	0	5574	0	2772	410	2874
0.70	2860	1509	0	3524	1613	1282
0.75	57990	7185	2606	5994	0	3976
0.80	148741	2078	6885	2158	665	3198
0.85	0	7929	121713	1012	16148	3774
0.90	3061	2145	47262	1422	232711	2174
0.95	0	5928	1003	7489	3603	6234
1.00	1091	3053	0	3494	1177	2700

Table 15: Intensity distribution integrated PMMA band along the line scan (on and between PMMA accumulations) with ultrasound turned on. Area of the accumulated particles are shown in rectangular region-.48 g/l PMMA
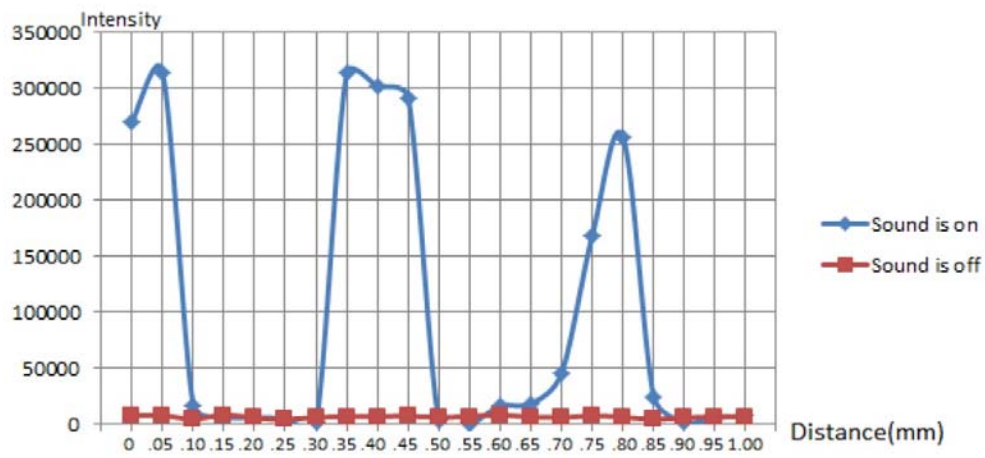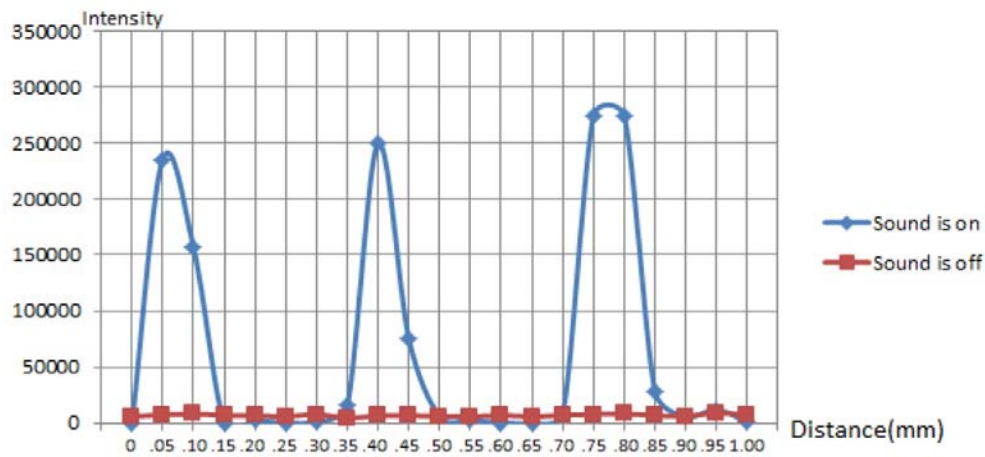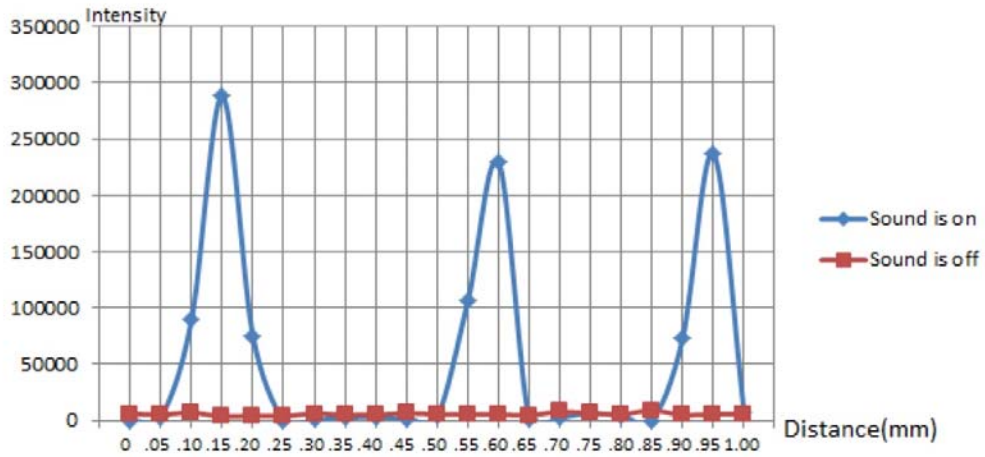
Distance (mm)	First experiment		Second experiment		Third experiment	
	Sound on	Sound off	Sound on	Sound off	Sound on	Sound off
0	76	5842	0	5487	270267	7968
0.05	3006	5138	326156	7316	314392	7687
0.10	89129	6851	156954	7963	17395	4407
0.15	288129	3393	0	6705	6372	8364
0.20	74870	3881	1853	6410	5830	5566
0.25	0	3566	0	5596	4960	4368
0.30	159	6135	999	7661	1543	5992
0.35	2290	4727	16485	4163	313489	6786
0.40	3106	4921	236156	6309	301224	6908
0.45	1093	6506	74685	6375	291863	7055
0.50	3522	5287	5751	6043	3876	5940
0.55	105928	5204	2363	5384	0	6926
0.60	229703	5220	0	6720	16478	8393
0.65	1570	4480	0	5383	18522	6121
0.70	2474	7754	8253	6798	45998	5778
0.75	6336	6415	275110	7657	168529	7363
0.80	3957	5314	274587	8059	257063	6202
0.85	0	8995	27910	6583	25104	4446
0.90	72650	4798	5587	5966	2116	5621
0.95	237477	5444	12081	8694	5536	6688
1.00	7636	5584	341	7128	7583	6578

Table 16: *Intensity distribution integrated PMMA band along the line scan (on and between PMMA accumulations) with ultrasound turned on. Area of the accumulated particles are shown*

	First experiment		Second experiment		Third experiment	
Distance(mm)	Sound on	Sound off	Sound on	Sound off	Sound on	Sound off
0	9973	5805	12886	8159	1526	4679
0.05	4962	6916	232524	7599	-1084	8611
0.10	-1096	6275	97514	7108	12558	7814
0.15	-18	6372	-902	8063	103873	7171
0.20	221	7081	1497	6036	80756	6411
0.25	7546	4926	-330	8360	82340	8043
0.30	54715	5998	2051	5765	6498	6595
0.35	48042	5600	3834	5735	-149	7464
0.40	26082	6200	133168	6778	1121	5854
0.45	3387	7050	78075	6628	103	6748
0.50	1438	5621	5513	4770	4809	5822
0.55	78	5821	1265	7190	70060	7262
0.60	21451	5852	5188	7668	41111	8097
0.65	40552	4752	6535	5185	3627	8297
0.70	40869	6728	25196	6230	1153	6163
0.75	41230	5416	76477	6128	3694	4852
0.80	2044	4716	146292	6146	2880	6578
0.85	-496	6126	197021	9047	30713	6794
0.90	692	4403	2666	5968	67927	7747
0.95	2279	6063	1905	4926	91822	7305
1.00	14145	4810	-1587	5949	118851	8929

Table 17: Intensity distribution integrated PMMA band along the line scan (on and between PMMA accumulations) with ultrasound turned on. Area of the accumulated particles are shown in rectangular region- 3.72 g/l PMMA
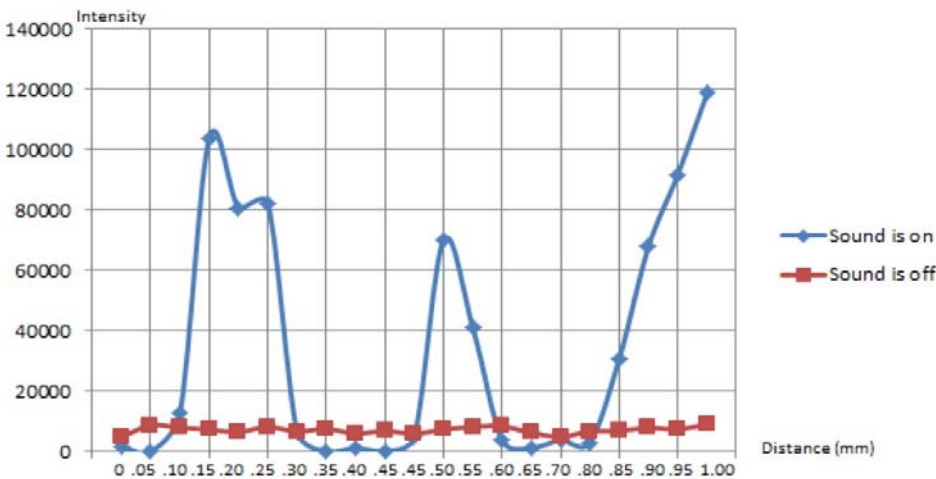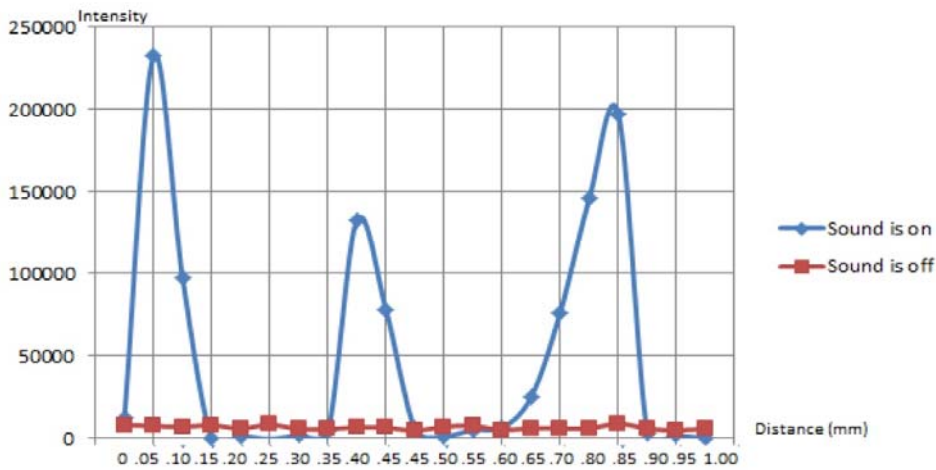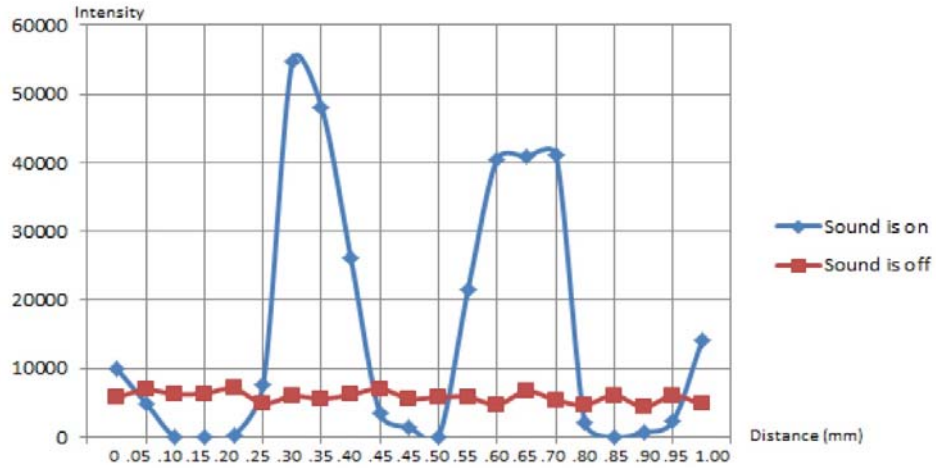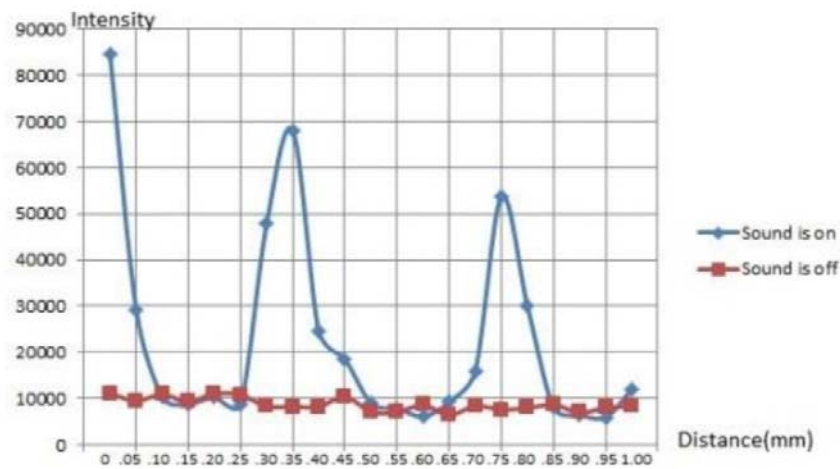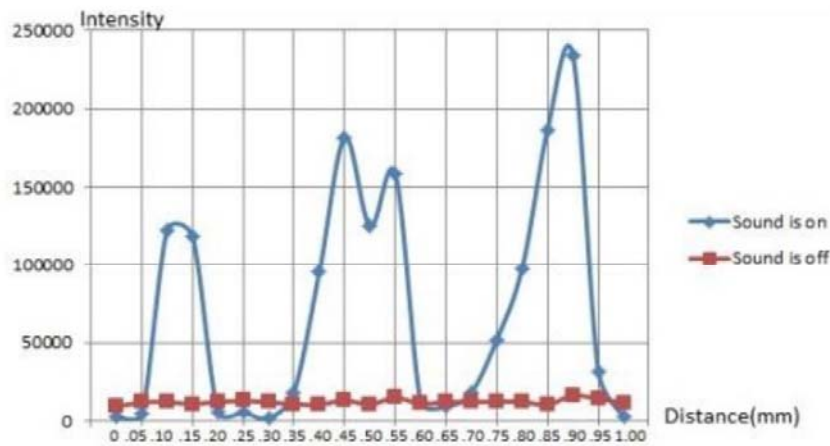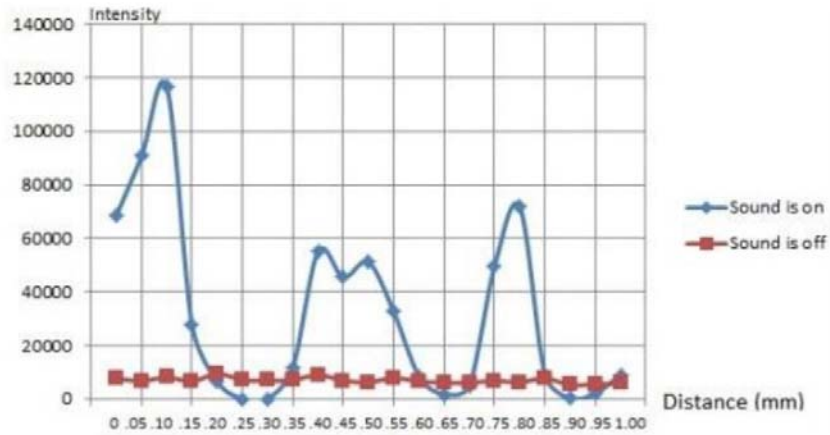
Distance(mm)	First experiment		Second experiment		Third experiment	
	Sound on	Sound off	Sound on	Sound off	Sound on	Sound off
0	68474	7492	2577	9498	84438	11117
0.05	90736	6642	4941	12047	29329	9548
0.10	116436	7953	122520	12359	10378	10887
0.15	27655	6481	118382	11005	8830	9317
0.20	6453	9268	6107	12590	10298	11078
0.25	-36	6997	5546	13071	8735	10820
0.30	-872	6818	1885	12184	47854	8373
0.35	11772	6945	18641	10953	68021	8252
0.40	55004	8890	95397	10737	24650	8253
0.45	45390	6745	181634	13323	18518	10411
0.50	50956	6128	124716	10890	9064	7155
0.55	32520	7717	158592	15093	7870	7090
0.60	8353	6509	12549	11151	6143	8625
0.65	1636	6019	9367	12375	9335	6448
0.70	5010	5934	18409	12388	16068	8428
0.75	49606	6714	52054	12625	53826	7627
0.80	71692	6128	97838	12513	30037	7997
0.85	8878	7631	186735	10522	8099	8660
0.90	89	5118	233960	16557	6482	7022
0.95	1979	5471	32074	14351	6010	7987
1.00	8914	5698	2805	11962	12000	8410

Table 18: *Scanning Y direction of 5.58 g/l PMMA when sound was on: Model name: Rxn1-785, Accumulations: 3, Exposure time: 3sec, Sound is on 2.04 MHz, 0.9 w, stirrer was on: 700 rpm*
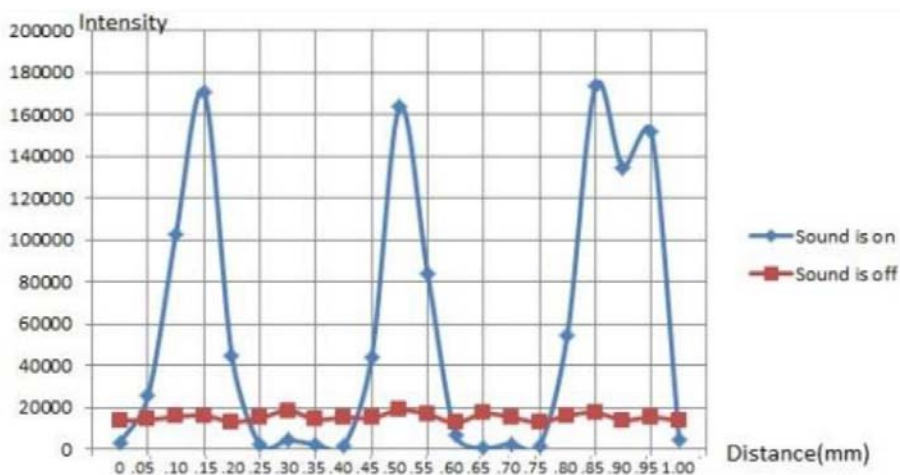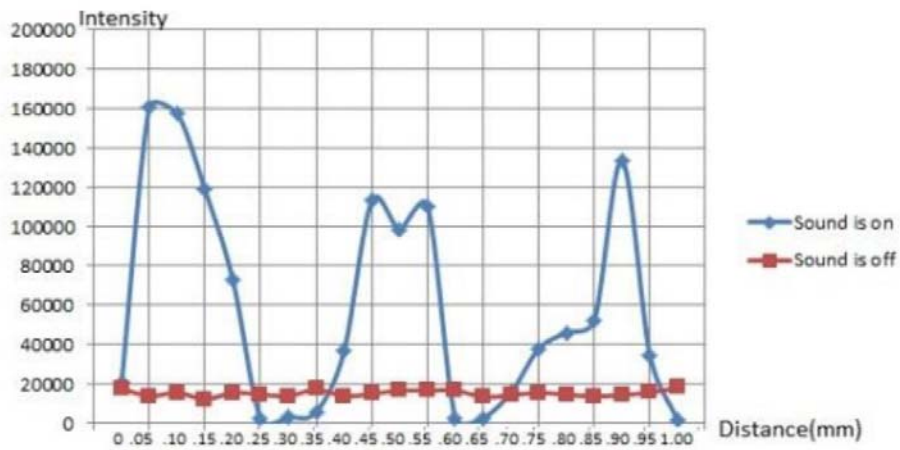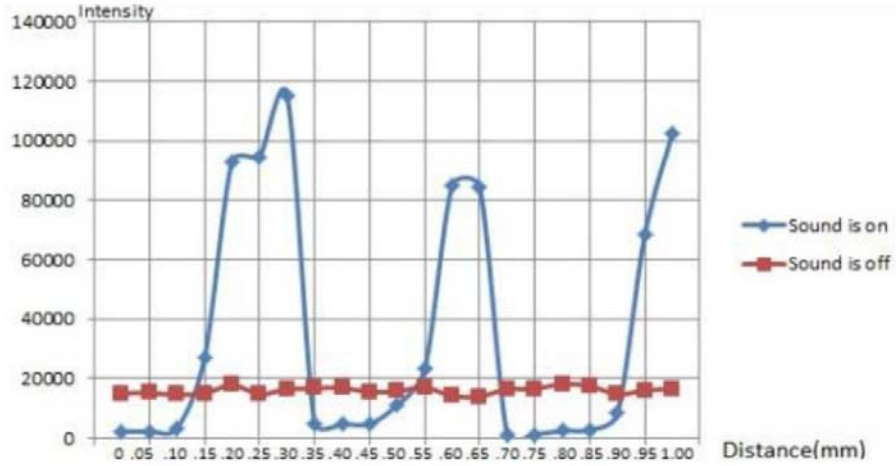
Distance(mm)	First experiment		Second experiment		Third experiment	
	Sound on	Sound off	Sound on	Sound off	Sound on	Sound off
0	2310	15127	21109	17746	3376	13655
0.05	2347	15220	160789	13867	25554	14063
0.10	3416	14677	157645	15642	103118	15582
0.15	27177	15110	118993	12218	170493	16210
0.20	93028	17896	72692	15526	44496	13136
0.25	94654	14860	2388	14688	2151	14911
0.30	115013	16505	3084	13917	4331	18546
0.35	5093	16830	5823	17325	2385	14279
0.40	4823	16923	36577	13844	1551	15268
0.45	4821	15628	113521	14948	43853	14972
0.50	11234	15789	98841	16861	163607	18733
0.55	23472	17126	110929	16712	84277	16828
0.60	85157	14178	2686	16840	6897	12686
0.65	84286	14076	2825	13386	549	17136
0.70	1138	16514	15697	14241	2699	15323
0.75	1242	16614	37824	15611	1462	12906
0.80	2486	18239	46095	14540	54712	16187
0.85	2874	17586	52038	13725	173475	17533
0.90	8292	14805	133777	14416	134301	13968
0.95	68464	16126	34679	15712	152066	15354
1.00	102669	16682	1746	18237	4444	13651

Table 19: *Scanning Y direction of 7.44 g/l PMMA when sound was on: Model name: Rxn1-785, Accumulations:3, Exposure time: 3sec, Sound is on 2.042 MHz*
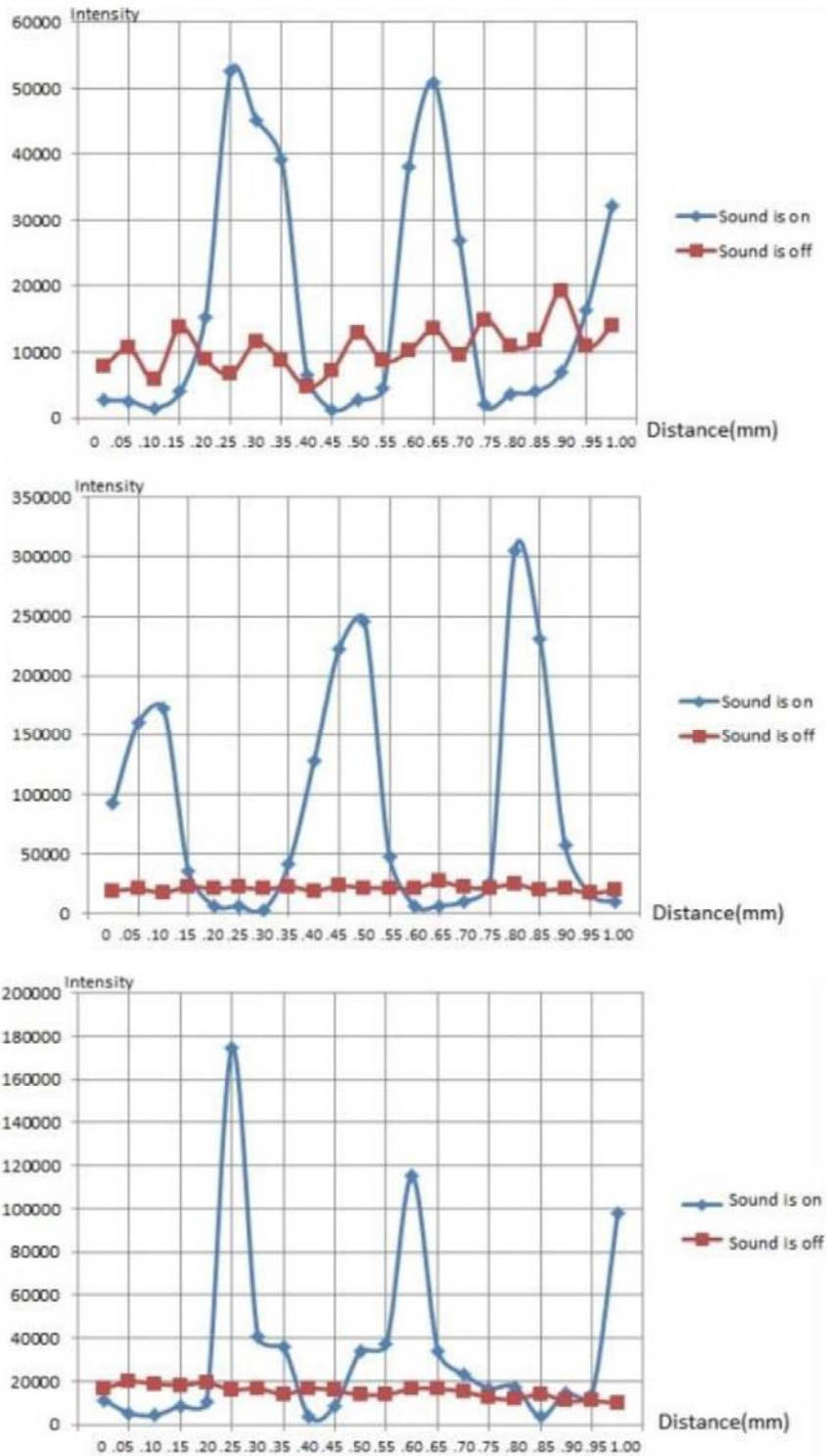
Distance(mm)	First experiment		Second experiment		Third experiment	
	Sound on	Sound off	Sound on	Sound off	Sound on	Sound off
0	2705	7821	92813	18817	11299	16600
0.05	2606	10582	160629	20323	5385	19763
0.10	1542	5818	172714	17338	4312	18857
0.15	3985	13795	35370	22423	8689	18126
0.20	15350	8870	6657	20591	10428	19337
0.25	52514	6680	6047	21822	174455	16041
0.30	45201	11519	3085	20286	40816	16712
0.35	39144	8777	41923	22565	35824	13997
0.40	6453	4685	128112	18939	3751	16741
0.45	1261	7230	222986	23027	8759	15605
0.50	2777	12880	246134	21242	34044	13835
0.55	4560	8613	47976	21283	37309	13842
0.60	38010	10121	6500	21085	115215	16638
0.65	50856	13456	6532	26280	34261	16449
0.70	26940	9468	10122	21645	23431	15306
0.75	2048	14926	25267	21169	16771	12465
0.80	3682	10986	305586	24520	17521	11569
0.85	3987	11669	231531	19184	3636	14108
0.90	6909	19144	57020	20545	14862	10929
0.95	16441	10919	15961	16911	14013	11121
1.00	32241	13963	9609	19404	97695	9727

Table 20: *Scanning Y direction of 9.3 g/l PMMA when sound was on: Model name: Rxn1-785, Accumulations:3, Exposure time: 3sec, Sound was on 2.042 MHz*

	First experiment		Second experiment		Third experiment	
Distance(mm)	Sound on	Sound off	Sound on	Sound off	Sound on	Sound off
0	6822	19740	6731	25988	117165	18690
0.05	3921	19253	13083	20748	15680	18684
0.10	127426	17119	7833	21166	8762	18959
0.15	114990	14280	20855	22288	5775	17126
0.20	40311	15291	148717	30691	11517	16955
0.25	4999	13181	271470	23493	87804	17072
0.30	4981	16105	89346	22694	195696	13809
0.35	4872	12949	22219	23974	138401	17021
0.40	14432	12339	29491	23723	61598	16004
0.45	116354	15908	11808	24773	24156	13221
0.50	136693	18954	49445	20329	18053	14037
0.55	65925	11272	215857	26545	10275	14184
0.60	17388	12445	234607	23333	15313	13298
0.65	19948	10331	71660	22977	89434	11413
0.70	13979	10290	10062	22833	137967	9772
0.75	24995	10283	6341	20697	80929	9382
0.80	106241	9416	9577	21918	34054	10020
0.85	159743	10498	33668	24425	17246	9484
0.90	98194	9158	76318	22807	22898	9257
0.95	58731	8009	237738	21303	34558	11393

Table 21: *Time-dependency of particles agglomeration in nodal planes. Area of the accumulated particles are shown in rectangular region _ PMMA 5.58 g/l*

		First Experiment		
Distance(mm)	1 Min	15 Min	30 Min	Without sound
0	13330	582	679	13135
0.05	180236	97059	13028	12772
0.10	126388	129283	111276	10099
0.15	132540	63633	88427	9026
0.20	22521	6065	10757	10983
0.25	8001	2790	3109	11578
0.30	7667	2199	1093	10928
0.35	3973	1177	1615	9365
0.40	51335	7437	24810	10129
0.45	75277	75576	105815	10800
0.50	111407	92163	77661	11657
0.55	194914	56064	56579	11188
0.60	101265	3154	5314	9046
0.65	12026	1643	3620	8337
0.70	7350	3405	617	7251
0.75	29877	1846	2259	7840
0.80	92742	30345	44443	10532
0.85	80217	80754	80017	8291
0.90	56482	44534	50429	8704
0.95	16768	2500	6619	8318
1.00	2484	-351	1912	9335

		Second time		
Distance(mm)	1 Min	15 Min	30 Min	Without sound
0	77162	36080	47673	5877
0.05	61875	60892	71815	4726
0.10	10781	19847	26490	4574
0.15	1569	3366	4737	4741
0.20	1299	2156	3023	5000
0.25	15808	4816	12150	8523
0.30	111110	67205	63291	6337
0.35	86032	71776	39292	7990
0.40	95693	87281	88974	7213
0.45	63106	50568	59357	7084
0.50	11532	9306	13254	6818
0.55	7281	2072	4767	5682
0.60	23887	3770	4599	8935

0.65	93993	23338	5453	8181
0.70	96733	31818	98536	5686
0.75	112454	91715	88725	8230
0.80	99078	102003	111083	10203
0.85	10731	21466	24333	10431
0.90	1561	660	1788	8855
0.95	5126	2066	2337	10585
1.00	32348	6714	2764	8965

		Third Experiment		
Distance(mm)	1 Min	15 Min	30 Min	Without sound
0	3306	3529	3774	5184
0.05	7682	7871	6380	4929
0.10	51328	57916	53155	5274
0.15	62198	62306	59575	6285
0.20	27180	61314	56021	6026
0.25	15714	21677	16993	6399
0.30	1863	4444	3525	5778
0.35	2267	2776	3138	6816
0.40	3057	5463	4439	6811
0.45	51517	9240	7968	6121
0.50	62842	60735	55714	6353
0.55	77805	77235	75991	4772
0.60	41551	37464	33397	6918
0.65	4335	4745	3395	4770
0.70	681	1420	2533	4215
0.75	6632	9092	3345	8752
0.80	76382	28474	59249	6054
0.85	82718	82336	87771	8144
0.90	97102	86706	97121	7608
0.95	78889	73515	88190	7669
1.00	13450	15185	11271	8404

Table 22: *Areas of agglomerated PMMA particles of 2.5 % Agar gel with 5.58 g/l PMMA*

Distance mm	First Experiment				Second Experiment				Third Experiment			
	1	2	mean	Stdev	1	2	mean	Stdev	1	2	mean	Stdev
0	34919	0	17459	24691	81249	78587	79918	1882	0	0	0	0
0.05	0	0	0	0	121457	119923	120690	1084	0	0	0	0
0.10	0	0	0	0	8803	12485	10644	2603	0	0	0	0
0.15	0	0	0	0	0	0	0	0	99121	96813	97967	1632
0.20	0	0	0	0	0	0	0	0	132614	138435	13552	4116
0.25	29495	38415	33955	6307	0	0	0	0	0	0	0	0
0.30	57979	63133	60556	3644	0	0	0	0	0	0	0	0
0.35	15096	42857	28976	19629	0	0	0	0	0	0	0	0
0.40	0	0	0	0	49005	46546	47775	1738	0	0	0	0
0.45	0	0	0	0	40497	50198	45347	6859	0	0	0	0
0.50	0	0	0	0	0	0	0	0	0	0	0	0
0.55	0	0	0	0	0	0	0	0	0	0	0	0
0.60	0	0	0	0	0	0	0	0	0	0	0	0
0.65	50055	50549	50302	349	0	0	0	0	0	0	0	0
0.70	55885	68767	62326	9108	0	0	0	0	0	0	0	0
0.75	154	32109	16131	22595	143505	144808	144156	921	0	0	0	0
0.80	0	0	0	0	81690	93991	87840	8698	0	0	0	0
0.85	0	0	0	0	18159	17433	17796	513	25950	26951	26450	707
0.90	0	0	0	0	0	0	0	0	5694	54750	30222	34687
0.95	0	0	0	0	0	0	0	0	61770	60875	61322	632
1.00	15670	0	7835	11080	0	0	0	0	0	0	0	0

Table 23: *t-test for three runs of PMMA Raman signal at different stirrer speed for x+800µm*

	Run1	Run2
Sum (counts)	113340	65723
Average	7083	4107
$\sum i\, X^2ij$	8.1E+08	2.7E+08
St. Dev	857	576
SS	1.1E+07	4988035
n	16	16

Finally, with having already calculated the mean sum of squares, the F-statistic is computed as follows:

$$F = \frac{MS\ between}{MS\ within} = \frac{70853600}{533665} = 132$$

The following null H_0 and alternative H_a hypotheses need to be tested:

H_0: $\mu_1 = \mu_2 = \mu_3$

H_a: Not all means are equal

The above hypotheses will be tested using an F-ratio for a t-test.

Since it is observed that F=132, it is then concluded that the null hypothesis H_0 is not rejected.

Using the P-value approach: The p-value is p = 0, and since p = 0 ≥, it is concluded that the null hypothesis is not rejected. Therefore, there is enough evidence to claim that not all 2 population means are equal, at α=0.5 significance level.

	Run1	Run3
Sum (counts)	113340	114106
Average	7083	7131
$\sum i\ X^2 ij$	8.1E+08	8.2E+08
St. Dev	857	837
SS	1.1E+07	1.1E+07
n	16	16

Finally, with having already calculated the mean sum of squares, the F-statistic is computed as follows:

$$F = \frac{MS\ between}{MS\ within} = \frac{18400}{718238} = 0.026$$

The following null H_0 and alternative H_a hypotheses need to be tested:

H_0: $\mu_1 = \mu_2 = \mu_3$

H_a: Not all means are equal

The above hypotheses will be tested using an F-ratio for a t-test.

Since it is observed that F=0.026, it is then concluded that the null hypothesis H_0 is not rejected.

Using the P-value approach: The p-value is p = 0.8739, and since p = 0.8739 $\geq \alpha$, it is concluded that the null hypothesis is not rejected. Therefore, there is enough evidence to claim that not all 2 population means are equal, at α=0.5 significance level.

	Run2	Run3
Sum (counts)	65723	114106
Average	4107	7131
$\sum i\ X^2ij$	2.7E+08	8.2E+08
St. Dev	576	837
SS	4988035	1.1E+07
n	16	16

Finally, with having already calculated the mean sum of squares, the F-statistic is computed as follows:

F=$\frac{\text{MS between}}{\text{MS within}} = \frac{73155600}{517107} = 141$

The following null H_0 and alternative H_a hypotheses need to be tested:

H_0: $\mu_1 = \mu_2 = \mu_3$

H_a: Not all means are equal

The above hypotheses will be tested using an F-ratio for a t-test.

Since it is observed that F=141, it is then concluded that the null hypothesis H_0 is not rejected.

Using the P-value approach: The p-value is p = 0, and since p = 0 ≥, it is concluded that the null hypothesis is not rejected. Therefore, there is enough evidence to claim that not all 2 population means are equal, at α=0.5 significance level.

Table 24: t-test for three runs of PMMA Raman signal at different stirrer speed for x+1000μm

	Run1	Run2
Sum (counts)	140346	135249
Average	8771	8453
$\sum i\ X^2 ij$	1.3E+09	1.2E+09
St. Dev	1434	1626
SS	3.1E+07	4E+07
n	16	16

Finally, with having already calculated the mean sum of squares, the F-statistic is computed as follows:

$$F = \frac{MS\ between}{MS\ within} = \frac{811856}{2351590} = 0.345$$

The following null H_0 and alternative H_a hypotheses need to be tested:

H_0: $\mu_1 = \mu_2 = \mu_3$

H_a: Not all means are equal

The above hypotheses will be tested using an F-ratio for a t-test.

Since it is observed that F=0.345, it is then concluded that the null hypothesis H_0 is not rejected.

Using the P-value approach: The p-value is p = 0.5612, and since p = 0.5612≥α, it is concluded that the null hypothesis is not rejected. Therefore, there is enough evidence to claim that not all 2 population means are equal, at α=0.5 significance level.

	Run1	Run3
Sum (counts)	140346	157477
Average	8771	9842
$\sum i\, X^2 ij$	1.3E+09	1.6E+09
St. Dev	1434	1417
SS	3.1E+07	3E+07
n	16	16

Finally, with having already calculated the mean sum of squares, the F-statistic is computed as follows:

$$F= \frac{MS\ between}{MS\ within} = \frac{9170973}{2032836} = 4.5$$

The following null H_0 and alternative H_a hypotheses need to be tested:

H_0: $\mu_1 = \mu_2 = \mu_3$

H_a: Not all means are equal

The above hypotheses will be tested using an F-ratio for a t-test.

Since it is observed that F=4.5 and thus > 0, it is then concluded that the null hypothesis H_0 is not rejected.

Using the P-value approach: The p-value is p = 0.042, and since p = 0.042≥, it is concluded that the null hypothesis is not rejected. Therefore, there is enough evidence to claim that not all 2 population means are equal, at α=0.5 significance level.

	Run2	Run3
Sum (counts)	135249	157477
Average	8453	9842
$\sum i\ X^2ij$	1.2E+09	1.6E+09
St. Dev	1626	1417
SS	4E+07	3E+07
n	16	16

Finally, with having already calculated the mean sum of squares, the F-statistic is computed as follows:

$$F= \frac{MS\ between}{MS\ within} = \frac{15440124}{2327400} = 6$$

The following null H_0 and alternative H_a hypotheses need to be tested:

H_0: $\mu_1 = \mu_2 = \mu_3$

H_a: Not all means are equal

The above hypotheses will be tested using an F-ratio for a t-test.

Since it is observed that F=6, it is then concluded that the null hypothesis H_0 is not rejected.

Using the P-value approach: The p-value is p = 0.0152, and since p = 0.0152≥α, it is concluded that the null hypothesis is not rejected. Therefore, there is enough evidence to claim that not all 2 population means are equal, at α=0.5 significance level.

References

1. *Douglas C. Giancoli. Physics for Scientists and Engineers with Modern Physics, Volume 3*

2. Long, D.A., *The Raman Effect: A Unified Treatment of the Theory of Raman Scattering by Molecules*. 2002: Wiley.

3. Pawley, J., *Handbook of Biological Confocal Microscopy*. 2012: Springer US.

4. Dieing, T., O. Hollricher, and J. Toporski, *Confocal Raman Microscopy*. 2011: Springer Berlin Heidelberg.

5. Wang, H., et al. *Spot size and depth of focus in optical data storage system*. 2007. SPIE.

6. Liu, Z., et al., *High resolution, high collection efficiency in numerical aperture increasing lens microscopy of individual quantum dots.* Applied Physics Letters, 2005. **87**(7).

7. Piston, D.W., *Concepts in Imaging and Microscopy. Choosing Objective Lenses: The Importance of Numerical Aperture and Magnification in Digital Optical Microscopy.* Biological Bulletin, 1998. **195**(1): p. 1-4.

8. Ross, S.T., J.R. Allen, and M.W. Davidson, *Chapter 2 - Practical considerations of objective lenses for application in cell biology*, in *Methods in Cell Biology*, J.C. Waters and T. Wittman, Editors. 2014, Academic Press. p. 19-34.

9. Gröschl, M., *Ultrasonic separation of suspended particles-Part I: Fundamentals.* Acta Acustica united with Acustica, 1998. **84**(3): p. 432-447.

10. Trujillo, F.J., et al., *Multiphysics modelling of the separation of suspended particles via frequency ramping of ultrasonic standing waves.* Ultrason Sonochem, 2013. **20**(2): p. 655-66.

11. Harris, N.R. and M. Hill, *Particle Manipulation Using Ultrasonic Fields*, in *Encyclopedia of Microfluidics and Nanofluidics*, D. Li, Editor. 2008, Springer US: Boston, MA. p. 1597-1602.

12. Ross-Johnsrud, B., E. Zabolotskaya, and Y. Ilinskii, *Acoustic manipulation of particles in standing wave fields*. 2016, Google Patents.

13. Presz, W.M., et al., *Large scale acoustic separation device*. 2016, Google Patents.

14. Hawkes, J.J. and W.T. Coakley, *Force field particle filter, combining ultrasound standing waves and laminar flow.* Sensors and Actuators B: Chemical, 2001. **75**(3): p. 213-222.

15.   Trampler, F., et al., *Multilayered piezoelectric resonator for the separation of suspended particles*. 1994, Google Patents.

16.   Glynne-Jones, P., et al., *Mode-switching: A new technique for electronically varying the agglomeration position in an acoustic particle manipulator.* Ultrasonics, 2010. **50**(1): p. 68-75.

17.   Gröschl, M., *Ultrasonic Separation of Suspended Particles - Part II: Design and Operation of Separation Devices.* Acta Acustica united with Acustica, 1998. **84**(4): p. 632-642.

18.   Koch, Cosima., Advances in Bioprocess Monitoring by Mid-Infrared Spectroscopy

19.   Woodside, S.M., B.D. Bowen, and J.M. Piret, *Measurement of ultrasonic forces for particle–liquid separations.* AIChE Journal, 1997. **43**(7): p. 1727-1736.

20.   Xi, X., et al., *Study on the bubble transport mechanism in an acoustic standing wave field.* Ultrasonics, 2011. **51**(8): p. 1014-25.

21.   Petersson, F., et al., *Free flow acoustophoresis: microfluidic-based mode of particle and cell separation.* Analytical chemistry, 2007. **79**(14): p. 5117-5123.

22.   Bassindale, P., et al., *Measurements of the force fields within an acoustic standing wave using holographic optical tweezers.* Applied Physics Letters, 2014. **104**(16): p. 163504.

23.   Koch, C., et al., *Ultrasonic manipulation of yeast cells in suspension for absorption spectroscopy with an immersible mid-infrared fiberoptic probe.* Ultrasound in medicine & biology, 2013. **39**(6): p. 1094-1101.

24.   Wienland,Karin., Hyperspectral imaging of hyphae and spores of penicillium chrysogenum using confocal Raman (micro) spectroscopy

25   Stochastic Processes and Applications: Diffusion Processes, the Fokker-Planck and Langevin Equations (Texts in Applied Mathematics) 2014th Edition

25.   Gherardini, L., et al., *A study of the spatial organisation of microbial cells in a gel matrix subjected to treatment with ultrasound standing waves.* Bioseparation, 2001. **10**(4): p. 153-162.

26.   Radel, S,. *Ultrasonically enhanced settling   the effects of ultrasonic plane wave fields on suspensions of the yeast Saccharomyces cerevisiae.pdf.*

27.   Gherardini, L., et al., *A new immobilisation method to arrange particles in a gel matrix by ultrasound standing waves.* Ultrasound in Medicine & Biology, 2005. **31**(2): p. 261-272.

28.   H.A Willis,MRs V.J.I.Zichy and P.J.Hendra ., The laser-Raman and Infra-red Spectra of Poly(Methyl Methacrylate)

29.   Greiner, W., *Relativistic quantum mechanics*. Vol. 3. 1990: Springer.

30.   Mohammed, A., *Theoretical Studies of Raman Scattering*. 2011, KTH.

31.   Wang, H., C.K. Mann, and T.J. Vickers, *Effect of Powder Properties on the Intensity of Raman Scattering by Crystalline Solids.* Applied Spectroscopy, 2002. **56**(12): p. 1538-1544.

32.   Woodside, S., et al. *Analysis of the forces responsible for ultrasonic resonance based cell separation*. in *ABSTRACTS OF PAPERS OF THE AMERICAN CHEMICAL SOCIETY*. 1997. AMER CHEMICAL SOC 1155 16TH ST, NW, WASHINGTON, DC 20036.

33.   Greenspan, M. and C.E. Tschiegg, *Tables of the Speed of Sound in Water.* The Journal of the Acoustical Society of America, 1959. **31**(1): p. 75-76.

34.   David, Tuschel. HORIBA Scientific, Edison, New Jersey, Selecting an excitation wavelenght for Raman spectroscopy

35.   QiangSun[a]ChaojianQin[b]., Raman OH stretching band of water as an internal standard to determine carbonate concentrations